CORA Cork Open Research Archive
Cartlann Taighde Oscailte Chorcaí

Title	Electrochemical sensor interface
Authors	Murphy, Aidan
Publication date	2023
Original Citation	Murphy, A. 2023. Electrochemical sensor interface. PhD Thesis, University College Cork.
Type of publication	Doctoral thesis
Rights	© 2023, Aidan Murphy. - https://creativecommons.org/licenses/by-nc-nd/4.0/
Download date	2026-11-16 09:31:49
Item downloaded from	https://hdl.handle.net/10468/14984



UCC
University College Cork, Ireland
Coláiste na hOllscoile Corcaigh

Ollscoil na hÉireann, Corcaigh

National University of Ireland, Cork



Electrochemical Sensor Interface

Thesis presented by

Aidan Murphy, BEEL

for the degree of

Doctor of Philosophy

University College Cork

Department of Electrical and Electronic Engineering

Head of School/Department: Prof. Liam Marnane

Supervisors: Dr. Ivan O'Connell and Dr. Alan O'Riordan

2023

Contents

Declaration vi

Abstract vii

Acknowledgements ix

Chapter 1 Introduction 1

1.1 References 4

Chapter 2 Literature Review 5

2.1 Electrochemical Sensors 5

2.1.1 Electrochemical Cell 5

2.1.2 Potentiostat Circuit 7

2.1.3 Electrochemical Sensor Circuit Model 9

2.1.4 Ultramicro Electroders 12

2.2 Voltammetric Sensing 13

2.2.1 Cyclic Voltammetry 13

2.2.2 Square Wave Voltammetry 16

2.3 Generator-Collector Voltammetric Sensing 17

2.3.1 Dual Working Electrode Sensors 19

2.3.2 Bipotentiostat 20

2.4 Electrochemical Impedance Spectroscopy 21

2.4.1 Electrochemical Impedimetric Immunosensors 22

2.4.2 EIS Plots 23

2.4.3 EIS Curve Fitting 24

2.4.4 Sensor Impedance 25

2.5 Portable Potentiostats 30

2.5.1 Trends in Portable Potentiostats & Current State of the Art 31

2.6 References 36

Chapter 3 Voltammetric Proof of Concept using ADuCM350 System on Chip..44
3.1 Introduction 44
3.2 Tyndall Ultramicro Electrodes and Nanowire Sensors 45
3.2.1 Voltammetric Scans Performed on Sensor 46
3.2.2 System Requirements 47
3.3 Analog Front End 50
3.3.1 Voltammetric Measurement using the ADuCM350 51
3.4 Development of System 54
3.4.1 Trans Impedance Amplifier 55
3.4.2 Defining Voltammetric Test Parameters of the System 57
3.4.3 ADuCM350 Offset Calibration 58
3.4.4 Programming Tests 58
3.4.5 Specifications 61
3.5 Benchmarking the proposed System vs Lab Equipment 62
3.5.1 Resistive Calibration 62
3.5.2 Ferrocene Calibration 64
3.5.3 Cyclic Voltammogram Calibration 67
3.5.1 Square Wave Voltammogram Calibration 68
3.5.2 Sources of Error 69
3.6 Conclusion 70
3.7 References 71
Chapter 4 Bipotentiostat System for Water Quality Monitoring 73
4.1 Introduction 73
4.2 Tyndall Interdigitated Ultramicroband Sensors 74
4.3 Dual Electrode System Proof of Concept 75
4.3.2 Custom Printed Circuit Board Realisation 83
4.3.3 Validation of the data acquisition PCB 87

4.4 Calibration of Sensor in River Lee Water 91
4.4.1 Dissolved Oxygen Sensor 91
4.4.2 Electrochemical Reaction in Water for Dissolved Oxygen 92
4.4.3 Dissolved oxygen detection and calibration plot 93
4.4.4 Limitations of the System 97
4.5 Conclusion 98
References 99
Chapter 5 EIS Disease Detection System 103
5.1 Introduction 103
5.2 Tyndall Immunosensors 105
5.3 CV Results 106
5.4 Portable Impedometric Potentiostat 108
5.4.1 Derivation of Specifications 109
5.4.2 ADuCM355 as a SoC for Impedance Measurements 112
5.4.3 Development of System 114
5.4.4 PCB Implementation 120
5.5 Results 125
5.5.1 Device Calibration 125
5.6 Limitations of System 132
5.7 Field Results 134
5.8 Conclusion 137
5.9 References 139
Chapter 6 Conclusions and Future Work 142
6.1 Conclusions and Summary 142
6.2 Future Work 144
Appendices 145
A.1 Acronyms 145

A.2 Peer Reviewed Publications 147
A.3 Publications Submitted 147
A.4 Code Used 148
A.5 PCB Schematics and Layouts 149

Declaration

"This is to certify that the work I am submitting is my own and has not been submitted for another degree, either at University College Cork or elsewhere. All external references and sources are clearly acknowledged and identified within the contents. I have read and understood the regulations of University College Cork concerning plagiarism and intellectual property."

Aidan Murphy

January 2022

Abstract

Recent advances in nanotechnology have led to the development of electrochemical sensors that utilize electrodes with a width of one micron or less. This increased sensitivity has opened up a range of new electrochemical sensing applications, allowing the technology to move beyond the confines of the laboratory and into real-world settings. However, the interfacial electronics used for these sensors are often too bulky for portable use and can be prohibitively expensive due to the low current measurement capability required from the instrument. To address this challenge, this thesis presents cost-effective measures for creating portable interfaces specifically designed for ultra-micro and nano-scale electrochemical sensors.

A portable data acquisition system has been developed to interface to nano and ultra-micro scale electrochemical sensors at the point of use through voltammetry. It can perform a range of voltammetric tests, including cyclic voltammetry, square wave voltammetry and generator collector voltammetry. The data acquisition system interfaces to a smartphone, operates from a rechargeable battery and is of suitable form factor to ensure that it's fully portable. By utilising commercially available components, this system has been developed to lower the barrier for entry for the development of emerging portable electrochemical sensing technologies at micro and nano scale.

A second data acquisition system has been developed to interface to nano and ultra micro electrochemical immunosensors through Electrochemical Impedance Spectroscopy. Results from the device were benchmarked against laboratory

equipment to ensure it is of suitable sensitivity to be fit for purpose. The printed circuit board has been designed such that it can be integrated into a handheld device suitable for operatives such as veterinarians. This system will aid in the detection of biological agents such as viruses and antibodies at the point of sample, particularly in electrochemical sensors designed for agricultural applications.

Acknowledgements

This thesis is the culmination of a lot of help from a lot of good people. First and foremost I'd like to thank my supervisor Ivan O'Connell. He had everything I could ask for in a supervisor, he gave me the freedom to work on the project whichever way I enjoyed most and also was a rock of knowledge and advice. No matter how silly the question was he would answer and never make me feel stupid! I am very thankful to him for all the support he gave me throughout the PhD.

Thanks to my co-supervisor, Alan O'Riordan for letting an engineer into his electrochemistry group. You kept pushing me to have the devices I made interface to as many of the sensors in your group as possible. I would have never contemplated trying to make a bipotentiostat if it wasn't for you!

Thanks to Niamh Creedon for taking me under your wing, especially when I was starting off. You made time for me whenever I had a question on chemistry and I'm very grateful for that.

Huge thanks to my friend Kathy 'Skip' Hanley, together we managed to talk to the 350 for the first time. Thanks for calming me down whenever I got stressed about electronics and for being the greatest captain in the history of the Tyndall annual staff vs student soccer match.

Another cohort of people I am very grateful for are the lads in Analog Devices who were working with the 350/355. Liam Riordan, Mike Looney, Sean Wilson, Michael Lambe and Neo Xu all gave me huge support and I'm grateful for their patience with me when I ran into trouble using their chips.

A big thanks to all my friends in Tyndall. Thanks Catherine Walsh and Nicola Cooney for helping me to keep my sanity. I really enjoyed our chats and your

company in the MCCI office! Big thanks to Anthony Wall for letting me bounce ideas off you and for being a mighty man in general… we'll always have Milan! Thanks to everyone in the B.2.29 electrochemistry lab for their patience with "the engineer" and showing me how to use equipment and find stuff in the lab! ! Over the course of the PhD I was lucky enough to work with some excellent electrochemists. Particular thanks to Ian Seymour, Caoimhe Robinson, Fernando Diaz, Luiza Wasiewska, Benjy O'Sullivan and Pierre Lovera for all the electrochemical knowledge you imparted on me!

Finally, a big thanks to my family, Roseanne, Denis (Flynn), Dad and Mary (mother), for all their love, support and guidance throughout my life. I wouldn't be at this stage of a PhD without them. Particular thanks for not exiling me when I was grumpy and locked down with covid when finishing the Thesis.

Chapter 1 Introduction

Technology has been advancing rapidly in the last half century and has had a profound impact on how the people live their day to day lives. One of the most consistent advancements has been in miniaturisation. Improvements in semiconductor device science have seen computers shrink from the size of rooms into our pockets. Such a trend is also occurring in analytical chemistry, particularly in electrochemical sensing. Since the first electrochemical sensor was developed in the 1950's [1], sensor form factors have been decreasing from the macro to sub-micro scale and have become more sensitive in the process.

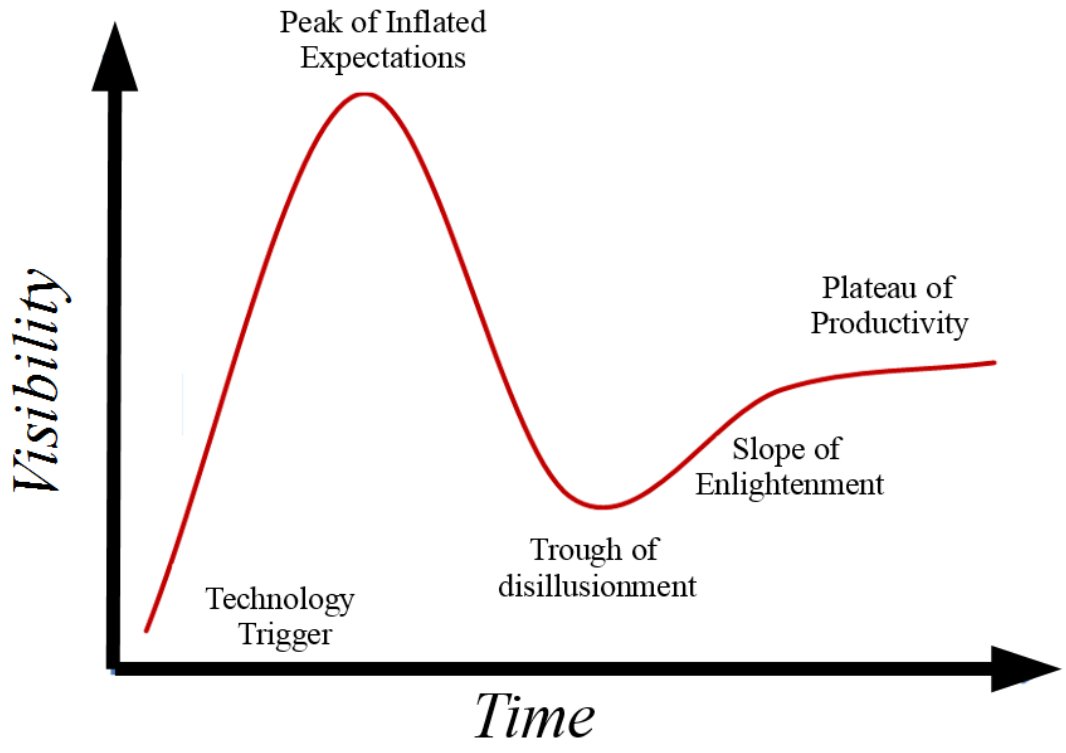


Figure 1.1: Gartner Hype Curve

The global electrochemical sensor market was valued at $6.19 billion in 2020 and is expected to grow 11.4% annually to $11.83 billion in 2026 [2]. Nano and sub-micro electrochemical sensors will gain a share of this market as the technology progress through the slope of enlightenment of the Gartner hype curve [3] as seen in Figure 1.1. This particular segment of the curve is where it is expected that further technological advancement will lead to increased adoption. Industries that have been early adopters of electrochemical nanosensors include medical, security and environmental monitoring industries, where high degrees of sensitivity and selectivity are paramount [4]. Another example of a technology that has passed the trough of disillusionment in the last decade include internet of things sensor systems [5]. They were at the peak of the hype cycle in 2015-2016 but as the technology matured, it became clear that some of the use cases were not practical. Today, internet of things sensors systems are still being developed [6],[7], but with a more realistic understanding of their capabilities.

Ubiquitous devices such as digital glucometers and pregnancy tests are early indicators that electrochemical sensing is moving out of the laboratory. The importance of shifting the use of these technologies out of the laboratory has been highlighted by the recent SARS-CoV-2 pandemic, where a rapid, onsite testing system would have been a powerful tool to reduce testing times and curtail the spread of the virus. Nano and sub-micro electrodes for electrochemical sensors have seen improvements in response time and specificity [5-8]. These advances should allow for point of sample electrochemical sensing to be performed in a wider variety of applications. The aim of this thesis is to develop low cost electronic interfaces for sub-micro to nano scale electrochemical sensors and highlight the main challenges

associated with them. The main use cases of the electronic interfaces will be for sensors used for water quality monitoring and agricultural applications.

1.1 References

[1] J. L.C.Clark, “Monitor and Control of Blood and Tissue Oxygen Tensions,” *American Society for Artificial Internal Organs,* vol. 2, no. 1, pp. 41-48, 1956.

[2] Mordor Intelligence, “Electrochemical Sensor Market - Growth, Trends, COVID-19 Impact, and Forecasts (2021 - 2026),” Hyderabad, 2021.

[3] A. a. J. F. Linden, “Understanding Gartner’s hype cycles Strategic Analysis Report Nº R-20-1971 Gartner,” Inc 88, 2007.

[4] A. O. Sean Barry, “Electrochemical nanosensors: advances and applications,” *Reports in Electrochemistry,* vol. 6, pp. 1-14, 2016.

[5] D. W. M. Arrigan, “Nanoelectrodes, nanoelectrode arrays and their applications,” *Analyst,* pp. 1157-1165, 2004.

[6] N. Hossain et. al, “High aspect ratio nano-fabrication of photonic crystal structures on glass wafers using chrome as hard mask", Nanotechnology, vol 25 pp. 301-355, 2014.

[7] P. Lovera et al., “Low-cost silver capped polystyrene nanotube arrays as super-hydrophobic substrates for SERS applications", Nanotechnology pp. 175502, 2014.

[8] N. Creedon et al., “Highly Sensitive SERS Detection of Neonicotinoid Pesticides. Complete Raman Spectral Assignment of Clothianidin and Imidacloprid", Journal of Physical Chemistry A, pp. 7238-7247, 2020.

Chapter 2 Literature Review

2.1 Electrochemical Sensors

Electrochemistry is the science that investigates the charge transfer at the electrode solution interface through a mechanism known as a *redox* reaction [1]. Redox reactions are a type of chemical reaction whereby an electron is transferred between two species. A species, in the context of chemistry, is a group of atoms or molecules that are made to go through a chemical reaction. The species that loses the electron is said to be *oxidised* and the body that gains an electron is *reduced*. For an electrochemical sensor, a potential voltage is applied at an electrode-solution interface to initiate a redox reaction between the two bodies. The current that is generated at the electrode by the oxidation or reduction of a species, also known as the faradaic current, is a direct indicator of the rate at which the chemical reaction is occurring [2].

2.1.1 Electrochemical Cell

Typical electrochemical sensors consist of three electrodes: the Working Electrode (WE), the Counter Electrode (CE) and the Reference Electrode (RE) as seen in Figure 2.1. The WE is typically where the reaction of interest takes place and is maintained at a fixed potential, often referred to as virtual ground. The RE is used to sense the potential of the solution under test.. Through the use of feedback provided by the RE, the potential of the CE is adjusted to obtain the desired solution-Working Electrode potential. The Reference Electrode is placed as near as possible to the WE to ensure that it senses the potential of the solution at the solution-electrode interface. The CE is used to apply an electric potential to the solution to

induce a potential difference at the WE-solution interface. It is also acts as a source or sink of electrons to accommodate for the electrochemical reaction. It is typically an order of magnitude larger in surface area than the WE in order to ensure sufficient transfer of electrons in the reaction.

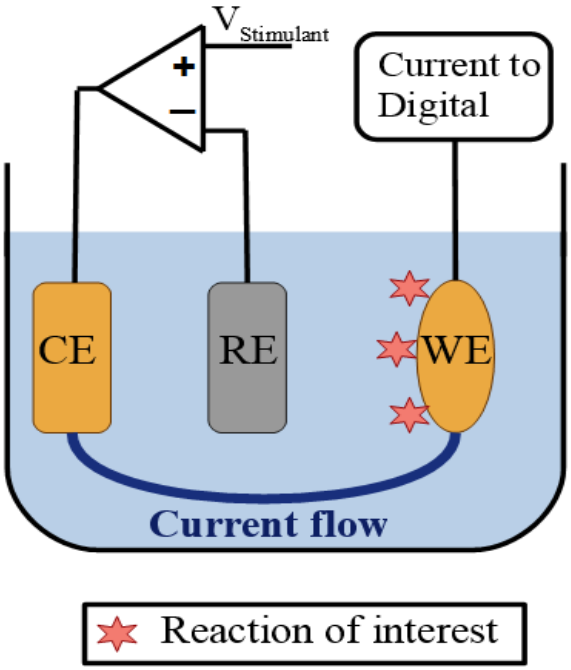


Figure 2.1: Three Electrode Electrochemical Sensor.

2.1.1.1*Aqueous and Pseudo Reference Electrodes*

Aqueous reference electrodes are commonly used as in an electrochemical sensor to provide a stable, well known electrode potential. Examples include the standard hydrogen electrode [3], which provides 0 V and the silver chloride electrode [4], which provides 0.197 V with respect to the standard hydrogen electrode. Pseudo reference electrodes do not provide a constant potential, but are easier to integrate into sensing solutions as they are solely a piece of an chemically inactive material such as platinum [5] or nickel [6]. A drawback is that regular calibration may be necessary to account for potential drift in pseudo reference electrodes.

To demonstrate the potential shift that different reference electrodes can provide, a test was performed using the same sensor and different reference electrodes. As shown in Figure 2.2, a potential shift in an electrochemical test known as a cyclic voltammogram can be seen between the two waveforms. Both waveforms used the same test parameters but utilised different reference electrodes. Due to the potential shifts seen in Figure 2.2, electrochemists must change the test parameters based on the reference electrode used.

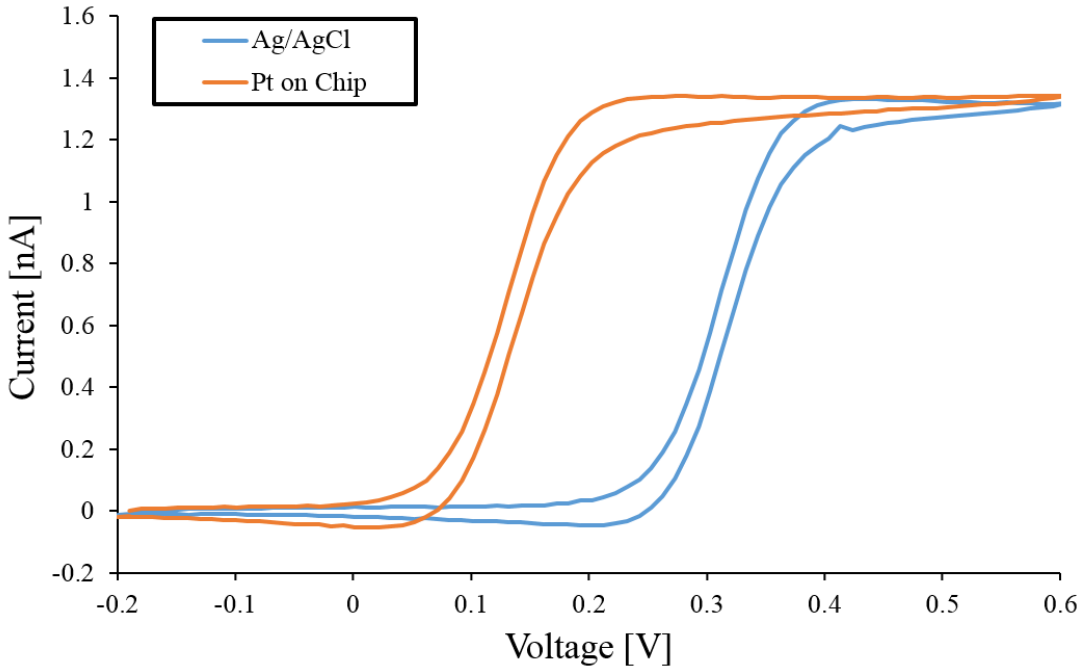


Figure 2.2: Electrochemical test using a silver/silver chloride aqueous reference electrode and a platinum on chip pseudo reference electrode.

2.1.2 Potentiostat Circuit

A potentiostat is the instrument used to interface to electrochemical sensors [7]. Its function is to induce the target electric potential difference between the RE and WE of the electrochemical cell under test and measure the resultant current at

the WE [8]. A simple potentiostat is illustrated in Figure 2.3, the main components of which are:

The Signal Generator provides the voltage signal to the CE which is necessary for the electrochemical test to be completed. It typically utilises a Digital to Analog Converter (DAC) to generate an analog input to the system.

The Electrometer measures the potential difference between the RE and CE and is used as the feedback signal in the potentiostat circuit. It is important that as little current flows though the RE as possible to ensure the electrode doesn't get polarised. A unity gain buffer is usually used in potentiostats to make the RE feedback path of high impedance.

The Control Amplifier is used to ensure that the voltage from the signal generator is inducing the required potential difference at the electrode solution interface. It is an op-amp that compares the electrometer voltage with the signal generator. It drives current into the system based on negative feedback from the measured cell to compensate for the IR drop due to solution resistance between the CE and WE.

The Current to Voltage Converter is used to convert the output current of the WE to a readable voltage for the Analog to Digital Converter (ADC) in the signal processor. The most common method of converting the current to a readable voltage, particularly for low current measurements, is through the use of a Trans-Impedance Amplifier (TIA) [9]. A resistive feedback TIA is shown in Figure 2.3.

The Signal Processor utilises an ADC to convert the analog voltage from the TIA into a digital signal. The sample rate of the ADC determines the highest frequency signal that can be measured and the resolution determines the number of increments of current that can be measured from the sensor [10]. To improve the quality of the TIA voltage to be read by ADC, potential gain amplifiers can be used to amplify the voltage and filters may also be used to remove any out of band signals.

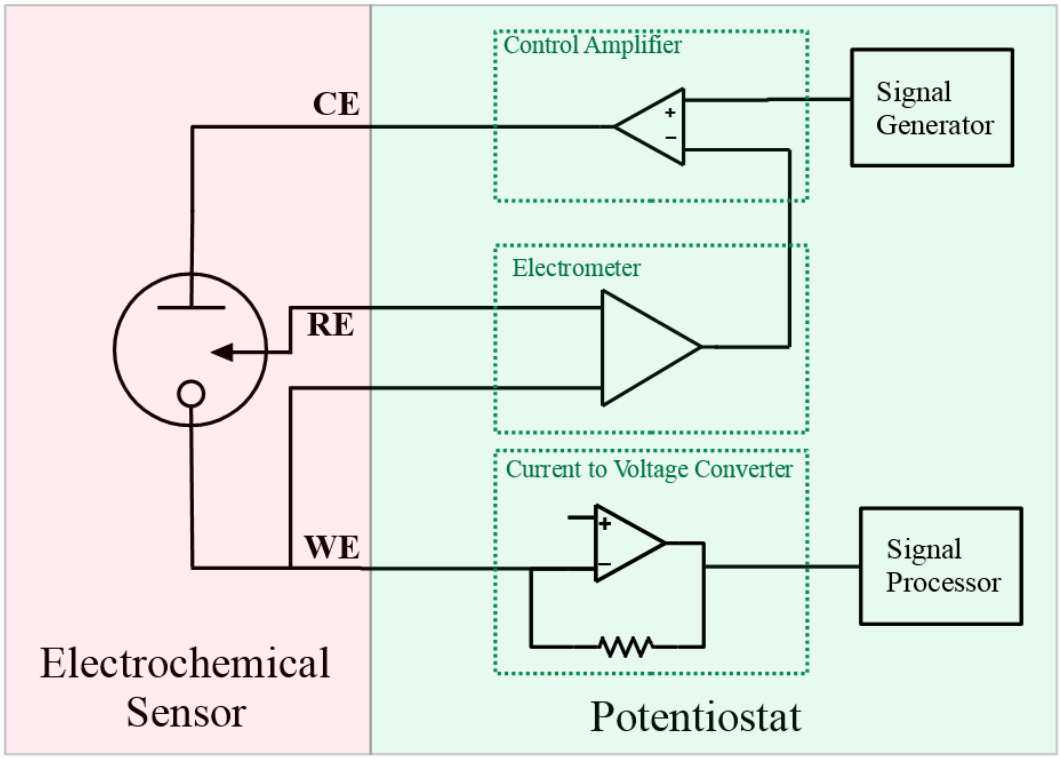


Figure 2.3: Potentiostat schematic for three electrode electrochemical cell.

2.1.3 Electrochemical Sensor Circuit Model

The electrode-electrolyte interface of an electrochemical sensor can be modelled by a Randles equivalent circuit as seen in Figure 2.4 [11] [12]. Although the Randles circuit is a simplistic model, it is a useful tool to identify and understand

the mechanisms at work in an electrochemical sensor. The model consists of: R_{sol} the electrolyte resistance, C_{dl} the double layer capacitance, R_{ct} the charge transfer resistance and Z_{war}, the Warburg impedance and is explained in more detail in Section 2.1.3.2. below.

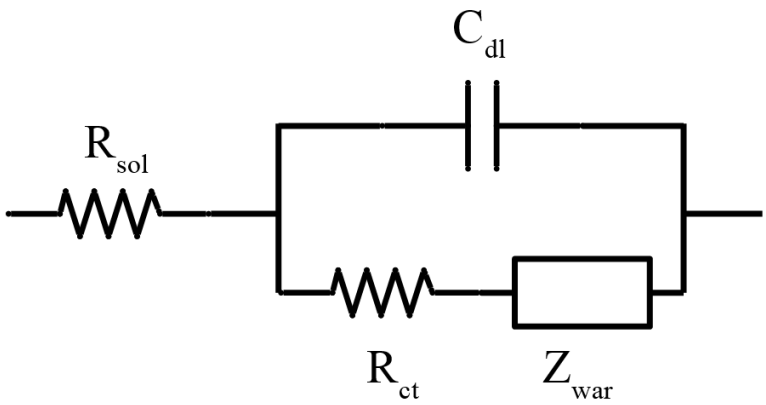


Figure 2.4: Randles circuit model of electrode-electrolyte interface.

2.1.3.1*Solution Resistance*

The solution resistance corresponds to the resistance offered by the ionic solution [13]. It is predominantly proportional to the physical distance between the CE and WE and the electrolytic composition of the solution. It is in series with the circuit model since the electrons associated with the chemical reaction must pass through the solution to reach the Counter Electrode. Three electrode electrochemical sensors can help mitigate the effects of solution resistance through the use of the RE.

2.1.3.2*Warburg Impedance*

The Warburg impedance represents the diffusion process of ions at work at the electrode-solution interface. Its impedance is related to the frequency of potential change at the electrode solution interface. At high frequencies the reactants don't have much time to move or diffuse before the potential changes again, this results in a small impedance.At low frequencies the reactants have more time to diffuse a

larger distance away from the electrode, resulting in a larger impedance. The effects of Warburg impedance become less pronounced for electrodes of smaller feature sizes as the reactions aren't diffusion limited. As the electrochemical sensors used in this thesis contain Ultra Micro Electrodes (UME) ie., electrodes with μm or sub μm feature sizes, the effects of Warburg impedance are negligible and is eliminated in the subsequent analysis.

2.1.3.3*Charge Transfer Resistance*

The R_{ct} represents the flow of ions from the electrode to the solution and vice versa through the redox reactions. It can be affected by the concentration of reactants, the applied potential at the WE – Solution interface, the nature of the redox reaction, the composition of the WE and the temperature of the solution. Charge transfer resistance is the most prevalent indicator of the reaction occurring for electrode surfaces that are at the micro or nano scale since Warburg impedance is negligible.

2.1.3.4*Double Layer Capacitance*

The C_{dl} occurs at any interface where an electrode becomes charged and oppositely charged molecules in the electrolyte are attracted to its surface. As seen from Figure 2.5, the first layer of negatively charged molecules are well attached to the electrode surface. Oppositely charged ions are subsequently attracted to the semi-permanent layer and are separated by a layer of neutral molecules thus creating a capacitor. The value of the C_{dl} depends on multiple factors including; the applied potential, the ionic concentration of the electrolyte, the temperature of the electrolyte and the roughness of the electrode. This is an effect predominately seen in

electrodes with a form factor greater than a mm^2. It inhibits sensor sensitivity and increases the amount of time it takes for the reaction to reach a steady state.

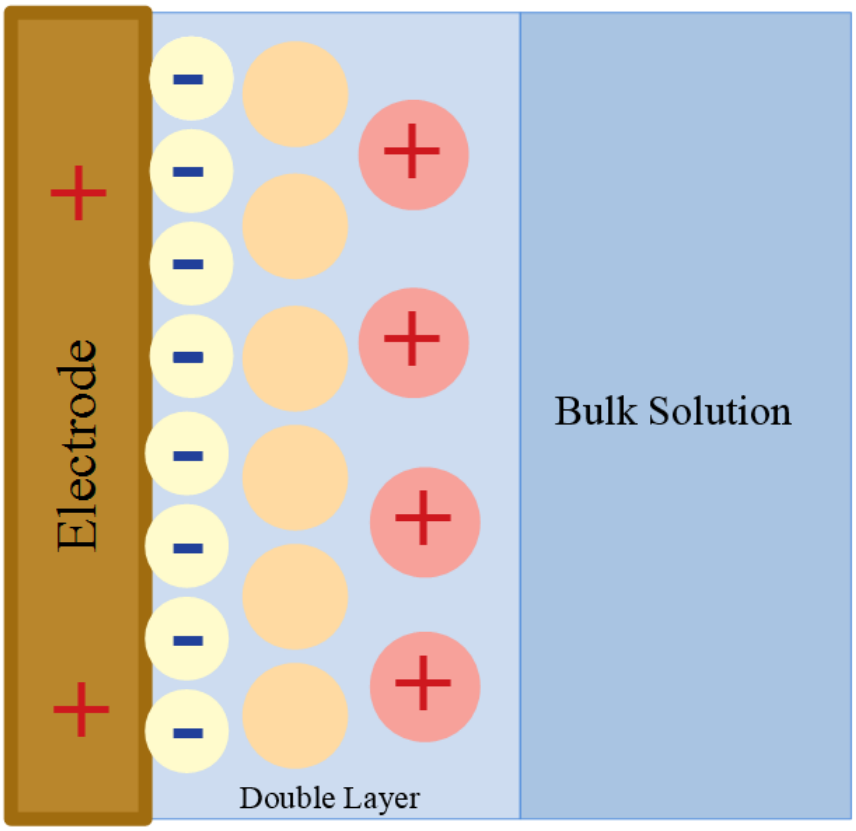


Figure 2.5: Simplified diagram of double layer capacitance for an electrochemical cell.

2.1.4 Ultramicro Electroders

Ultramicro electrodes (UME) refer to a WE with a critical dimension of 25 µm or less [14]. Sensors that utilise an UME offer many advantages over existing sensors, specifically in terms of their response time and sensitivity, resulting from their feature size [15]. The response time is superior due to improved mass transport of the analyte to the electrode. This is as a result of radial (3-dimensional) diffusion becoming more dominant for smaller feature sizes, which allows the reaction to reach a steady state faster. Despite their lower output currents, ultramicro electrochemical sensors have a superior signal to noise ratio compared to macro

electrodes [16]. This is as a result of the diffusion layer becoming smaller as the electrode decreases in size, resulting in reduced capacitive effects. Other advantages include a smaller sensor size, requiring a smaller sample volume and less solution resistance. This makes these sensors particularly suited for field deployment for point of test applications for an optimum sensitivity response time solution.

Despite their advantages, UMEs also have several limitations. For instance, the specialized equipment required for their fabrication and testing can result in higher manufacturing costs, making them prohibitively expensive for some applications. Moreover, UMEs are more fragile than their larger counterparts, and their small size can make them more sensitive to environmental factors like temperature and humidity. As a result, they may require more frequent calibration than sensors with larger electrodes, which can be both time-consuming and costly.

2.2 Voltammetric Sensing

Voltammetry involves applying a known electric potential difference between the solution and WE while measuring the resultant current from the induced redox reaction [17]. The current is plotted against the voltage applied, over the course of the test to produce a voltammetric curve. Information from the analyte can be inferred from the resultant chart, which is called a voltammogram, an example of such is shown in Figure 2.6 (a).

2.2.1 Cyclic Voltammetry

Cyclic Voltammetry (CV) is one of the most commonly used voltammetric techniques. It requires a applied electric potential to be ramped and usually starts and finishes at an initial specified potential. CV is used to infer both qualitative and

quantitative information about the electrochemical reaction. The most prominent test parameters include the maximum and minimum values of the voltage ramp and the scan rate (V/s), which is the rate at which the electric potential is swept [2]. The initial potential of the voltammogram is set at a voltage where no redox reaction takes place and is swept to a value where the electrochemical reaction of interest takes place as illustrated in Figure 2.6 (a).

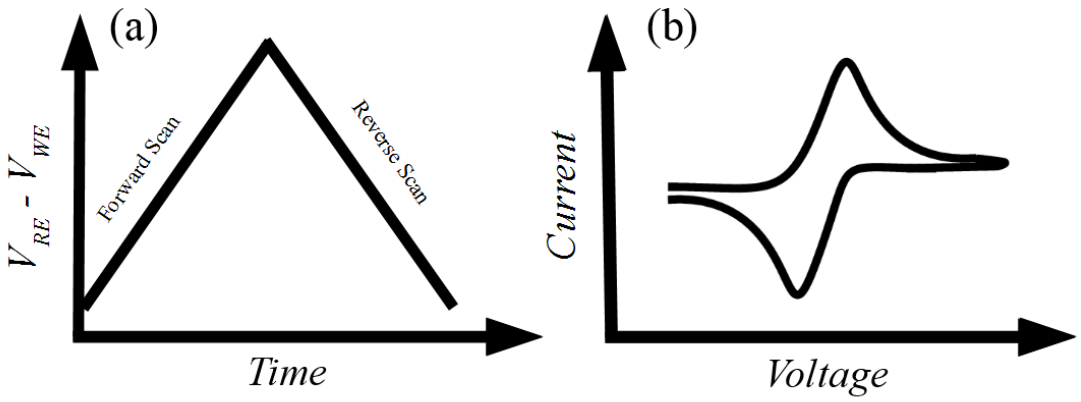


Figure 2.6: (a) CV voltage ramp, (b) Typical current response from CV.

2.2.1.1.1 Points of interest on CV Scan

When reading a CV curve, the predominant points of interest are the oxidation or reduction peaks of the waveform. These peaks can correspond to the concentration of the analyte in the solution. The nature of the peak is an indicator of the kinetics of the electrochemical reaction at the electrode solution interface. If the peak is flat then the reaction reached a steady state and the flow of electro-active species to the electrode surface was limited. If there is a pronounced peak, as seen in Figure 2.6 (b), it is due to double layer capacitance. The diffusion co-efficient or electroactive surface area can be deduced from the peak value of the cyclic voltammogram trough the Randles-Sevik equation [2]. The steady state current can

be an indicator of the surface area of the electrode, which is of particular interest to nano-scale electrochemical sensors.

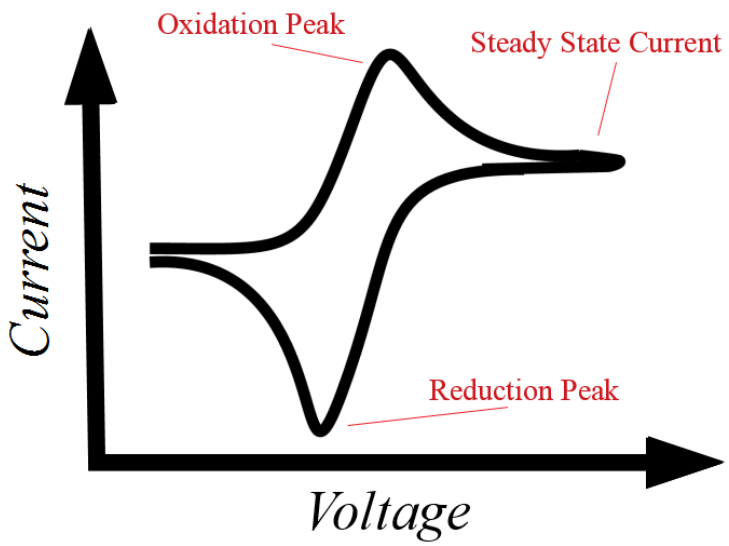


Figure 2.7: Points of interest on CV.

2.2.1.1.2 CV Shape

If the oxidation and reduction peak values are not within a margin of 58mV within each other, then the reaction may not be reversible [4]. This may be due to a slow electron transfer in the reaction or a chemical step preventing the species to be oxidised or reduced back to its original state.

Cyclic Voltammetry can also show presence of short-lived intermediate reactions that result in the product of the redox species [5]. As shown in Figure 2.8, it is usually represented by separate peaks along the voltammogram. The shape of the intermediate and redox peaks can give an indication to the stability and lifetime of the both the reactants and products. Such peaks may also represent electroactive contaminates reacting in the solution.

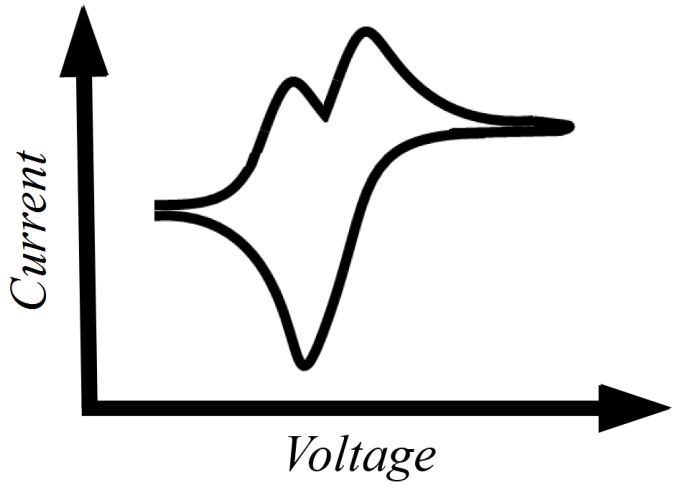


Figure 2.8: Cyclic Voltammogram with two peaks, an example of an intermediate reaction that can be seen in a voltammetric test.

2.2.2 Square Wave Voltammetry

Square Wave Voltammetry (SWV) [18] involves applying a ramped square wave to the sensor, as illustrated in Figure 2.9 (a), and measuring the difference in current at the end of the trough and peak of each period, as shown in Figure 2.9 (b). SWV is a sensitive electroanalytic technique as it is a pseudo differential measurement, which means low frequency background noise is nullified. It is more likely to be used for detecting lower concentration levels compared to CV, as its peaks can be an indicator of the concentration of the species of interest as well. Similarly to CV, the ramp commences at a voltage where no redox reaction takes place and is ramped until the reduction or oxidation reaction occurs. The main test parameters include the maximum and minimum values of the voltage ramp, scan rate and both the frequency and amplitude of the square wave.

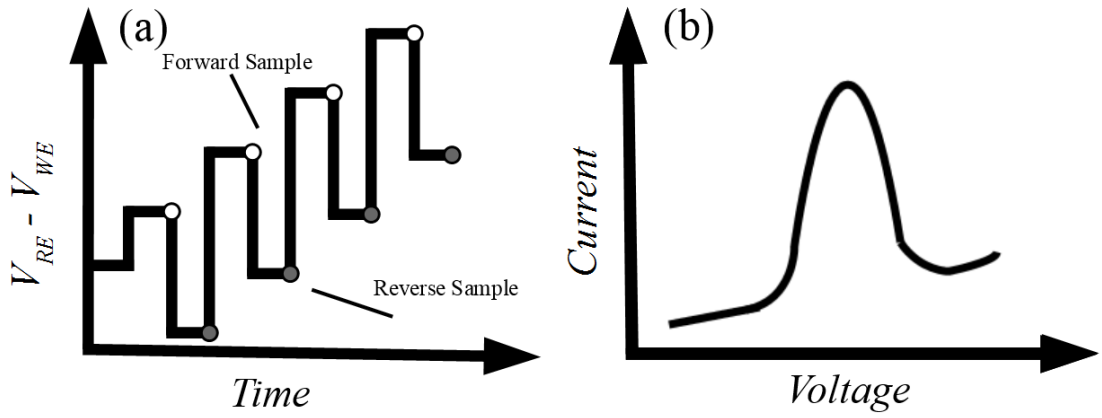


Figure 2.9: (a) SWV voltage ramp, (b) Typical current response from SWV.

2.3 Generator-Collector Voltammetric Sensing

Generator-collector voltammetry [19] is a technique that utilises two working electrodes. It utilises redox cycling to enhance the sensitivity of the sensor under test. Redox cycling is a process whereby the same analyte can be oxidised and reduced a multitude of times between two working electrodes in close proximity. One electrode, the generator is used to oxidise or reduce the species of interest while the second electrode, the collector usually reverses the reaction as shown in Figure 2.10. The more reduction and oxidation cycles the analyte undergoes between the generator and collector, the larger the signal and the more sensitive the sensor becomes.

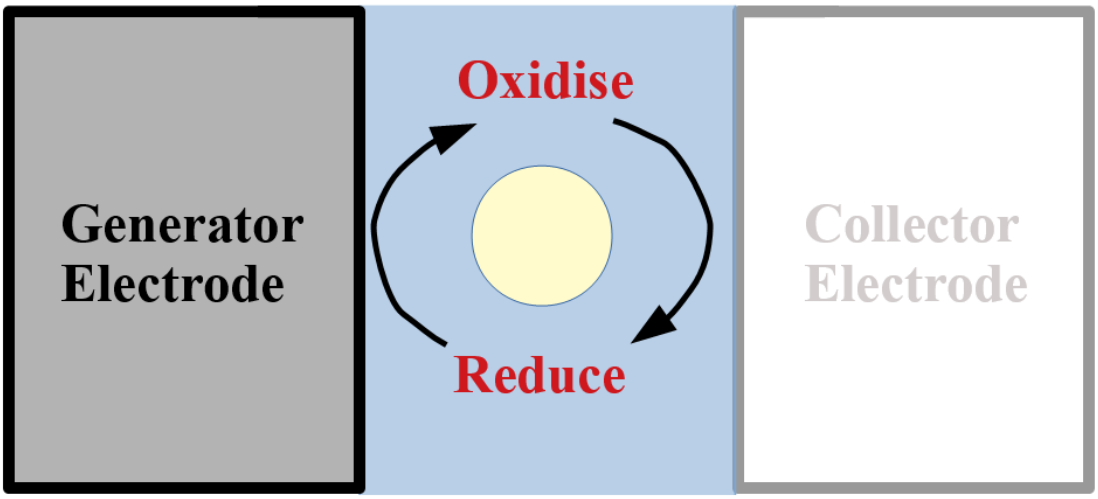


Figure 2.10: Example of redox cycling between generator and collector electrodes.

In general this involves performing the voltammetric test of interest at the first working electrode (WE1), while keeping the second working electrode (WE2) at a constant potential with respect to the reference electrode. Shown in Figure 2.11 is an example of this where a cyclic voltammogram is performed at WE1 and WE2 is held at a constant potential.

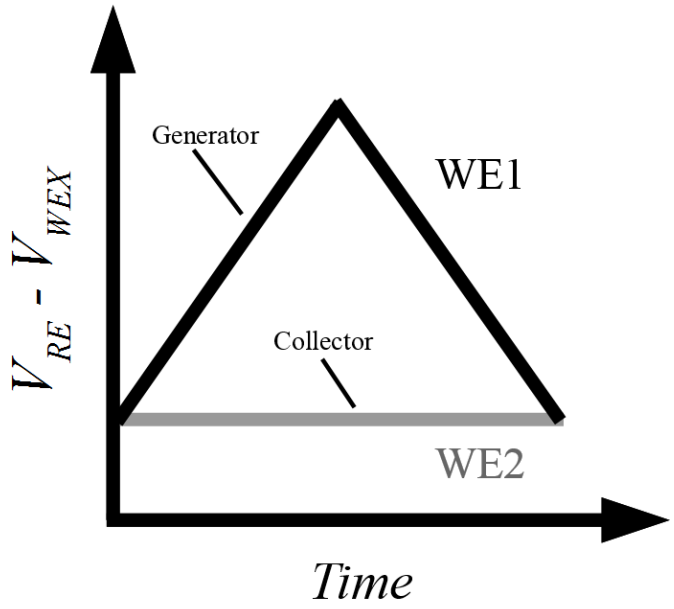


Figure 2.11: Example of voltage levels of generator collector voltammogram for WE1 and WE2.

2.3.1 Dual Working Electrode Sensors

The first generator-collector sensor was developed in the 1950's and was called the rotating ring disk sensor [20]. It comprised of a disc generator electrode, surrounded by a ring collector electrode and this was spun by a motor in order to transport the species to the collector through using a centrifugal force. With advances in technology, particularly in the miniaturisation of electrode form factors, generator collector sensors have become less complex as their closer proximity has meant the species can be transported between the collector and generator without the need of external assistance [21].

One such configuration that is used for ultramicro scale sensors known as interdigitated electrodes [22]. It consists of two electrode "combs" separated by a gap, as illustrated in Figure 2.12. In an interdigitated configuration the species diffuses across the gap between the electrodes. If the electrodes are closer together, the probability of the generated species diffusing to its corresponding generator or collector electrode is increased. A key indicator of the performance of the sensor is the collection efficiency, which is the fraction of the collected current divided by the generated current from the redox reaction. Ultramicro scale interdigitated electrodes have recorded efficiencies more than 99% [23].

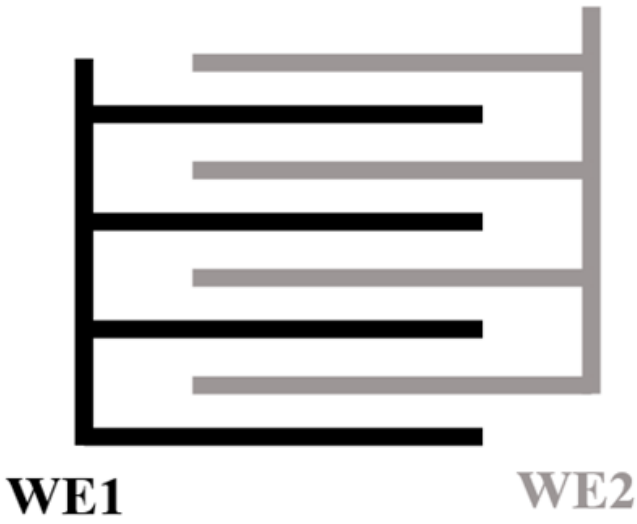


Figure 2.12: Interdigitated Electrode Array showing both the WE1 and WE2 consisting of 4 electrodes each separated by a gap.

2.3.2 Bipotentiostat

Bipotentiostats can be regarded as potentiostats but with the added functionality of potential control and current measurement at a second working electrode. The electrochemical potential of WE1 and WE2 are set by *e1* and *e2* respectively, as shown in Figure 2.13, which is an example of a bipotentiostat circuit [24]. As in standard potentiostats, to induce a specified potential difference at the electrode solution interface, WE1 is maintained at a virtual ground while the CE drives the solution potential, using the RE as feedback. The potential at WE2 is changed with reference to WE1. By using WE1 as a reference point, it ensures the difference at the electrode-solution interface is accurate with respect to the solution without the need for second RE as feedback.

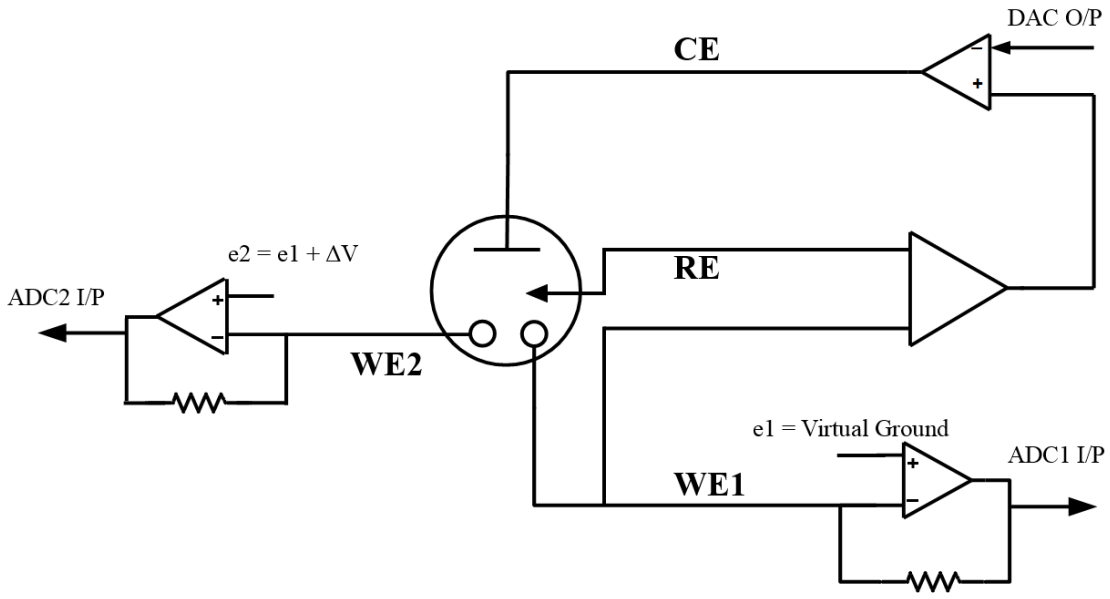


Figure 2.13: Example of bipotentiostat circuit, with a control amplifier, electromoter and two trans-impedance amplifiers.

2.4 Electrochemical Impedance Spectroscopy

In the voltammetric techniques described previously, the electrode is driven to a condition far from equilibrium through the application of a voltage and the response is observed. Electrochemical Impedance Spectroscopy (EIS) allows for interrogation of the sensor at equilibrium. This is done by applying a small, biased AC signal to the sensor and information regarding the sensors impedance is determined [25]. The frequency range explored in EIS varies depending on the specific system being studied, but it ranges from mHz to GHz range. Factors such as the electrode/electrolyte system being employed and the rate at which the reaction of interest is occurring on the electrode surface determine the frequency range of interest for the EIS scan.

This technique allows for far less deterioration of the WE surface as a small AC signal is used as opposed to large DC biases in voltammograms. It also enables

measurements to be taken over a longer time period, which can be averaged and improve the sensitivity of the reading for both the electronics and sensor. Through measuring the cell at equilibrium, models can be used to interpret the response more easily. The equivalent resistance and capacitances that are extracted can be regarded as a representation of the interfacial phenomena occurring at the electrode surface. EIS is used in corrosion sensing [26], batteries [27], fuel cells [28] and paint characterisation [29].

2.4.1 Electrochemical Impedimetric Immunosensors

Impedimetric immunosensors can be used to detect either an antibody or antigen [30]. An antigen is a substance that would cause an immune system to produce antibodies against it, for example, a virus, fungi or bacteria. Immunosensors are affinity based because of the tendency of antibodies and antigens to form stable complexes. Bioreceptor probes, such as antibodies are immobilised on the electrode surface [31]. This allows for the selective detection a target of interest such as a virus which can be seen in Figure 2.14. A bound antibody/antigen pair creates an insulating layer on the electrode surface, changing its electrical characteristics across a range of frequencies. EIS is used to characterise this phenomena, where the resistive and capacitive elements are used to model the electrode surface. This is done to gauge the extent of the affinity based reaction and discern the concentration of the target in the solution. Applications of this class of sensor include, human health [32], animal health [33], food security [34] and the environment [35].

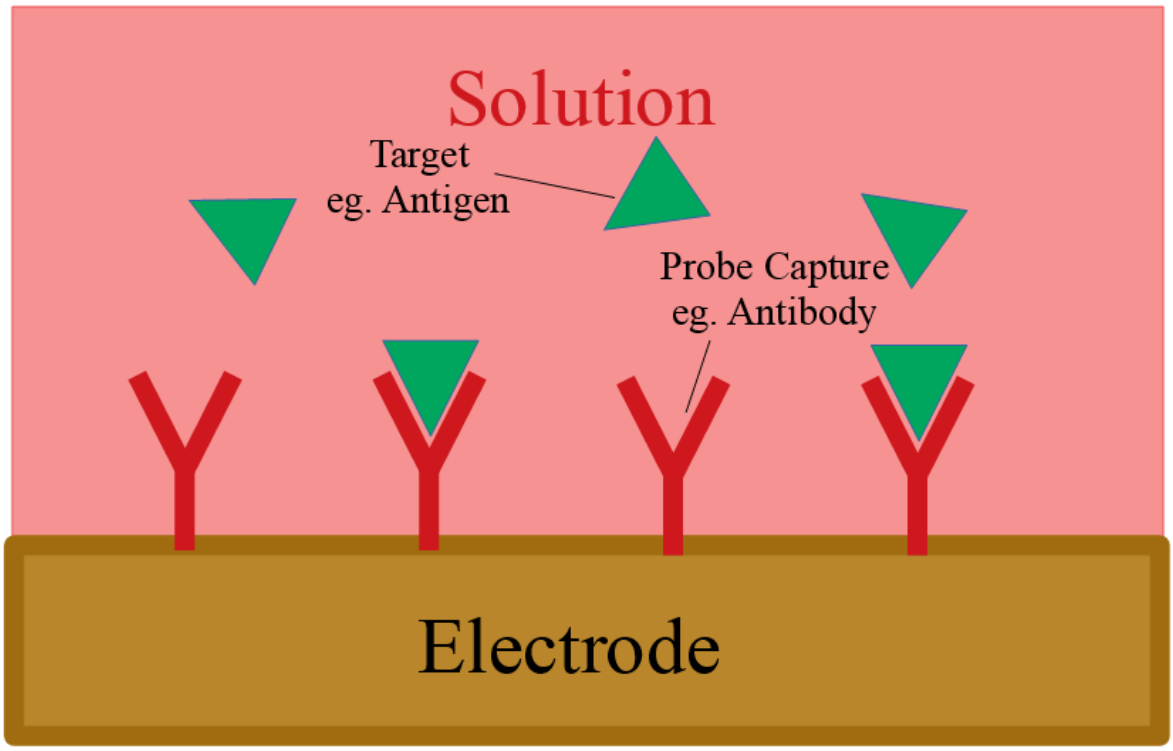


Figure 2.14: Example of affinity based sensing for electrochemical impedimetric immunosensor. The target can be seen binding with the probe capture, which, in turn will create an insulating layer on the electrode surface.

2.4.2 EIS Plots

The applied signal's frequency is usually swept across a range of values and the results are plotted as Bode or Nyquist plots as shown in Figure 2.15 (b-d) below. The Nyquist plot graphs the real against imaginary impedance from high frequency values to low. It is used for curve fitting which will be discussed in the next section. The Bode plot shows the absolute impedance and phase and shows more clearly how the system reacts to different excitation frequencies.

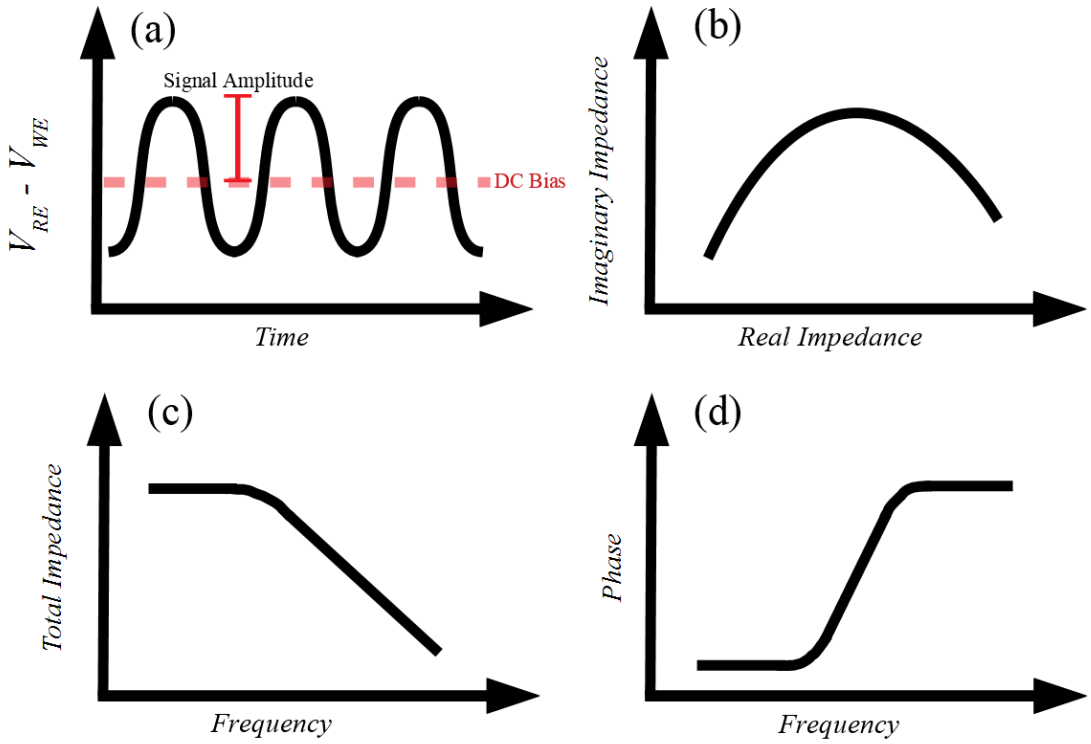


Figure 2.15: EIS applied signals and resultant graphs: (a) AC signal applied with a DC bias, (b) Nyquist Plot of real vs imaginary impedance, (c) Bode Plot of frequency vs total impedance, (d) Bode Plot of frequency vs phase.

2.4.3 EIS Curve Fitting

Equivalent circuit generation is the most common method of analysing EIS data [36]. As seen from Figure 2.16, the solution resistance corresponds to the real impedance value at the high frequency origin of the curve. The charge transfer resistance can be extracted by finding the diameter of the Nyquist plot. The double layer capacitance can be extracted by:

$$C_{dl} = \frac{1-\omega R_{ct}}{\omega} \tag{2.1}$$

where ω is the angular frequency at the centre of the EIS scan, which can also be described by:

$$\omega = 2\pi f \tag{2.2}$$

where *f* is the frequency at the centre of the EIS scan.

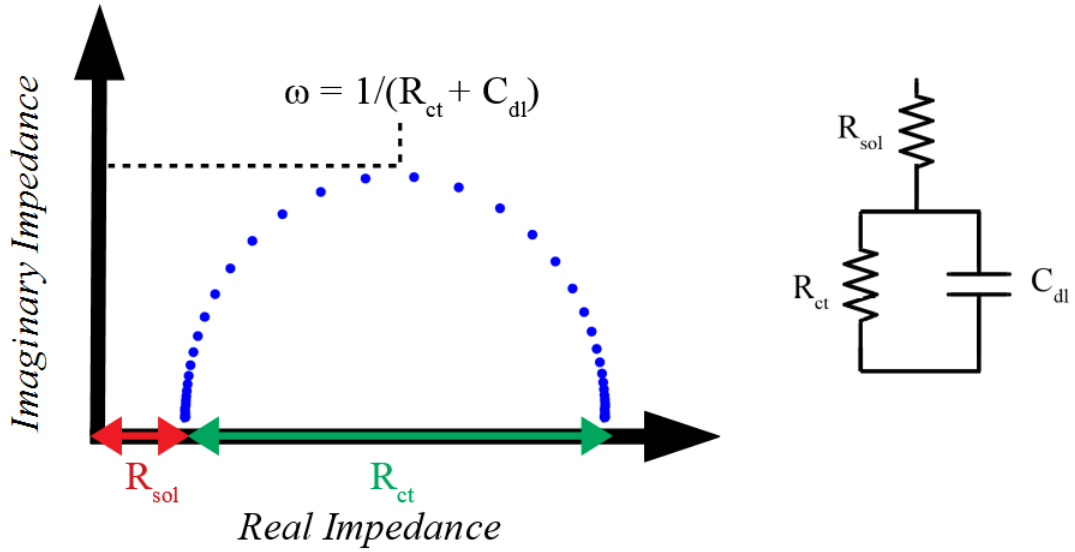


Figure 2.16 Randles circuit feature extraction from EIS Nyquist plot and simplified Randles circuit.

2.4.4 Sensor Impedance

Information on the impedance of the cell can be extracted by comparing the input voltage applied to the electrochemical sensor and the resultant output current. Where, the input voltage is:

$$e = Esin(2\pi ft) \tag{2.3}$$

where *E* is the voltage amplitude, *t* is time and *f* is the frequency of the waveform. The resultant output current will have a phase shift relative to the input voltage, it can be represented as follows:

$$i = Isin(2\pi ft + \Phi) \tag{2.4}$$

where *I* is the current and *Φ* is the phase shift relative to the input voltage. Using The same principles of phase shift hold true for the complex components of the input and output voltage:

$$e = E\ exp(j2\pi ft), \tag{2.5}$$

and

$$i = Iexp(j2\pi ft) \tag{2.6}$$

where j is the complex impedance component. Ohms law can be used to represent the impedance of the of the system:

$$Z_{tot} = \frac{e}{i} \tag{2.7}$$

To understand the system it can be useful to interpret the impedance by its real and imaginary vectors by:

$$Z_{tot} = Z_{re} - jZ_{im} \tag{2.8}$$

which can be plotted on a Nyquist plot, similar to Figure 2.15 (b). It can also be useful to separate its modulus and phase elements, which can graphed on a Bode plot, where: $Z = |Z_{tot}|$, (2.9)

and

$$\Phi = \arctan\left(\frac{Z_{im}}{Z_{re}}\right). \tag{2.10}$$

Impedance measurements used to be performed using an impedance bridge where one would use resistors and capacitors to match with the device under test [37]. This was useful for the measurement of an impedance at one frequency, but with electroanalytic techniques like impedance spectroscopy requiring measurements across multiple decades of frequencies, a different approach was needed. Modern instrumentation utilise either frequency or time domain measurements to extract the impedance. Frequency domain measurements are performed with Frequency Response Analysers (FRA). Alternatively, Fourier transforms can be used to interpret data in the time domain using with spectrum analysers.

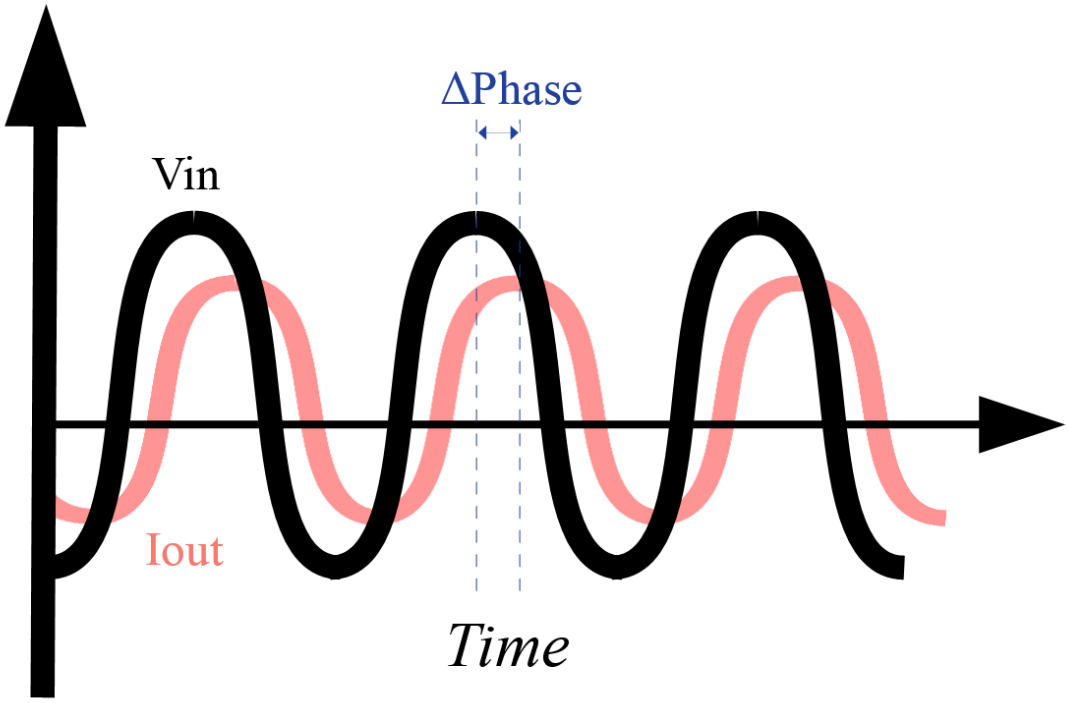


Figure 2.17: Representation of the applied sinusoidal input voltage and resultant current output of an EIS excitation signal, which stimulated at a given frequency.

2.4.4.1*Frequency Response Analysers*

The basic principle of performing an impedance measurement using a frequency response analyser is seen in Figure 2.18. A sinusoidal excitation signal is generated e(t), by the signal generator, and applied to the potentiostat along with a DC bias, E_{DC}. The resultant current, which is in reality is a voltage signal that is fed into a mixer and integrated over a set time, usually several times the period of the test frequency [2]. A longer period of integration will improve the accuracy measurement. The resultant current is also mixed with the input signal 90^0 out of phase and integrated. Results of the test correspond to the real and imaginary impedances of the cell. This process can be repeated over a range of frequencies to obtain a Nyquist or Bode EIS plot. This process, which is also known as the lock in technique is used for high precision measurements on electrochemical sensors [38]. Measuring multiple frequencies using this technique requires additional circuitry and

this method is incapable of measuring harmonic responses of the cell outside the excitation frequency.

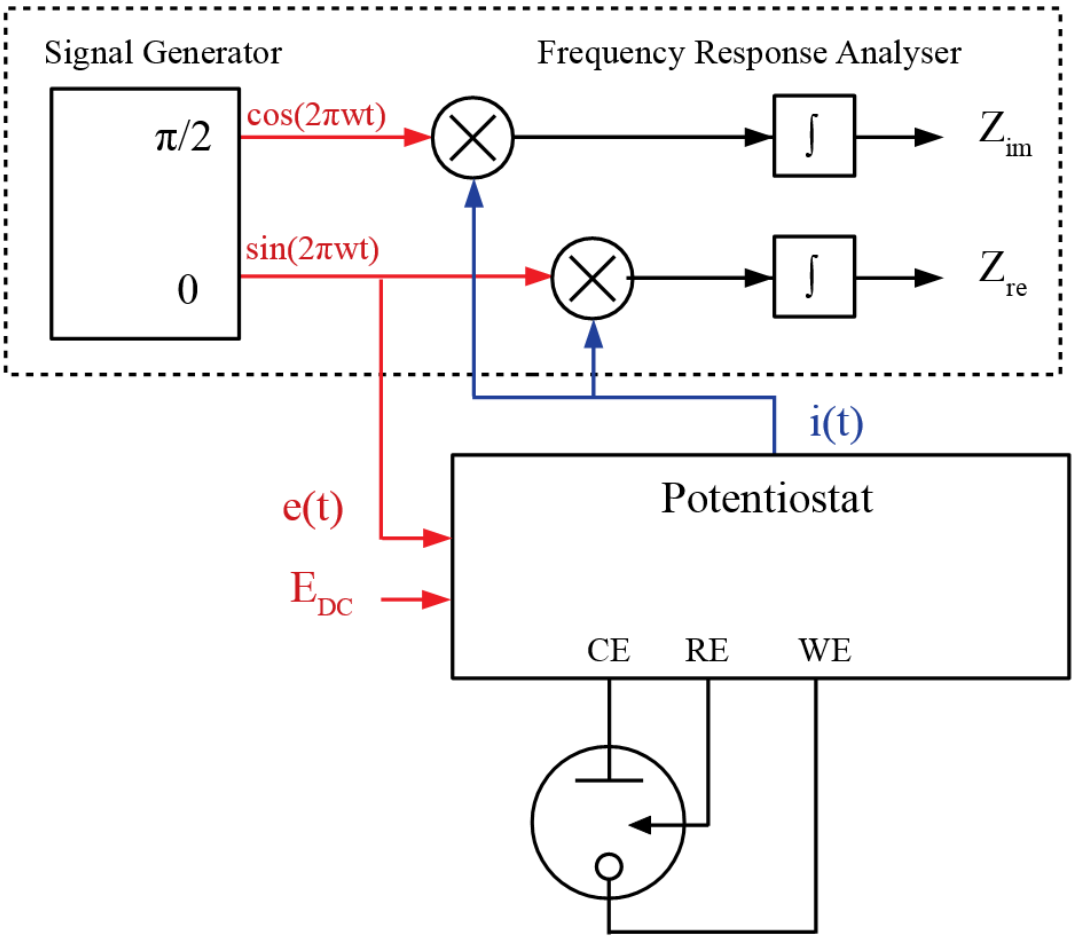


Figure 2.18 Example of system used to measure the impedance of an electrochemical cell based on a frequency response analyser. The red lines in the diagram represent the voltage paths , while the blue represent the resultant current path. The crosses in the diagram represent signal mixers.

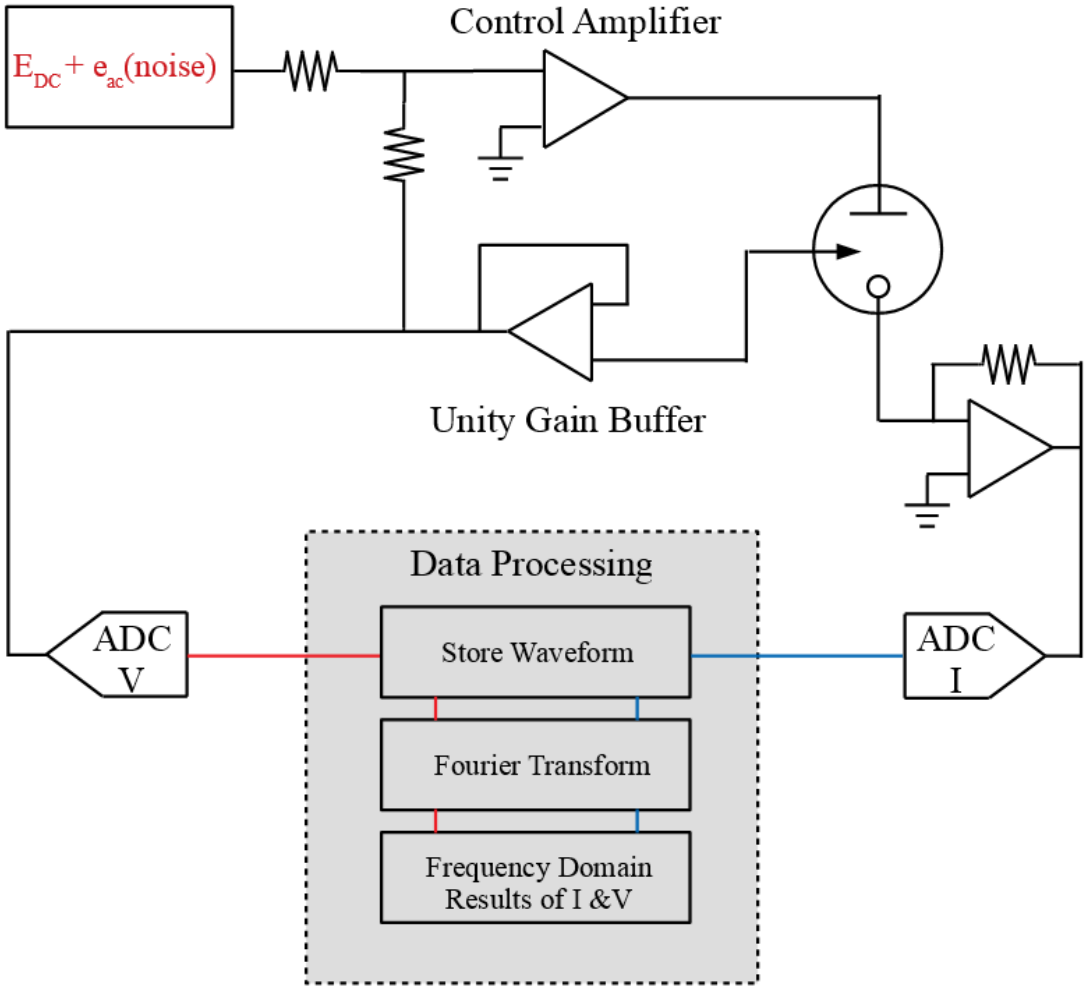


Figure 2.19: Example of typical potentiostatic apparatus, including control amplifier, unity gain buffer and trans-impedance amplifier with ADCs to measure both the applied voltage and resultant current. Also included, are the data processing steps used for Fourier analysis of AC current and voltage.

2.4.4.2 *Time Domain Measurements*

In time domain measurements the potential variation applied is a pulse or white noise signal and the current is recorded with respect to time. Through the use of a conversion method such as a Fourier transform the impedance magnitude and phase spectral responses can be plotted with respect to frequency. This method can allow for several different excitation signals to be applied to the sensor

simultaneously. Measuring multiple frequencies at once can dramatically reduce test time. This is important as electrochemical measurements can be time sensitive due to how quickly surface properties can change on the WE of sensors.

For such measurements, the input voltage and output current are typically measured directly using ADC's. Both the input voltage and output current can be converted to their frequency domain representations through a Fourier transform and the impedance can be calculated.

2.5 Portable Potentiostats

Current laboratory equipment, such as the Autolab PGSTAT302N potentiostat [7] shown in Figure 2.20, can work across a large range of applications but are expensive, difficult to use, require skilled operators and don't readily support in field testing. To support in field testing, portable potentiostats are becoming more application specific. They generally sacrifice the versatility of laboratory equipment to simplify the device and reduce both form factor and cost. Portable potentiostats can fall under the following categories:

- Ultra small instruments, intended to be in vivo or wearable [39].
- Multiplexed instruments, intended to interface to arrays of sensors or electrodes [40].
- Low cost instruments, intended to lower the barrier of entry for a sensor to be used at the point of sample [41].

The aim of this thesis is to enable the use of ultramicro scale electrochemical sensors at the point of sample through low cost portable devices. Each device will either

interface via an impedimetric test or by voltammetry to a single or dual WE electrochemical sensor.

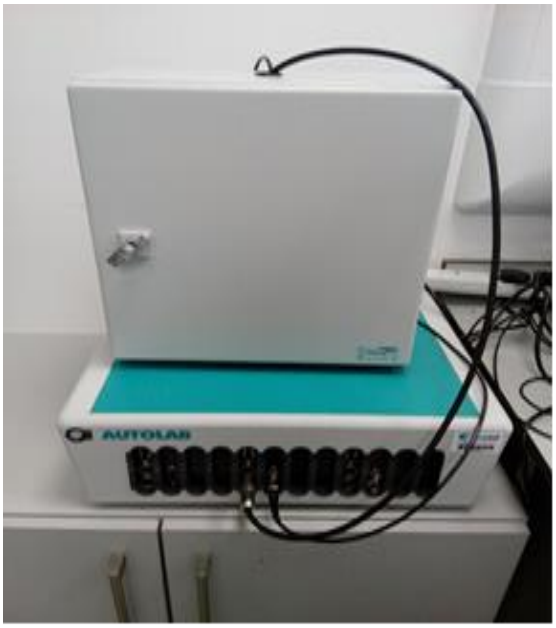


Figure 2.20: Laboratory based benchtop potentiostat, the Autolab PGSTAT302N and a Faraday cage.

2.5.1 Trends in Portable Potentiostats & Current State of the Art

In the recent years, there has been a trend for handheld commercial potentiostats to move away from laptop interfaces and include Bluetooth capability in order to be interfaced to via smartphone [42]. This can negate the need for a laptop, which is less suitable for in field use. It can also reduce the bill of materials cost for the potentiostat as an LCD or touchscreen is no longer required. In future years the potentiostats will become less and expensive and of smaller form factor with more devices such as the Sensit Smart on the market.

Potentiostat manufacturers are beginning to develop cost effective means of interfacing to electrochemical sensors at the point of sample. These portable

potentiostats have limited specifications compared to other commercial interfaces, but are significantly smaller, less expensive and easier to configure. An example of such a device is the Sensit Smart, which is useful for emerging sensors that don't require a large voltammogram range or high resolution. It is a cost effective means of attempting field measurements while the sensor is early in its development cycle. It uses a smartphone as its power source and interface, this may be the trend other portable potentiostat manufacturers take in the future.

Two tables comparing commercial, open source and research grade potentiostats made in the last decade that are suitable for field measurements are given in Table 2.1 and Table 2.2 below. This highlights the recent trends in portable electrochemical sensing.

2.5.1.1 *Voltammetric Potentiostats*

Voltammetry is the most popular branch of electrochemical tests and as a result there are a multitude of low cost research and open source potentiostats in recent literature [43], [44], [45]. Nano electrochemical sensors are currently not available off the shelf due to their emerging nature. This is reflected in many of the open source potentiostats such as the Ministat [46] and UWED [47], which do not have the current sensing ability to read output currents in the nA range. Some of the commercial and open source portable potentiostats have measurement ranges suitable to interface to ultramicro and nano electrochemical sensors such as the Dstat [48] and EmStat 3 [49], but lack the capability to interface to dual WE sensors. This work will address the gap both in the literature and commercial world, and introduce the first low cost instrument that can interface to ultramicro and nano scale dual electrode sensors.

2.5.1.2 *Impedimetric Potentiostats*

Impedimetric immunosensors in the ultramicro to nano scale require a large impedance measurement range of up to 1 GΩ due to their feature size. They also require frequency measurements from 1 kHz to the sub Hz range, which will be discussed further in Chapter 5. Commercial portable potentiostats such as the Palm Sens 4 [50] and Interface 1010B [51] are capable of interfacing to such sensors but are at too high a price point to be viable for use as a mass produced handheld reader for a many emerging immunosensors, particularly in the agriculture industry. An application in the literature of similar specifications to the immunosensors were EIS measurements for corrosive monitoring, as seen in Grassini [52]. These measurements required larger amplitude input voltages than were suitable for the immunosensors used in this thesis. This thesis contributes to the state of the art through presenting a low cost portable instrument that has the capability of interfacing to ultramicro to nano scale impedimetric immunosensors.

Table 2.1: Comparison of portable voltammetric potentiostats.

System	Voltage Range (V)	Measurement Range	Bipotentiostat?	Size(mm)	User Interface	Development Stage	Cost	Year
Pruna et al. [43]	±2.5	-	No	120x70	PC	Research	$300	2018
Huang et al. [53]	±2	200nA - 20mA	No	45x5	PC/USB	Research	-	2017
Baranwal et al. [45]	±1.5	Up to 10µA	No	-	Touchscreen	Open Source	$48.28	2021
MiniStat [46]	±1.2	±100µA	No	27x20	App/Bluetooth	Open Source	$80	2019
Cheapstat [54]	±0.99	100nA – 50µA	No	140x66	PC/USB	Open Source	<$80	2011
Dstat [48]	±1.5	600fA (min limit)	No	92x84	PC/USB	Open Source	$120	2015
UWED [47]	±1.5	±180 µA	No	51x34	App/Bluetooth	Open Source	$61.50*.	2018
Dobbelaere et al. [55]	±8	2uA – 20mA	No	-	PC/USB	Open Source	<$100	2017
Sun et al. [69]	±8	1nA – 200µA	No	39x15.5	Smartphone Module	Open Source	-	2017
Sensit Smart [42]	-1.7 to 2	100nA – 5mA	No	43x25	App/Bluetooth	Commercial	$1250	2019
Interface 1010B [51]	±12	10nA-1A	No	270x240	PC/USB	Commercial	$7600	-
910 PSTAT mini [56]	±2.048	10nA-100uA	Yes	80x54	PC/USB	Commercial	-	2012
Em Stat3 [49]	±5	1nA-10mA	No	67x50	PC/USB	Commercial	$1850	-
PalmSens 4 [50]	±10	100 pA - 10 mA	Yes	157x97	App/Bluetooth	Commercial	$4300	2019
1200C [57]	±5	1nA-10mA	Yes	178x114	PC	Commercial	$3000	-
PocketStat 2 [58]	±10	100pAto10 mA	No	160x67	PC/USB	Commercial	$4300	2019

Table 2.2: Comparison of portable impedimetric potentiostats.

System	Frequency Range	Measurement Range	Phase Accuracy	Magnitude Accuracy	Size(mm)	User Interface	Development Stage	Cost	Year
Grassini et al. [52]	0.01Hz-100kHz	100Ω-10GΩ	3^0	5%	102x53	PC/USB*	Research	160$	2018
H Jiang et al. [59]	17Hz-17kHz	10 Ω -10kΩ	0.30^0	0.50%	81x66	App/Audio-jack	Research	-	2016
Huang et al. [44]	1Hz-10kHz	-	0.1^0-1.2^0	1.2% - 9.8%	-	PC/USB	Research	~30$	2011
J. Jiang et al. [60]	2kHz-100kHz	~1 Ω -10kΩ	-	-	67x53	App/Bluetooth	Research	-	2014
P-Villagrasa et al [61]	10Hz-100kHz	100 Ω -100kΩ	12.1^0 (max)	12.3% (max)	-	Remote control	Research	-	2014
Adabbo et al [62]	1kHz-2.2MHz	~1 Ω -10kΩ	3^0	2%	-	PC/Serial	Research	-	2019
Harder et al. [63]	3kHz-150kHz	-(~1kΩ)	5^0	1	-	App/Bluetooth	Research	-	2016
Zhang et al [64]	20kHz	~100kΩ -1MΩ	5^0	<2	-	App/Bluetooth	Research	-	2015
Chuang et al. [65]	1Hz-100kHz	~~200kΩ-2MΩ	NA	3.47	-	PC/USB	Research	-	2016
Lentka [66]	0.1Hz-100kHz	1Ω -10MΩ	1^0	1.5	-	PC/USB	Research	-	2017
Pruna et al. [43]	0.1Hz-10kHz	~1Ω -20kΩ	-	-	120x70	PC/UART	Research	300$	2018
Tsai et al. [67]	11kHz-101kHz	1Ω-10kΩ	0.74^0-4.96^0	3.21%-10.61%	160x170	Touchscreen	Research	-	2014
Sensit Smart [42]	0.016Hz-200kHz	10Ω-100MΩ,	-	-	18x30	App/Bluetooth	Commercial	1250$	2019
Interface 1010B [51]	10uHz - 20kHz	<1mΩ >1GΩ	1^0	1%	270x240	PC	Commercial	7600$	2017
µStat-i 400 [68]	1mHz - 1MHz	-	-	-	100x132	Bluetooth/PC	Commercial	-	-
PalmSens 4 [50]	10uHz - 1MHz	<1Ω >1GΩ	1^0	1%	157x97	App/Bluetooth	Commercial	4300$	2019
PocketStat 2 [58]	10uHz - 1MHz	-	-	-	160x67	PC/USB	Commercial	4300$	2019

2.6 References

[1] C. G. Zoski, Handbook of Electrochemistry, Amsterdam: Elsevier, 2007.

[2] A. J. Baird and L. R. Faulkner, Electrochemical Methods - Fundamentals and Applications, New York: John Wiley & sons, 2001.

[3] R. W. Ramette, "Outmoded terminology: The normal hydrogen electrode," *Journal of Chemical Education*, vol. 64, no. 10, p. 885, 1987.

[4] R.G. Bates et al., "Standard potential of the silver-silver chloride electrode," *Pure Appl. Chem*, vol. 11, no. 12, p. Pure Appl. Chem, 1976.

[5] B.K.K Kassem et al., "Platinum as a Reference Electrode in Electrochemical Measurements," *Platinum Metals Review*, vol. 52, no. 2, pp. 100-106, 2008.

[6] C. Duarte-Guevara et al., "On-chip metal/polypyrrole quasi-reference electrodes for robust ISFET operation," *Analyst*, vol. 140, pp. 3630-3641, 2015.

[7] Metrohm, "PGSTAT302N," Herisau, https://www.metrohm.com/en/products/electrochemistry/autolab-modular-line/PGSTAT302N (Assessed December 2021).

[8] D.A. Skoog et al., Principles of Instrumental Analysis, Harcourt Brace College Publishers, 1997.

[9] K. Hanley et al., "Current readout circuit for point-of-care infectious disease diagnostics in animal health," in *NORCAS*, Talinn, 2018.

[10] M. Pelgrom, Analog-to-Digital Conversion, Helmond: Springer, 2017.

[11] J. E. B. Randles, "Kinetics of rapid electrode reactions," *Discussions of the*

Faraday Society, vol. 1, pp. 11-19, 1947.

[12] Z. Wang et al., "Equivalent Impedance Models for Electrochemical Nanosensor-Based Integrated System Design," *Sensors,* vol. 21, no. 9, p. 3259, 2021.

[13] R. R. N Sekar, "Electrochemical impedance spectroscopy for microbial fuel cell characterization," *J. Microb. Biochem,* vol. 6, no. 2, 2013.

[14] A. Wahl et al., "Electroanalysis at Ultramicro and Nanoscale Electrodes:," *Journal of The Electrochemical Society,* vol. 61, no. 2, pp. 3055-3060, 2014.

[15] D. W. M. Arrigan, "Nanoelectrodes, nanoelectrode arrays and their applications," *Analyst,* pp. 1157-1165, 2004.

[16] K. Aoki, "Theory of ultramicroelectrodes," *Electroanalysis,* vol. 5, no. 8, pp. 627-639, 1993.

[17] P. Kissinger, Laboratory Techniques in Electroanalytical Chemistry, Second Edition, Revised and Expanded, Taylor & Francais, 1996.

[18] L. Ramaleu, "Theory of square wave voltammetry," *Analytical Chemistry,* vol. 41, no. 11, pp. 1362-1365, 1969.

[19] E.O. Barnes et al., "Generator-collector double electrode systems: A review," *The Royal Society of Chemistry,* vol. 137, no. 5, pp. 1068-1081, 2012.

[20] A. Feldman et al., "Radial transport times at rotating ring-disk electrodes. Limitations on the detection of electrode intermediates undergoing homogeneous chemical reacti," *Journal of Electroanalytical Chemistry (1959),* vol. 9, no. 5-6, pp. 395-399, 1959.

[21] F. Zhu et al., "Double electrode systems with microelectrode arrays for electrochemical measurements," *Reviews in Analytical Chemistry,* vol. 34, no.

3-4, 2015.

[22] T.A. Postlethwaite et al., “Interdigitated Array Electrode as an Alternative to the Rotated Ring−Disk Electrode for Determination of the Reaction Products of Dioxygen Reduction,” *Analytical Chemistry,* vol. 68, no. 17, p. 2951–2958, 1996.

[23] K. Ueno et al., “Fabrication and electrochemical characterization of interdigitated nanoelectrode arrays,” *Electrochemistry Communications,* vol. 7, no. 2, pp. 161-165, 2005.

[24] J. Mason et al., “A Redox-Enzyme-Based Electrochemical Biosensor with a CMOS Integrated Bipotentiostat,” in *IEEE Biomedical Circuits and Systems (BIOCAS)*, Beijing, China, 2009.

[25] J. R. M. Evgenij Barsoukov, Impedance Spectroscopy: Theory Experiment and Applications, Wiley, 2005.

[26] G. D. Davis, C. M. Dacres and L. Krebs, “EIS-Based In-Situ Sensor for the Early Detection of Coatings Degradation and Substrate Corrosion,” in *Corrosion,* Orlando, 2000.

[27] M. Crescentini et al., “Online EIS and Diagnostics on Lithium-Ion Batteries by Means of Low-Power Integrated Sensing and Parametric Modeling,” *IEEE Transactions on Instrumentation and Measurement,* vol. 70, pp. 1-11, 2020.

[28] G. Wiezell et al., “Steady-state and EIS investigations of hydrogen electrodes and membranes in polymer electrolyte fuel cells: I. Modeling,” *Journal of the Electrochemical Society,* vol. 153, no. 4, p. A749, 2006.

[29] A. Mahdavian et al., “Another approach in analysis of paint coatings with EIS measurement: phase angle at high frequencies.,” *Corrosion Science* , vol. 48,

no. 12, pp. 4152-4157, 2006.

[30] I. Prodromidis et al., “Impedimetric immunosensors—A review,” *Electrochimica Acta,* vol. 55, no. 14, pp. 4227-4233, 2010.

[31] M. K. Sezgintürk et al., “A review on impedimetric biosensors,” *Artificial Cells, Nanomedicine, and Biotechnology,* vol. 44, no. 1, pp. 248-262, 2014.

[32] J. Leva-Bueno et al., “A review on impedimetric immunosensors for pathogen and biomarker detection,” *Medical Microbiology and Immunology,* no. 209, p. 343–362, 2020.

[33] J. Tang et al., “Amplified impedimetric immunosensor based on instant catalyst for sensitive determination of ochratoxin A,” *Biosensors and Bioelectronics,* vol. 89, pp. 386-392, 2016.

[34] G. Yang et al., “Development of an impedimetric immunosensor for the determination of 3-amino-2-oxazolidone residue in food samples,” *Analytica Chimica Acta,* vol. 706, no. 1, pp. 120-127, 2011.

[35] E. Valera et al., “Impedimetric immunosensor for atrazine detection using interdigitated μ-electrodes (IDμE's),” *Sensors and Actuators B: Chemical,* vol. 125, no. 2, pp. 526-537, 2007.

[36] A. Lasia, Electrochemical impedance spectroscopy and its applications. In: Modern Aspects of Electrochemistry no.32, Kluwer Academic/Plenum, 1999.

[37] S. C. D. Roy, “Impedance Measurement by a Resistive Bridge,” *IEEE Transactions on Education,* vol. 10, pp. 50-51, 1967.

[38] K. Kishore and S. A. Akbar, “Evolution of Lock-In Amplifier as Portable Sensor Interface Platform: A Review,” *IEEE Sensors,* vol. 20, no. 18, pp. 10345 - 10354, 2020.

[39] R.D. Beach, “Sub et al.miniature implantable potentiostat and modified commercial telemetry device for remote glucose monitoring,” *IEEE Transactions on Instrumentation and Measurement,* vol. 48, no. 6, pp. 1239 - 1245, 1999.

[40] Yaoxing Hu et al., “A portable multi-channel potentiostat for real-time amperometric measurement of multi-electrode sensor arrays,” in *International Symposium on Circuits and Systems (ISCAS)*, Montreal, QC, Canada, 2016.

[41] A.F. Diaz Cruz et al., “A low-cost miniaturized potentiostat for point-of-care diagnosis,” *Biosensors and Bioelectronics,* vol. 62, pp. 249-254, 2014.

[42] PalmSens, Sensit/SMART, potentiostat for smartphone and tablet, Accessible(https://www.palmsens.com/wp-content/uploads/2020/04/Sensit-Smart-description-1.pdf), Houten, 2021.

[43] R. Pruna et al., “A low-cost and miniaturized potentiostat for sensing of biomolecular species such as TNF-α by electrochemical impedance spectroscopy,” *Biosensors and Bioelectronics,* vol. 100, no. 15, pp. 533-540, 2018.

[44] X. Huang et al., “A fast and simple electrochemical impedance spectroscopy measurement technique and its application in portable, low-cost instrument for impedimetric biosensing,” *Journal of Electroanalytical Chemistry*, vol. 657, no. 1-2, pp. 158-163, 2011.

[45] A.R. Baranwal et al., “Development of Completely Automated Poly Potential Portable Potentiostat,” *ECS Journal of Solid State Science and Technology,* 2021.

[46] S.D. Adams et al., “MiniStat: Development and Evaluation of a Mini-

Potentiostat for Electrochemical Measurements," *IEEE Access,* vol. 7, pp. 31903-31912, 2019.

[47] A. Ainla et al., "Open-source potentiostat for wireless electrochemical detection with smartphones," *Analytical Chemistry,* vol. 90, no. 10, pp. 6240-6246, 2018.

[48] D.M. Dryden and A.R. Wheeler, "DStat: A versatile, open-source potentiostat for electroanalysis and integration" *PloS one,* vol. 10, no. 10, 2015.

[49] PalmSens, EmStat 3 and 3+ potentiostats, Accessible (https://www.palmsens.com/wp-content/uploads/2020/04/EmStat-series-description.pdf), Houten, 2018.

[50] PalmSens, "PalmSens4 Potentiostat/Galvanostat/Impedance Analyzer Rev 1", Accessible (https://www.palmsens.com/wp-content/uploads/2020/07/PalmSens4-description.pdf), Houten, 2021.

[51] Garmy Instruments, Interface 1010 Potentiostat/Galvanostat/Zero Resistance Ammeter, Accessible (https://www.gamry.com/assets/Uploads/Interface-1010-Brochure-2020.pdf), Philadelphia, 2019.

[52] S. Grassini et al., "A simple Arduino-based EIS system for in situ corrosion monitoring of metallic works of art," *Measurement,* vol. 114, pp. 508-514, 2018.

[53] Chun-Yueh Huang et al., "Design of a Portable Mini Potentiostat for Electrochemical Biosensors," in *IEEE Electronic and Automation Control Conference (IAEAC),* Chongqing, 2017.

[54] A.A. Rowe et al., "CheapStat: an open-source,"Do-It-Yourself" potentiostat for analytical and educational applications," *PloS one,* vol. 6, no. 9, 2011.

[55] T. Dobbelaere et al., "A USB-controlled potentiostat/galvanostat for thin-film

battery characterization," *Hardware X*, vol. 2, pp. 34-39, 2017.

[56] Metrohm, 910 PSTAT mini, Herisau, Accessed 2021 (https://www.metrohm.com/en/products-overview/electrochemistry/portable%20potentiostats/29100010).

[57] CH Instruments, Inc, Model 1200C Series Handheld Potentiostat/Bipotentiostat, Austin, Acessed 2021 (https://www.chinstruments.com/chi1200.shtml).

[58] Ivium Technologies, pocketSTAT2, Acessible (https://www.ivium.com/wp-content/uploads/2019/09/pocketstat2MCFcell.pdf), Eindhoven, 2019.

[59] H. Jiang et al., "An Audio Jack-Based Electrochemical Impedance Spectroscopy Sensor for Point-of-Care Diagnostics," *IEEE Sensors*, vol. 17, no. 3, pp. 589-597, 2017.

[60] J. Jiang et al., "Smartphone based portable bacteria pre-concentrating microfluidic sensor and impedance sensing system," *Sensors and Actuators B: Chemical*, vol. 193, no. 31, pp. 653-659, 2014.

[61] J. Punter-Villagrassa et al., "A portable point-of-use EIS device for in-vivo biomedical applications.," *IEEE Design of Circuits and Integrated Systems*, 2014.

[62] T. Addabbo et al., "On the Suitability of Low-Cost Compact Instrumentation for Blood Impedance Measurements," *IEEE Transations on Instrumentation and Measurement*, vol. 68, no. 7, pp. 2412-2424, 2019.

[63] R. Harder et al., "Smart Multi-Frequency Bioelectrical Impedance Spectrometer for BIA and BIVA Applications," *IEEE Transactions on Biomedical Circuits and Systems*, vol. 10, no. 4, pp. 912-939, 2016.

[64] D. Zhang et al., "Smartphone-based portable biosensing system using

impedance measurement with printed electrodes for 2,4,6-trinitrotoluene (TNT) detection," *Biosensors and Bioelectronics,* vol. 70, no. 15, pp. 81-88, 2015.

[65] C. Chuang et al., "Immunosensor for the ultrasensitive and quantitative detection of bladder cancer in point of care testing," *Biosensors and Bioelectronics,* vol. 84, no. 15, pp. 126-132, 2016.

[66] G. Lentka, "Scalable Measurement System for Multiple Impedance Gas Sensors," *Journal of Metrology Society of India,* vol. 32, no. 3, pp. 223-228, 2017.

[67] S. Tsai et al., "Battery-powered portable instrumentsystem for single-cell trapping, impedancemeasurements, and modeling analyses," *Electrophoresis,* vol. 35, pp. 2392-2400, 2014.

[68] Metrohm, μStat-i 400 Bipotentiostat/Galvanostat/Impedance Analyzer (EIS), Philadelphia, Accessed 2021 (https://www.metrohm.com/en/products-overview/electrochemistry/portable%20potentiostats/STAT-I-400).

[69] Sun, A., Venkatesh, A.G. and Hall, D.A., 2016. A multi-technique reconfigurable electrochemical biosensor: Enabling personal health monitoring in mobile devices. IEEE transactions on biomedical circuits and systems, 10(5), pp.945-954.

Chapter 3 Voltammetric Proof of Concept using ADuCM350 System on Chip

3.1 Introduction

At present, the majority of electrochemical sensing applications require a laboratory environment to perform a diagnosis. This means of diagnostics is expensive and requires a long turn around time. Today, a sample is typically taken at the source be that a clinical setting for medical diagnostics, river for environmental monitoring and then shipped to the appropriate lab. This can jeopardise the integrity of the sample unless it is preserved in a known, stable and contained environment. During a lab diagnosis process, the sample may have to go through a number of treatment steps, many of which must be carried out highly skilled personnel. To reduce costs, these tests are sometimes pooled, meaning further delays to identify which individual samples are positive [1]. Once a result is obtained by the laboratory, it must be communicated efficiently, securely and appropriately back to the client. This is particularly important where the specific test being undertaken is a clinical test impacting an individual's health. These processes typically can take at least three working days. However, in addition to the sample capture, secure transport and actual test, there is a significant management overhead in relation to the tracking and management of individual samples to ensure that they are tested within an appropriate timeframe [2]. If there is any unforeseen delay, it can result in unnecessary stress and the original issue developing such that the test results are no longer relevant.

A suitable means of addressing this problem is through the development of an inexpensive portable device that can interface to electrochemical sensors at the point of sample. This chapter describes a proof of concept of a portable

electrochemical interface system that could interface to electrochemical sensors with form factors at or below 1μm, using the Tyndall ultramicro band and nanowire sensors as an example. It details the motivation behind the initial prototype and its results in comparison with benchtop laboratory equipment. This chapter is based on the paper Advanced Data Acquisition for Emerging Nano Electrochemical Sensors, presented at the IEEE I2MTC conference 2018, Houston [3].

3.2 Tyndall Ultramicro Electrodes and Nanowire Sensors

For the Tyndall nanowire and UME sensors, the CE and WE are fabricated using gold while the pseudo reference electrode is made of platinum. Both gold and platinum were used as they are inert metals that are less prone to unwanted secondary reactions. As seen in Figure 3.1. (a), the CE and RE are placed in parallel and are as close as possible to the WE. This design was used to ensure consistency between results at each electrode by ensuring each WE is at an equal distance from CE and RE. For the Tyndall sensors fabrication process [4] [5] [6], the width of the gold UMEs are 1 μm and nanowires are 100 nm. The height of the electrodes are 50 nm. A passivation layer of silicon nitride with a window exposing the working electrodes is used to ensure the solution only interfaces with the WE and doesn't react with the interconnection tracks. The window is typically at an opening of 45 μm and can be seen as the dark area in Figure 3.1 (b). This allows for an active electrode area of 49.5 pm^2 for an ultramicro electrode that's 1 μm wide and 50 nm high. As seen in Figure 3.1 (c), a quantity of the solution under test can be deposited into the sample well, which is aligned over all of the electrodes. The amount of solution required to perform the electrochemical test is small, which is reflected in the 100 μL sample well volume. The constituents of the sensor can be easily interfaced to using a micro Secure Digital (SD) connector PCB.

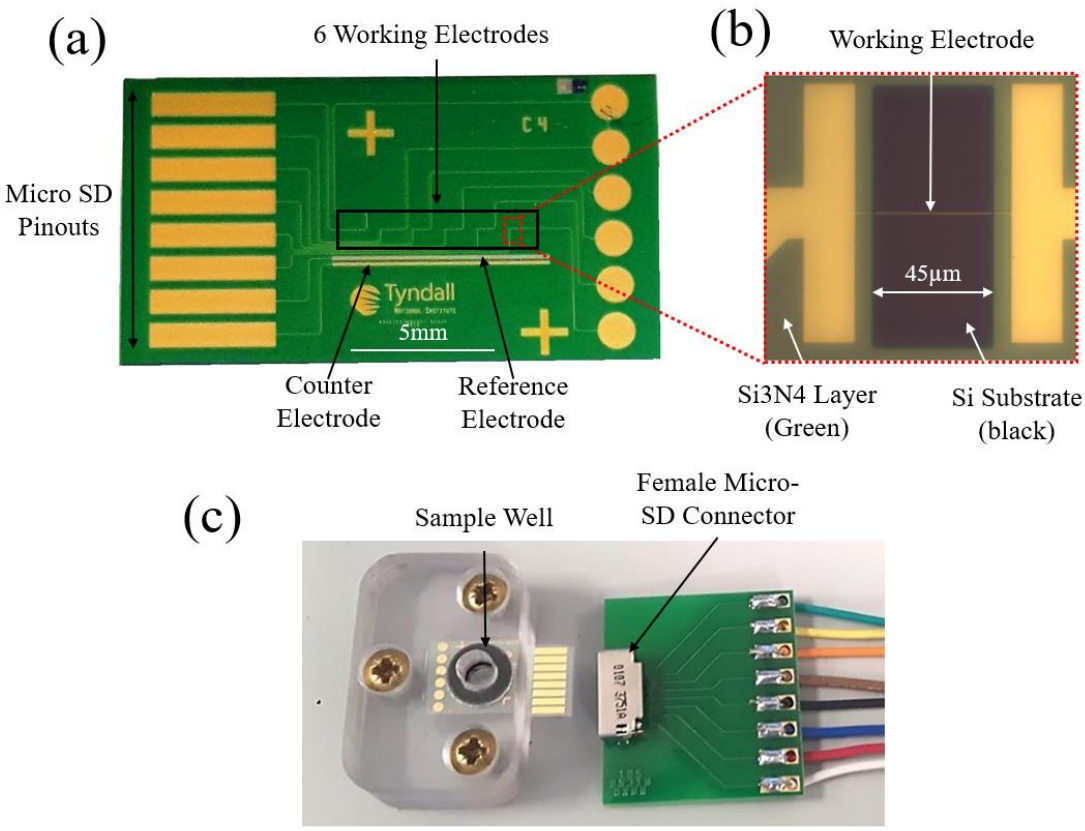


Figure 3.1: (a) Tyndall ultramicro sensor chip, (b) Optical micrograph of ultramicro electrode, (c) Chip holder and micro SD connector.

3.2.1 Voltammetric Scans Performed on Sensor

The voltammetric scans performed on the Tyndall ultramicroband sensors are CV and SWV. In order to characterise the sensors, CVs are performed using ferrocene monocarboxylic acid (FcCOOH). FcCOOH is a suitable compound as it's routinely used to characterise electrochemical sensors due to its easily reversible redox reaction [7]. A laboratory grade table top potentiostat such as the Autolab PGSTAT302N is used to perform the necessary tests on the sensor. For FcCOOH characterisation, the voltammetric test is typically swept from -0.2 V to 0.6 V at a scan rate of 100mV/s. An example of the resultant current outputs from the microband sensors, using a laboratory potentiostat can be seen in Figure 3.2.

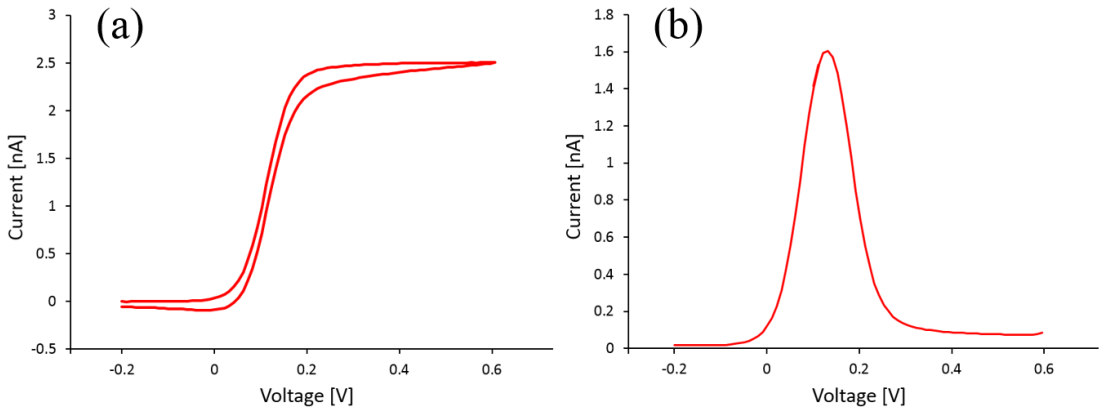


Figure 3.2: Electrochemical tests performed on 1um ultramicro band sensor using 1mM FCOOH using laboratory potentiostat Autolab PGSTAT302N; (a) CV at 100mV/s, (b) SWV at 10Hz, swept at 100mV/s.

3.2.2 System Requirements

To enable in-field deployment of electrochemical sensors, a portable data acquisition system platform needs to be developed that has comparable accuracy to dedicated laboratory based instrumentation. It must also have the required robustness to support different interrogation methods and at the same time, withstand the physical challenges of deployment to the field, for use by unskilled operators. Table 3.1 describes the minimum requirements that need to be met in order to have a viable point of care solution for electrochemical sensors.

Using the Tyndall developed nanowire sensors as a lead example, a requirements table has been derived for this data acquisition system. As presented in Table 3.2, an inexpensive portable system is required that could quickly perform electrochemical tests with similar accuracy to a laboratory potentiostat.

Table 3.1: Requirements of point of care system in order to be fit for purpose.

Parameter	Requirement
Portability	Must be capable of operating at the point of care
Cost	Suitable price point for deployment as a portable field solution.
Speed	Tests carried out in the field must be within a convenient timeframe to the end user.
Sensitivity	Similar results to a lab based potentiostat for UMEs would be ideal, if device returns results that have a linear relationship to concentration, it would still be fit for purpose.

Table 3.2: Requirements of point of care data acquisition system.

Parameter	Requirement
Portability	Handheld Device
Cost	100-500$
Speed	<1min
Sensitivity	Minimum 50pA resolution
Required Tests	Cyclic Voltammetery, Square Wave Voltammetry

Depending on the dimensions of the electrode, the peak current of a CV can vary from 1 nA to 3 nA for the standard 1 mM FcCOOH concentration. A minimum resolution of 50 pA is proposed as a suitable level of precision based off the minimum current output of the ultramicro band sensors. Due to the low current magnitudes being measured and sensor iterations that will require a larger current measurement window, a high resolution ADC is required in the region of 16bits.

As mentioned previously, the standard voltammogram requires a -0.2 V to 0.6 V potential to be applied at the WE-solution interface. A suitable incremental voltage step of the ramp was 10 mV [4]. Therefore the DAC required to provide the

necessary control signal does not need to be of a high order resolution or output voltage range.

Although the final aim of the system is to be encapsulated as a handheld device, the intent of the first proof of concept is to ensure that the prototype could interface to the electrochemical sensors with the required degree of accuracy. Therefore, the proposed system will be interfaced with a using a laptop as represented in Figure 3.3. In order to process the ADC data, control the DAC and interface to a suitable device, such as a laptop, a microcontroller is also required in the system.

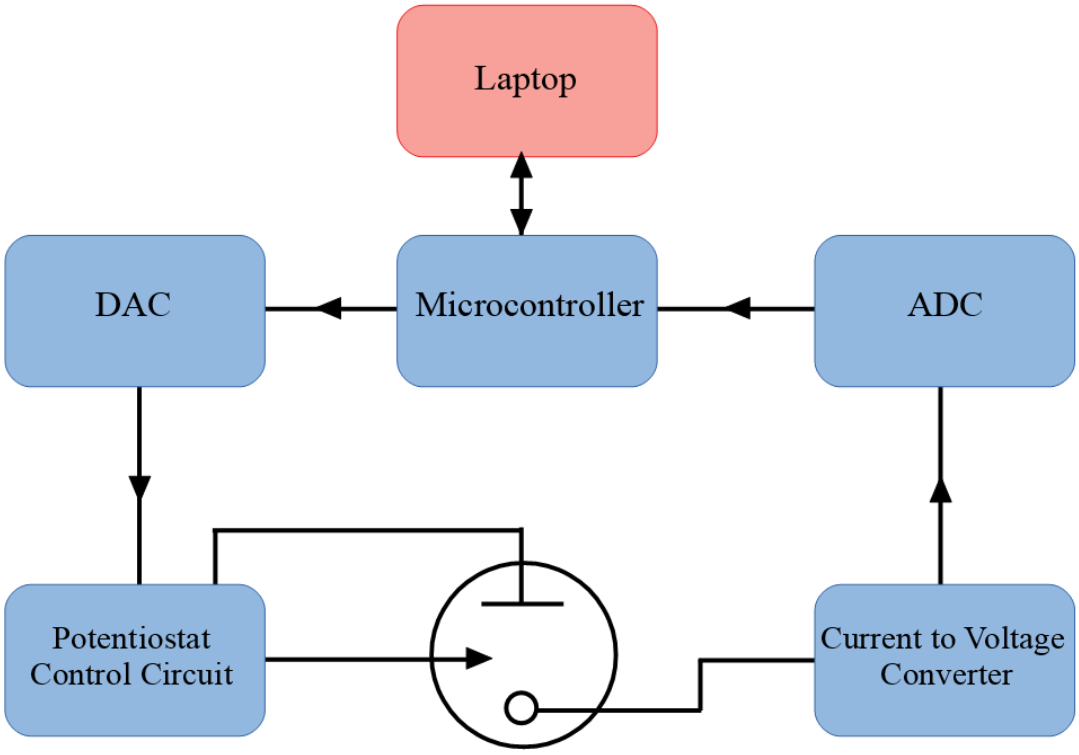


Figure 3.3: Block diagram of proposed system, consisting of a microcontroller for control of the system, DAC to provide an input signal to the potentiostat control circuit, a current to voltage converter and an ADC to read the resultant voltage from the voltammetric test.

3.3 Analog Front End

Commercial potentiostat Analog Front Ends (AFEs) have been designed on Integrated Circuits (ICs) for portable digital electrochemical interfaces such as glucometers in the past decade [8]. In recent years, such components have become available to purchase commercially. Texas Instruments released the LMP91000 in 2011 [9] and Analog Devices released the ADuCM350 in 2014 [10]. Both these products included the potentiostatic control circuitry, current to voltage converters, ADCs and DACs necessary to interface to commercial electrochemical sensors. The supply voltage of each of the chips are of a suitable range to allow for battery powered operation. These products offer a viable alternative to creating portable custom potentiostats using a multitude of discrete components. Both devices had the potential of being capable to interface to ultramicro band sensors, without the need for excessive external components. As a result, this work utilised this technology for the design of the point of care device as it could be manufactured at a fraction of the cost and size.



Figure 3.4: Roche Accu-Chek, which utilises the ADuCM350.

Although the ADuCM350 is more expensive than the LMP91000, it has more functionality which was applicable to the ultramicro band sensor application. It has a built in switch matrix, that enables the device to interface to six working electrodes which is suited to the configuration of the ultramicro band SD sensors. Another advantage is that it has a built in ARM Microprocessor. Both the microprocessor and switch matrix are essential constituents of the final in field solution. Therefore, using the ADuCM350 requires less external components and PCB footprint is required for the final solution. This ultimately will enable a lower cost solution with higher reliability resulting from the reduced number of components. Example code is also provided for the operation of the chip which promotes a faster prototyping process.

Table 3.3: Comparison Table for Prospective AFEs.

Parameter	**ADuCM350**	**LMP9100**
Potentiostatic control circuit	Yes	Yes
Cost	5.23$	3.27$
Supply Voltage	2.5 V -3 .6 V	2.7 V - 5.25 V
Microcontroller	Yes	No
Multiplexer	Yes	No

3.3.1 Voltammetric Measurement using the ADuCM350

3.3.1.1*AFE Current Path*

As seen in Figure 3.5, for voltammetric measurements with the ADuCM350, the current flows through the D and T nodes via the electrochemical sensor. The current path is created by buffering and conditioning the stimulus voltage to the

counter electrode, via the D node, while the maintaining the working electrode at a fixed common mode of 1.1 V through the T node. The resultant current is converted to a voltage using the resistor for the TIA, (RTIA) on the feedback path of the trans impedance amplifier. The resultant voltage seen at the ADC can be represented by:

$$V_{ADC} = I_{Tnode}\, x\, R_{TIA}. \tag{3.1}$$

Where V_{ADC} is the voltage seen at the ADC and I_{Tnode} is the current observed at node T, or the current produced by the electrochemical reaction.

3.3.1.1*AFE Voltage Feedback Path*

Potentials can be probed differentially through the use of the P and N nodes. The P and N nodes voltages are used as feedback for control of the DAC output. uffer amplifiers are utilised to provide high impedance paths to ensure a negligible amount of current flows through the nodes. This helps to ensure that the RE doesn't get polarised and that the reaction current only flows through the D and T nodes. As seen in Figure 3.5, the ADuCM350 is used to perform a three wire configuration electrochemical measurement by joining the N node internally with the T node through the switch matrix.

3.3.1.1*ADuCM350 Calibrations and Signal Processing*

For DC measurements, the calibration resistor, RCAL, is used for the generation of an accurate current source to calibrate the ADC and TIA signal paths prior to a voltammetric test. As seen in Figure 3.6, offsets sensed through the use of the calibration resistor are stored in registers. These values are used to calibrate out their associated error after the ADC measurement. Buffers, gain resistors and antialiasing filters are used after the TIA stage to precondition its output voltage to a

more readable signal for the ADC. The function of the antialiasing filter is to remove or reduce high frequency components of the analog signal prior to digitisation.

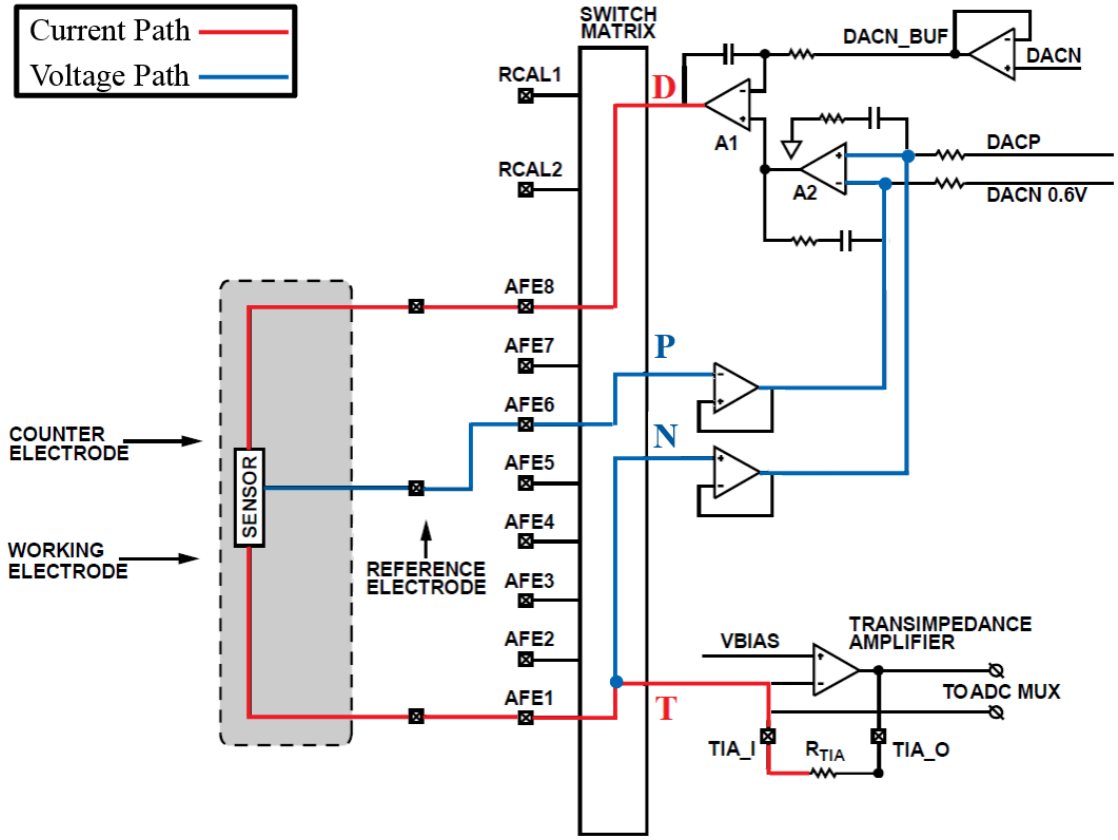


Figure 3.5: ADuCM350 AFE excitation loop for three electrode electrochemical sensor.

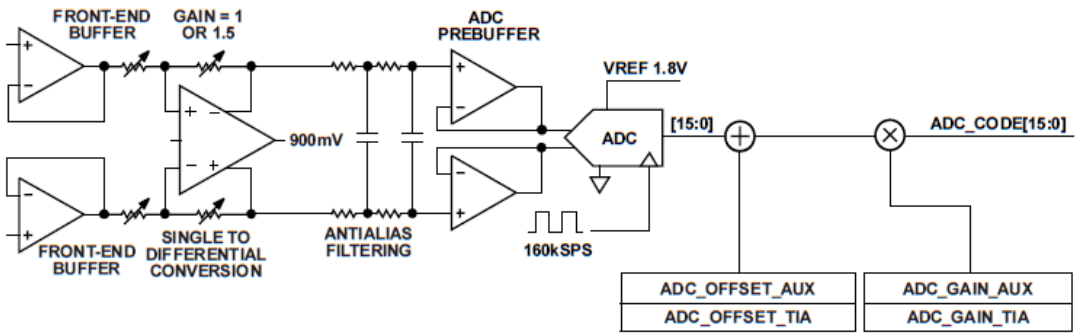


Figure 3.6: Post TIA signal processing for ADuCM350.

3.4 Development of System

In order to achieve a proof of concept with the ADuCM350, its evaluation board, the EVAL- ADuCM350 [11], is used initially as shown in Figure 3.8. A J-link connector enables emulation via serial wire and also supports UART communication with the ADuCM350. A breakout board is used to easily change certain external components such as the trans-impedance resistor and calibration resistors.

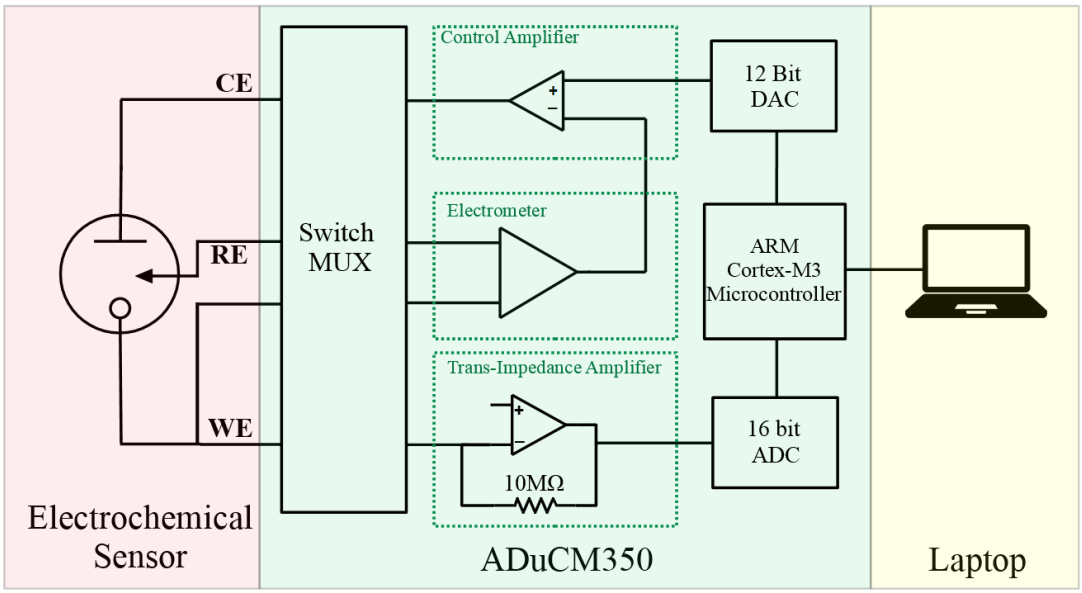


Figure 3.7: Simplified block diagram of ultramicro electrochemical interface proof of concept using ADuCM350 evaluation board.

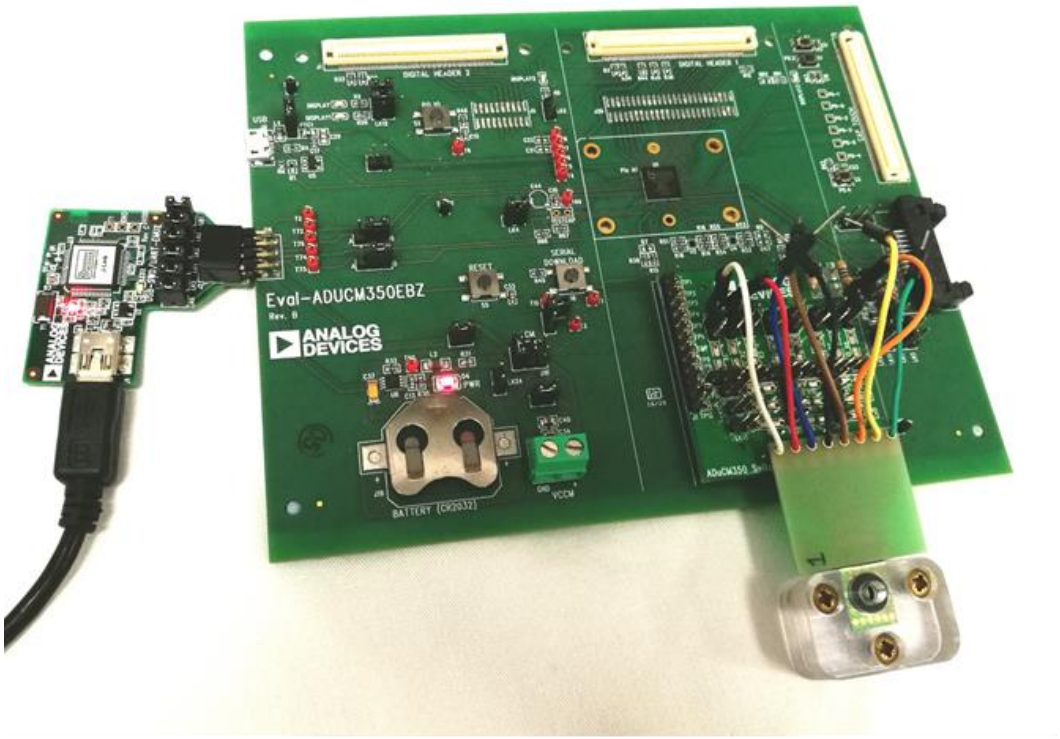


Figure 3.8: System interfacing to electrochemical sensor.

3.4.1 Trans Impedance Amplifier

Although typical ultramicro and nano electrochemical sensors have peak voltammogram values of 1 nA – 3 nA, maximum current reading can reach 60 - 70 nA under certain considerations. This is because of the need for the system to interface to interdigitated ultramicro band sensors which will be discussed in the next chapter. Due to the fact that the ADuCM350 has a relatively high resolution, 16 bit ADC, a single trans impedance resistor is used across all current ranges of the electrochemical sensors interrogated. This saves the need of incorporating a multiplexed array of different RTIA values to enable measurements at different ranges of current values. The ADC input channel is optimised for a ± 0.75 V output from the TIA. Therefore, the sizing of the RTIA is based on this voltage range. For

the TIA in the ADuCM350 the guide sizing of the trans impedance resistor is governed by the following equation:

$$RTIA = \frac{\mathrm{Vout}_{TIA}}{\mathrm{I}_{max}}, \tag{3.2}$$

and

$$RTIA = \frac{750\ \mathrm{mV}}{70\ \mathrm{nA}} = 10.70\ M\Omega. \tag{3.3}$$

where, $\mathrm{Vout_{TIA}}$ is the maximum input voltage swing into the TIA and $\mathrm{I_{max}}$ is the maximum current that the system is required to measure. A 10 MΩ resistor is used as the gain resistor for the trans-impedance amplifier of the ADuCM350. This resistor value is readily available commercially and it allows for a slightly larger current measurement range. The theoretical current resolution of the ADuCM350, not including the effects of noise can be described as:

$$I_{RES} = \frac{V_{ADC}}{N_{bits} A_{ADC} R_{TIA}} \tag{3.4}$$

Hence,

$$I_{RES} = \frac{3.6}{2^{16} x 1.5 x 10^{7}} = 3.64\ pA \tag{3.5}$$

where V_{ADC} is the input voltage range of the ADC and in the case of the ADuCM350 is 3.6 V, $\mathrm{N_{bits}}$ is the number of bits available from the ADC, which in this case is 16 bits and $\mathrm{A_{ADC}}$ is the gain applied to the signal prior to ADC measurement. This resolution is deemed suitable for voltammogram measurements using ultramicro band and nanowire electrochemical sensors. To determine the maximum current range of the system:

$$I_{RANGE} = I_{RES} N_{bits} \tag{3.6}$$

Hence,

$$I_{RANGE} = 3.64x2^{16} = 238\,nA \tag{3.7}$$

Where I_{RANGE} is the maximum current range of the system. Therefore a current range of ± 119 nA can be achieved for the system.

3.4.2 Defining Voltammetric Test Parameters of the System

The ADuCM350 has a common mode of 1.1 V for the WE and a maximum applied voltage of 2.2V but headroom issues are experienced close to its voltage limits. This means that the applied voltammetric range of ± 0.8 V is a more appropriate representation of its limits. A staircase sweep, consisting of voltage steps of 10 mV is used as standard for all voltammetric tests that are performed. The required scan rate of the system is 100 mV/s. This is limited by the DAC settling time which has been found to be a minimum of 37 ms. For a voltage step of 10 mV;

$$Sr_{max} = \frac{\mathrm{V}_{step}}{\mathrm{t}} \tag{3.8}$$

$$Sr_{max} = \frac{10\mathrm{mV}}{0.037\mathrm{s}} = 270.27 mV/s \tag{3.9}$$

Where Sr_{max} is the maximum scan rate, V_{step} is the applied voltage step and *t* is the minimum amount of time the step can be performed in, i.e. the DAC settling time. This means the required scan rate of 100 mV/s can comfortably be achieved.

The maximum applied frequency of the SWVs, F_{max}, is also limited by the DAC settling time;

$$F_{\max} = \frac{1}{T} = \frac{1}{2t}, \tag{3.10}$$

which results in:

$$F_{max} = \frac{1}{2x0.037s} = 13.51\ Hz. \tag{3.11}$$

A 10 Hz measurement is suitable for SWV measurements using the nanowire and ultramicro band electrochemical sensors.

3.4.3 ADuCM350 Offset Calibration

A 1 MΩ RCAL resistor is used for the system to calibrate the ADC and TIA signal paths that were mentioned earlier in section 3.3.1.1. It could be seen that there was still offset in the voltammetric tests despite the ADC calibration performed using RCAL. This noise is mostly due to the switch matrix, which has a typical leakage of up to 0.5 nA when the switches are on, as described in the ADuCM350 datasheet [12]. The error manifests as an offset when using the ADuCM350. In order to counteract this error, an open circuit measurement is performed prior to each voltammetric test and the resultant open circuit current value is calibrated against subsequent measurements.

3.4.4 Programming Tests

Embedded C++ programmes have been developed and configured by the author, using the IAR Embedded Workbench [13]. These scripts enable the electrochemical sensor under test to be appropriately configured and biased for the different modes of operation, specifically for Cyclic Voltammetry and Square Wave

Voltammetry. The rate at which the voltammetric test would sweep through the designated voltage range, the scan rate and the frequency of square wave voltammograms can be configured on the scripts.

3.4.4.1*Data Flow*

The resultant ADC codes are transmitted through Universal Asynchronous Receiver-Transmitter via COM ports and displayed using a serial console called PuTTY [14]. For experiments involving a comparison against benchtop laboratory equipment in this chapter, the ADC codes were converted into their corresponding current values and DC offset was calibrated using a MATLAB script [15]. This data is subsequently graphed using Microsoft Excel [16].



Figure 3.9: Data Flow of System for experimental calibrations vs benchtop potentiostat.

3.4.4.2*LabVIEW Display*

When characterising the nanowire electrochemical sensors, it is useful to display the current output of the voltammogram in real time as any defective electrodes can be identified in the first few seconds of the scan. This ensures that the characterisation effort can be focused on the electrodes that are shown to work. This especially important when characterising novel structures as their reliability is often unknown and may be severely limited. The practice of displaying the results in real time is also commonplace for commercial lab potentiostats. Therefore a real-time LabVIEW [17] display has been created for both prototyping and demonstrative purposes. The program processes the raw ADC codes from the system and converts

them to their corresponding current values, which are subsequently displayed in real time on the laptop. A block diagram of the LabVIEW code can be seen in the Appendix.

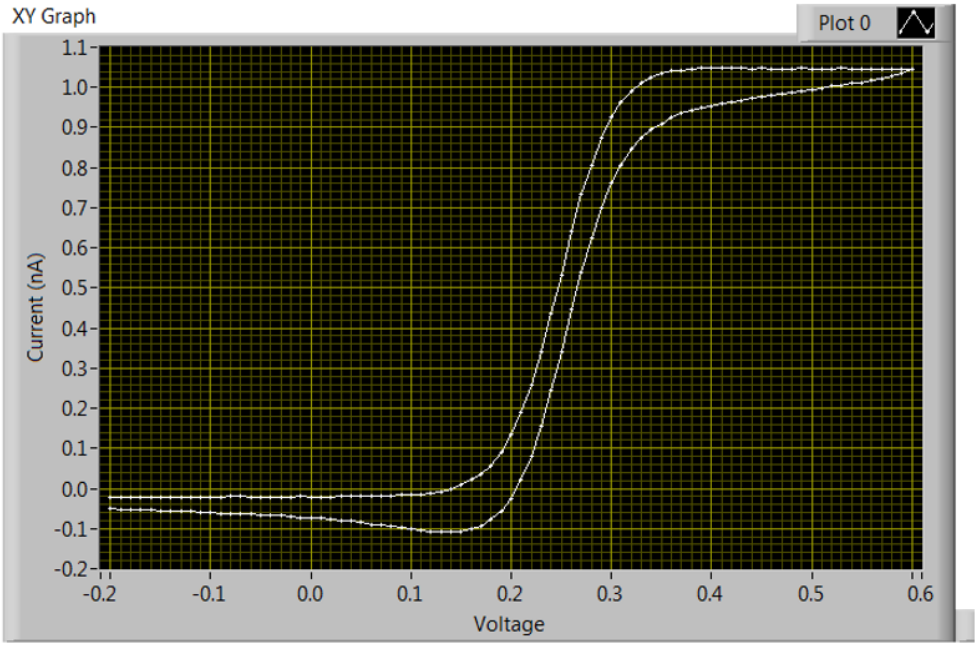


Figure 3.10: Ferrocene scan on ultramicro band electrochemical sensor using the proposed system on LabVIEW display.

3.4.4.3*Multiplexed Working Electrodes*

The system is required to interface to the six working electrodes on the Tyndall electrochemical sensors. The switch matrix built into the ADuCM350 has been utilised to enable the user to interface to all electrodes on the sensor without manually switching wires. This is of particular use as a time efficient means of identifying defective electrodes when characterising the sensor with FcCOOH. This also ensures that any parasitics are consistent from one working electrode to another and also that it's consistent across sensors. As seen in Figure 3.11, WE5 and WE6

did not provide the expected steady state response which showed that the electrodes were damaged.

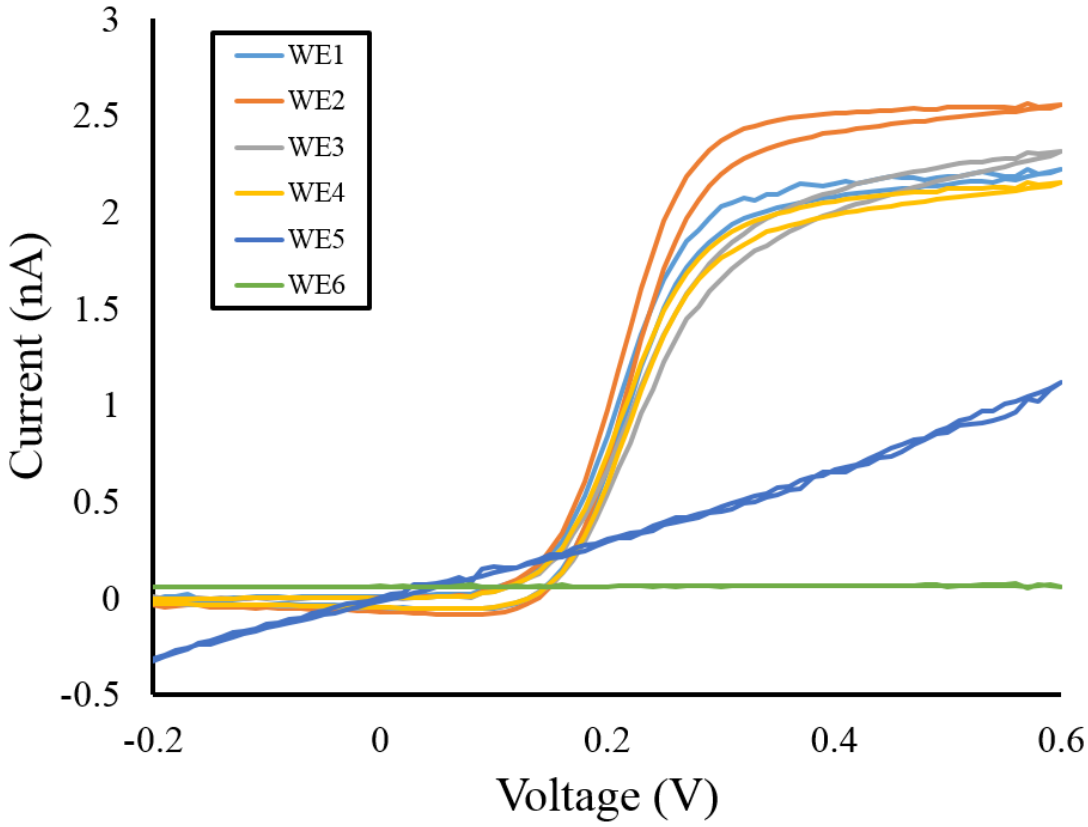


Figure 3.11: Multiplexed output ultramicro band sensor in FcCOOH using proof of concept system, demonstrating that the proposed system can interface to multiple Working Electrodes.

3.4.5 Specifications

The performance of the proof of concept is shown in Table 3.3. It is clear that it had the capability of interfacing to the ultramicro electrochemical sensors within the required specifications through CV and SWV.

Table 3.4: System Specifications for proof of concept system.

Parameter	Requirement
Voltammetric Tests	CV, SWV
Maximum Current	100 nA
Voltage step	10 mV
Scan Rate Limit (CV)	250 mV/s
Frequency Limit (SWV)	10 Hz
Resolution	3.6 pA
Voltage Scan Limits	± 0.8 V

3.5 Benchmarking the proposed System vs Lab Equipment

In order to verify the system as a proof of concept, it is necessary to benchmark the system against state of the art benchtop laboratory equipment.

3.5.1 Resistive Calibration

To calibrate the proposed system, a cyclic voltammogram was performed using a 100 MΩ resistance across the complete voltage range of the system as shown in Figure 3.12. This is a useful way to ascertain whether the proposed data acquisition system is fit for purpose while also removing any electrochemical noise. For comparison, a CV scan was also performed on a dummy cell of 100 MΩ resistance using a laboratory grade benchtop potentiostat, the Autolab PGSTAT302N. For laboratory based measurements the device under test is placed inside a faraday cage as standard, to negate the potential effects of any environmental electromagnetic noise. Therefore the dummy cell was placed in the faraday cage for the PGSTAT302N measurements.

It was found that there was a gain error when using the ADuCM350 evaluation boards resulting in a 3.5% current output gain across the voltage window using the 100 MΩ dummy cell. According to the laboratory potentiostat, using the line of best fit, the resistance measured was 98.34 MΩ, whereas the ADuCM350 measured 101.85 MΩ. Due to the fact that the evaluation board for the ADuCM350 was built for configurability rather than high precision measurements, there were many potential leakage paths on the TIA channel resulting in the gain error that can be seen in Figure 3.11. In further chapters in this thesis, this gain error is accounted for through the use of dedicated low noise TIA channel paths for each WE. As a proof of concept, the performance of the chip is deemed acceptable for measuring currents in the 0 - 100 nA range.

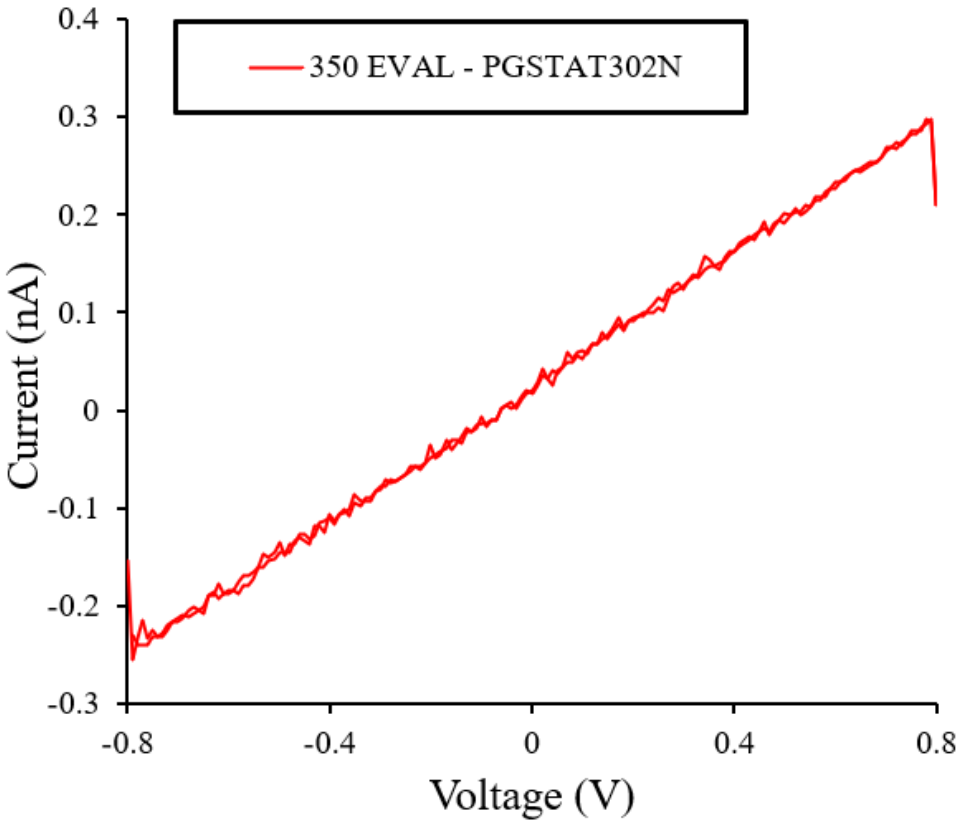


Figure 3.12: Difference between cyclic voltammetry scans for both potentiostat systems using 100 MΩ resistor, swept at 200 mV/s.

3.5.2 Ferrocene Calibration

To ensure that the system could adequately control and measure the resultant current from the electrochemical sensors, calibrations were performed using FcCOOH against a laboratory potentiostat.

3.5.2.1*Improvements to Apparatus*

Initial test results were more noisy and overly sensitive to environmental vibrational noise. This was due to the fact that the wires used to interface to the sensor were excessively long. Jumper cables of that were 20cm long were used for the CV shown in Figure 3.13 (a). Once the signal paths were made as short as possible, as depicted in Figure 3.8, the resultant voltammograms were less noisy as seen in Figure 3.13 (b).

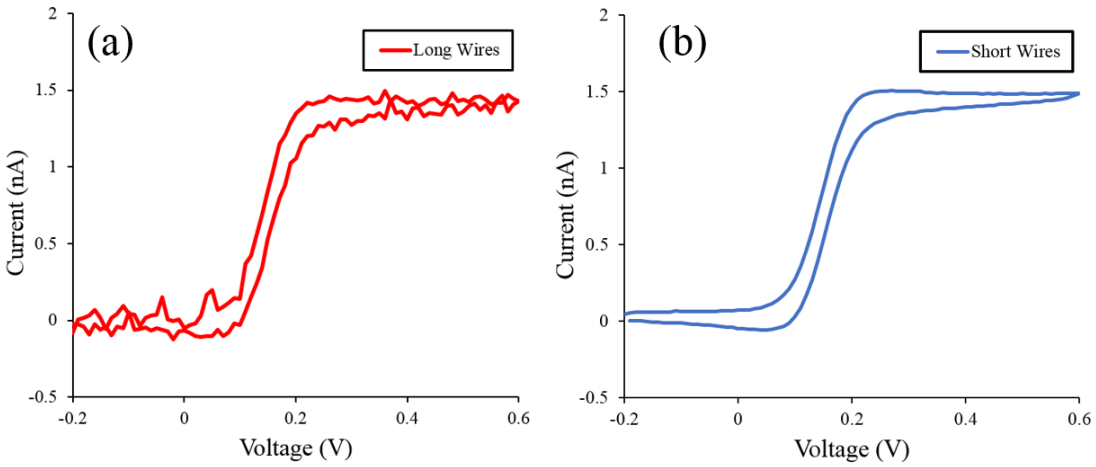


Figure 3.13: Ferrocene scan using (a) long wires and (b) short wires, to interface between proposed system and electrochemical sensor.

3.5.2.1*Pre Excitation Voltage*

A pre excitation voltage is applied to equalise the electrode with its environment. It is predominantly used to address the double layer created at the working electrode prior to testing. The double layer is formed due to the working

electrodes' metal work function that induces a slight ionic charge once placed in solution. Oppositely charged ions in solution will migrate to the surface of the electrode to counter this charge creating an interfacial double layer capacitance. When no pre excitation voltage is used, a current spike can be seen at the start of the voltammogram due to this double layer capacitance. This spike is of no analytical interest, so, prior an electrochemical test, a potential equal to the initial potential value of the scan is applied to the sensor for five seconds before any data is recorded. This current spike becomes more dominant the further the initial voltage is pushed from the sensors' equilibrium. Therefore a CV was performed from 0.8 V to -0.2 V to highlight this effect.

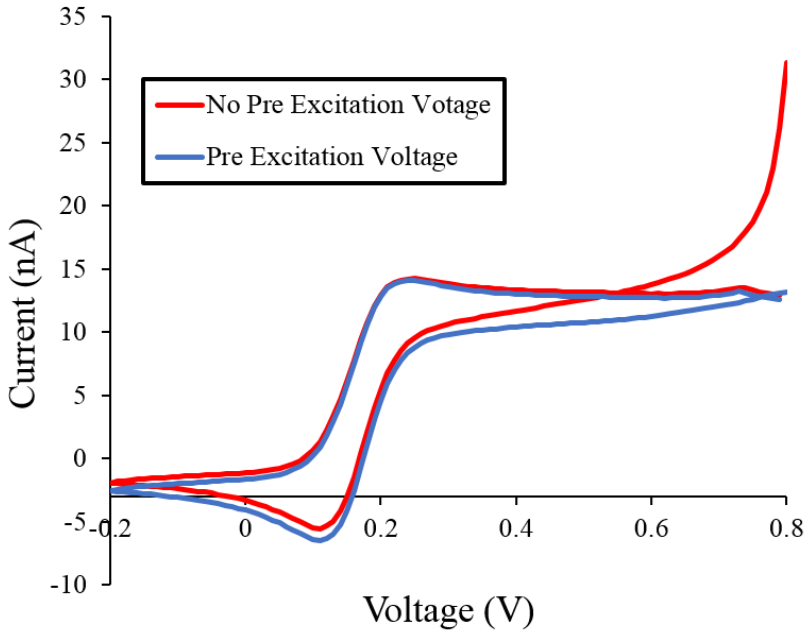


Figure 3.14: 0.1mMol FcCOOH CV, scanned from 0.8 V to -0.2 V at 100mV/s using no pre-excitation voltage and a pre-excitation voltage to interface between the proposed system and an interdigitated electrochemical sensor.

3.5.2.2 *2 vs 3 Electrode Electrochemical Measurements*

As shown in Figure 3.15, for two electrode electrochemical measurements, both the counter and reference electrode are connected. The reference electrode is used for standard three wire electrochemical measurements.

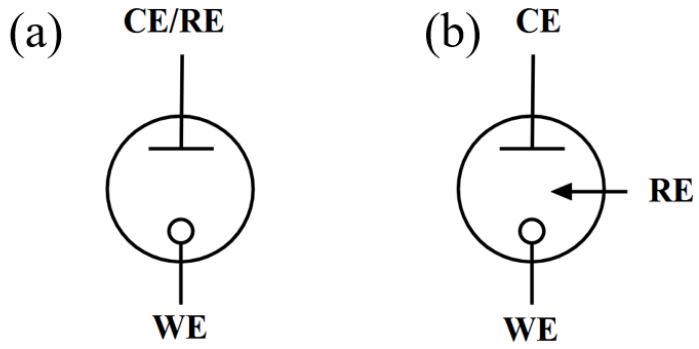


Figure 3.15: Connections of Counter, Reference and Working electrode for (a) 2 electrode and (b) 3 electrode measurements.

The solution resistance of the ultramicro sensors is small compared to macro electrodes due to the reduced distance between the counter and working electrodes. Therefore the effects of the reference electrode are less pronounced but still necessary for micro to nano scale electrochemical sensors. To demonstrate the effect of not using a reference electrode, a CV was performed using the same ultramicroband sensor for both a two and three electrode configuration. A small potential shift can be seen between the three and two wire electrochemical cell measurements as shown in Figure 3.16. The predominant reason for using the reference electrode in nano and ultramicro scale electrochemical sensors, is to decrease the likelihood of potential shift in repeat scans.

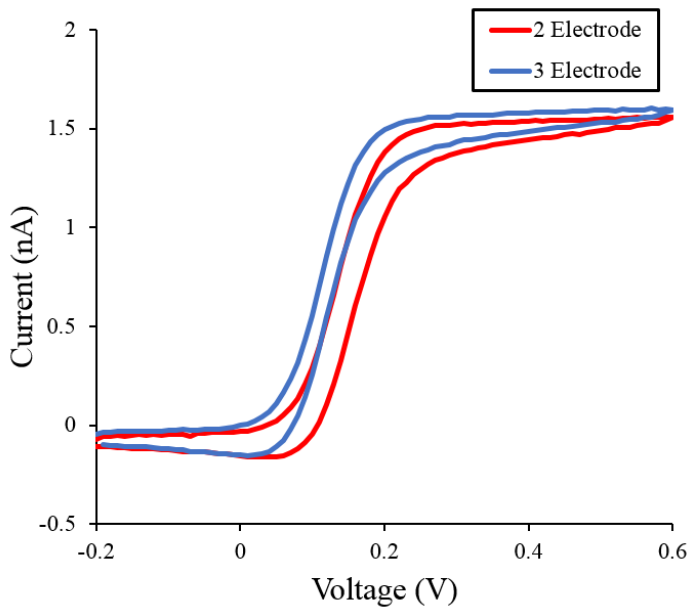


Figure 3.16: 2 vs 3 electrode electrochemical measurements for the same ultramicroband electrochemical sensor using proposed system.

3.5.3 Cyclic Voltammogram Calibration

Through implementing the correct lab procedure and good practice, shortening wires and introducing a pre scan, the ferrocene calibration results are more closely in line with the benchtop equipment. To compare the system to the laboratory potentiostat, CV scans were performed for five different FcCOOH concentrations on both the laboratory potentiostat and proposed data acquisition system. To allow for consistency, each test was performed on the Autolab first and subsequently on the proposed system. When examining the CV curves, two of the main points of interest are the peak current and the redox potentials. For FcCOOH, the peak current is an indicator of its concentration in the solution while, the redox potentials, which are the points where the curve enters and leaves steady state, should be between 0 V and 0.2 V for the on chip reference electrode. The peak currents varied by up to 4 % between the two potentiostats, while the redox

potentials varied by up to 5 mV, which is deemed acceptable. Figure 3.16 demonstrates the ability of the proposed low cost electrochemical data acquisition system to produce results comparable to dedicated laboratory instrumentation across a range of concentrations.

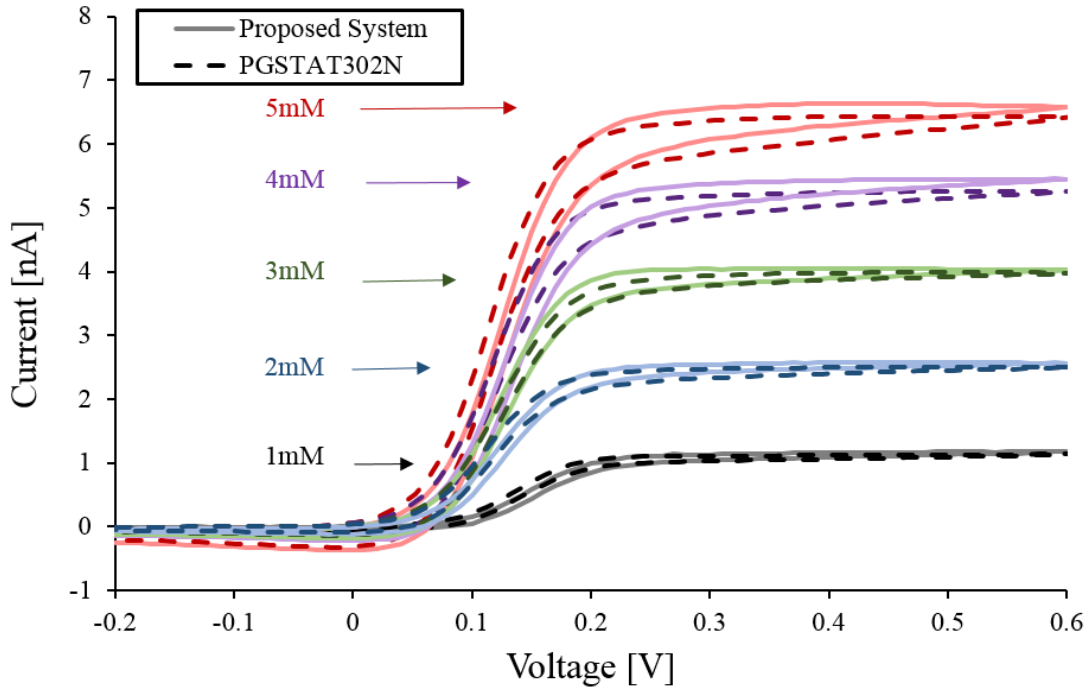


Figure 3.17: Cyclic voltammetry scan measuring varying concentrations of FcCOOH using nanowire sensor, swept at 100 mV/s, where the solid line is the result obtained using the proposed system. While the dashed line is the result obtained using the PGSTAT302N.

3.5.1 Square Wave Voltammogram Calibration

A square wave voltammogram was performed to demonstrate that different voltammetric tests could be executed using the proposed system, as illustrated in Figure 3.17. A difference in peak current magnitude of 68 pA was measured when compared to the Autolab potentiostat, this is considered to be within an acceptable margin of error.

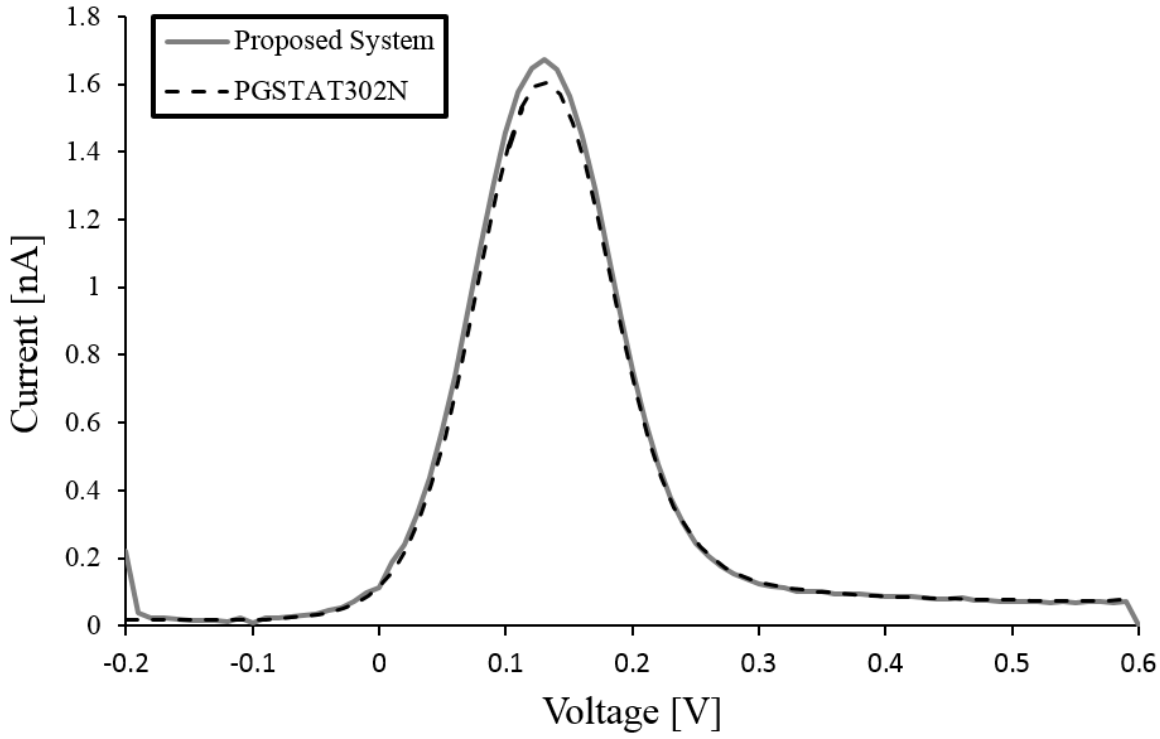


Figure 3.18: Square wave voltammogram at 10Hz, swept at 100mV/s of 1mM FcCOOH using microband sensor.

3.5.2 Sources of Error

All the measured results agree well with the laboratory potentiostat given that variations will occur with scans performed on the same electrode due to the repeatability of electrochemical sensors. Factors that may have contributed to the difference were polarization of the pseudo reference electrode and the deposition of FcCOOH on the electrode surface.

3.6 Conclusion

A low cost, portable point of care data acquisition proof of concept has been developed and demonstrated, which is suitable to interface to ultramicro and nanowire electrochemical sensors. Through a calibration using both an equivalently sized resistor and ultramicro scale electrochemical sensors, a clear indication of the performance of the system was achieved. Results have shown accuracies comparable to a table top, laboratory based potentiostat for cyclic and square wave voltammograms. The cyclic voltammetry calibration also showed the system's ability to differentiate between varying concentrations of FcCOOH clearly. Thus the proposed system was deemed fit for purpose.

3.7 References

[1] G. Zhang et al., “Effect of pooling samples on the efficiency of comparative studies using microarrays,” *Bioinformatics,* vol. 21, no. 24, pp. 4378-4383, 2005.

[2] L. Cates et al., “Laboratory costs of diagnosing TB in a high multidrug-resistant TB setting,” *The International Journal of Tuberculosis and Lung Disease,* vol. 25, no. 3, p. 228, 2021.

[3] A. Murphy et al., “Advanced data acquisition for emerging nano-electrochemical sensors,” in *IEEE International Instrumentation and Measurement Technology Conference (I2MTC)*, Houston, 2018.

[4] K. Dawsonn et al., “Electroanalysis at discrete arrays of gold nanowire electrodes,” *Electrochimica Acta,* vol. 101, pp. 169-176, 2013.

[5] K. Dawson et al., “Fully integrated on-chip nano-electrochemical devices for electroanalytical applications,” *Electrochimica Acta,* vol. 115, pp. 239-246, Jan 2014.

[6] K. Dawson et al., “Electroanalysis at Single Gold Nanowire Electrodes,” *The Journal of Physical Chemistry,* vol. 116, no. 27, p. 14665–14673, Jun 2012.

[7] R. R. Gagne et al., “Ferrocene as an Internal Standard for Electrochemical Measurements,” *Inorg. Chem,* vol. 19, pp. 2854-2855, 1980.

[8] R.L. Brazg et al., “New Generation Blood Glucose Monitoring System Exceeds International Accuracy Standards,” *Journal of Diabetes Science and Technology*, vol. 10, no. 6, p. 1414–1415, 2016.

[9] T. Instruments, LMP91000 Sensor AFE System: Configurable AFE Potentiostat

for Low-Power Chemical Sensing Applications Revised, Dallas, 2014.

[10] Analog Devices, “16-Bit Precision, Low Power Meter On A Chip with Cortex-M3 and Connectivity,” Analog Devices, Norwood, 2014.

[11] Analog Devices, EVAL-ADuCM350EBZ User Guide, Boston, 2014.

[12] Analog Devices, 16-Bit Precision, Low Power Meter On A Chip with Cortex-M3 and Connectivity Rev B, Boston, 2017.

[13] IAR Systems, “Iar Embedded Workbench 7.5,” Uppsala, Sweeden, 2015.

[14] Bitvise, Putty, "www.putty.org", (Assessed Jan '21).

[15] MATLAB, MATLAB R2016a, New Mexico, 2016.

[16] Microsoft, Excel 2013, Seattle, 2013.

[17] National Instruments, LabVIEW 2012, Austin, 2012.

Chapter 4 Bipotentiostat System for Water Quality Monitoring

4.1 Introduction

As mentioned in chapter 1, ultramicro scale electrochemical sensors are gaining traction for a variety of new applications including point of care clinical diagnostics and in field environmental monitoring. To address this growing need, several research groups are currently developing nano and ultramicro scale electrochemical sensors for point of sample tests [1-4]. Although many new electrochemical sensing technologies have and are being developed, it is challenging deploy them outside of a research laboratory due to the expensive bulky benchtop equipment required to interrogate these electrochemical sensors. Currently, to achieve proof of concept at the point of measurement, an electronic engineer must be hired to create a customised solution for the sensor in question [5-7], however, even then such systems often are not sufficiently robust to deal with sensor to sensor variations that regularly occur early in the development cycle. For electrochemical sensors utilising two working electrodes, the development of a custom acquisition system is even more onerous. While there are some commercial systems currently available [8-9], to date they are often prohibitively expensive.

While low-cost potentiostats have been developed [10-12], they typically do not support bipotentiostatic capabilities or have the sufficient resolution to support the pico-Amp currents associated with nano and ultramicro scale electrochemical sensors. This chapter proposes a portable electrochemical acquisition system, which utilises

commercial components and provides ease of use via a smartphone application and Bluetooth connection. The system can act as a low cost solution for electrochemists who want to explore their sensors capabilities in a portable or end application setting, without requiring a significant investment. It is envisaged that the system will be of particular use to nano-scale electrochemical sensing technologies that typically require the use of two WEs, which is not readily supported today. This chapter is based on the paper 'Portable Data Acquisition System for Nano and Ultra-Micro Scale Electrochemical Sensors', IEEE Sensors Journal [13], and Generator Collector Voltammetry Data Acquisition for Nanowire Interdigitated Sensors, presented at the IEEE Nano conference 2018, Cork [14].

4.2 Tyndall Interdigitated Ultramicroband Sensors

The Tyndall interdigitated sensors use the same SD chip topography as the single electrode sensors, as described in section 3.2. The only difference is that the second set of WE's are interfaced to via the contact pads at the opposite end of the chip, as illustrated in Figure 4.1 (a). This requires a sensor holder with springed pins to enable a connection with the circular contact pads for the second set of working electrodes as seen in in Figure 4.1 (c). The interdigitated comb structure can be seen between the two gold WEs in Figure 4.1 (b). The width of the electrodes is 1µm and the distance between the electrodes is either 1 µm, 2 µm or 10 µm depending on the sensor and application.

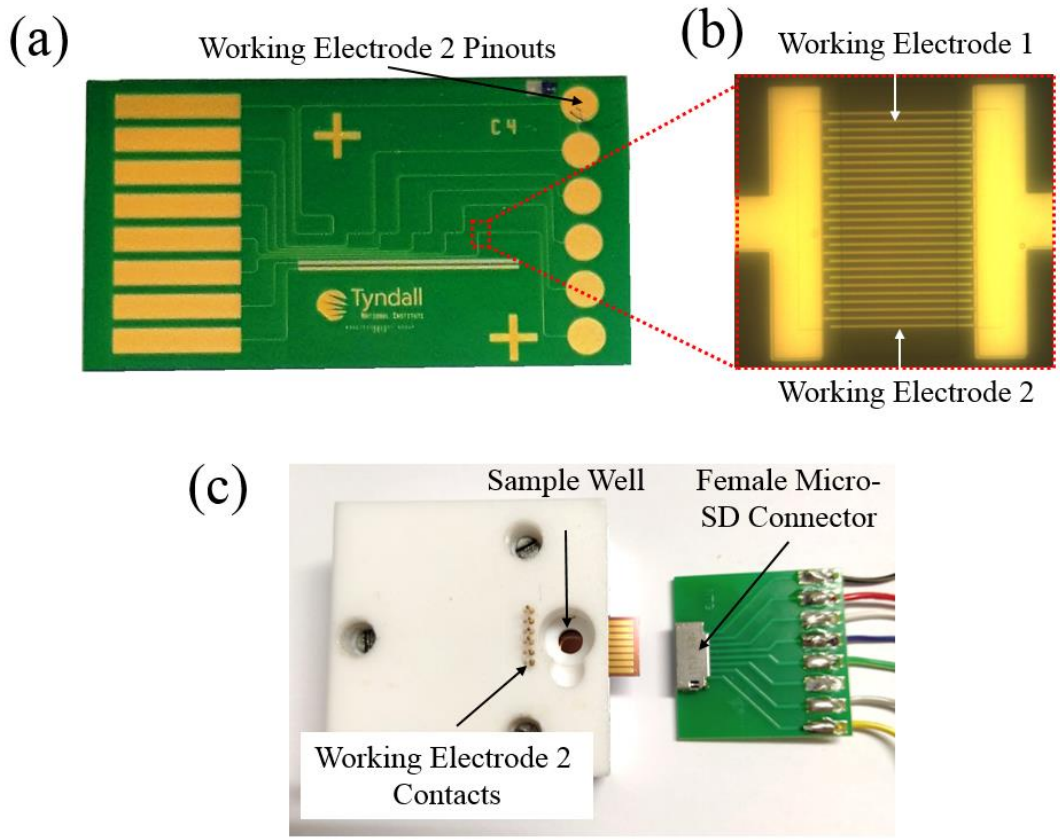


Figure 4.1: (a) Tyndall ultramicro band sensor chip with CE , RE and 6 WE1 accounting for the contact pads on the lefthand side and 6 WE2 accounting for the contact pads on the right hand side, (b) Optical micrograph of interdigitated 1µm ultramicro band with 2µm spacing, (c) Interdigitated chip holder and micro sd connector.

4.3 Dual Electrode System Proof of Concept

In order to interface to the Tyndall interdigitated sensors and perform a generator collector test as described in section 2.3, the system has to perform CV and SWV while also maintaining a fixed potential at the second working electrode. This must also be performed while having the current sensing capability for ultramicro scale electrochemical sensors i.e. the ability to detect current in the nano and pico amp ranges, which is done in the previous chapter.

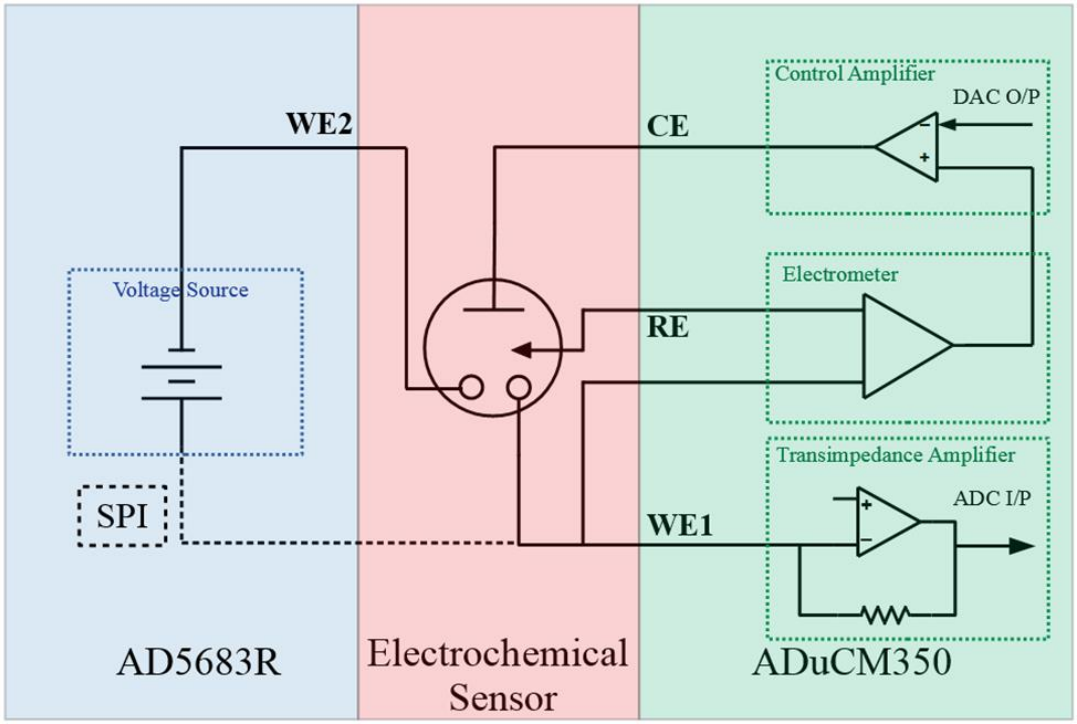


Figure 4.2: Circuit diagram of dual electrode interface system proof of concept, which includes the potentiostatic circuit from Chapter 3 and a voltage source to maintain a constant potential between WE1 and WE2.

As illustrated in Figure 4.2, the ADuCM350 is used to drive and control the CE, RE and WE 1 (Working Electrode 1). As described in the previous chapter, the ADuCM350 also indirectly controls the potential of the solution in the sensor that is being interrogated, through the CE by sensing the potential of the solution via the RE. The resultant current of the electrochemical reaction at the WE1 electrode is converted to a voltage using the integrated trans-impedance amplifier in the ADuCM350. This voltage is subsequently converted to a digital signal using the ADC. The AD5683R DAC [15], a 16 bit DAC with a range of up to 2.5 V, provides an additional independent stimulus for WE2 (Working Electrode 2). Serial Peripheral Interface is the protocol used to enable master slave communication between the ADuCM350 and AD5683R.

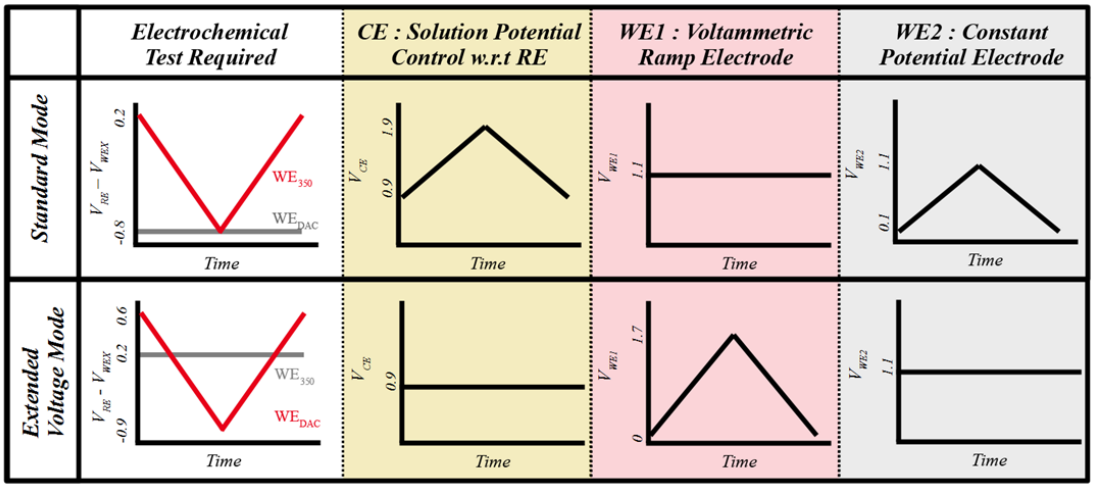


Figure 4.3: Voltage levels applied by system to realise standard and extended voltage levels.

4.3.1.1*Standard Voltage Mode*

The system can perform a voltammetric test in a range of ± 0.8 V at WE1 with respect to the solution. As outlined in the previous chapter, this is achieved in the case of a single WE based sensor by maintaining the WE at a virtual ground (1.1V) and driving the potential of the solution, via the CE, such that the potential difference between WE1 and the solution is maintained at a user specified value with respect to the RE. This varies from sensor to sensor and is also a function of the analyte under observation. As seen in Figure 4.3, for dual electrode measurements, the AD5683R is used to maintain a constant potential difference, specified by the user, relative to the CE. As depicted in Table I, the voltammogram in this mode is limited to ± 0.8V as the DAC driving the CE in the ADuCM350 experiences headroom issues outside an absolute range of 0.3V to 1.9V. As seen in Table 4.1, the range of all voltammograms for dual electrode sensing varies depending on the potential specified at WE2 (Working Electrode 2). In the standard operating mode, this is limited only by the ability of the AD5683R to mirror the potential at the CE at

the specified offset. In Figure 4.4, it can be seen that the proposed system is capable of supporting the requirements of this application.

4.3.1.2*Extended Voltage Mode*

In certain measurements, it is required to measure the resultant current at the collector electrode, WE2, which maintained at a constant potential during a dual electrode electrochemical test. The data acquisition system has been developed to integrate this capability. In the extended voltage mode, the voltage at WE2 and the solution is maintained at a constant potential through the ADuCM350, and the AD5683R is utilised to perform the necessary voltage sweep at the WE1, which is depicted in Figure 4.3.

Table 4.1: System Specifications.

General Specifications			
Current Resolution	3.6 pA		
Current Range	± 100 nA		
Max Scan Rate	0.2 V/s		
Measurement WE Virtual Ground	1.1 V		
System Voltage Ranges			
	WE2 (Constant Potential)		
	-0.8 V	**0 V**	**0.8 V**
Standard Mode			
Voltammetric Test Range (WE1)	-0.8 V to 0.3 V	-0.8 V to 0.8 V	-0.6 V to 0.8 V
Extended Voltage Mode			
Voltammetric Test Range (WE1)	-1.9 V to 1.6 V	-1.1 V to 1.4 V	-0.3 V to 2.2 V

In this mode of operation, there is also the possibility of applying a wider range of voltage potentials during the voltammogram sweep as the solution is maintained at a constant potential. This allows for the full 0 V to 2.5 V range of the AD5683R DAC to be utilised, which is reflected in the wider voltammogram range seen in Table 4.1.

4.3.1.3*Proof of Concept Results*

To show the ability of the system to perform a generator collector test and induce redox cycling between the two working electrodes in an interdigitated sensor, an electrochemical test was performed using 1mM FcCOOH. Cyclic Voltammetry was the test incorporated using the generator collector technique. The potential of the collector electrode was scanned from -0.2 V to 0.6 V against a platinum on chip reference electrode at a scan rate of 100mV/s while the generator electrode was biased at a potential of -0.2 V.

As a control, a cyclic voltammogram sweep was also performed on the same sensor, without the control of the generator electrode. The ratio of the two graphs is also used to determine the amplification factor of the electrode. Amplification factor is the ratio of redox current while both the collector and generator are biased, i.e. in dual mode, against the current achieved from biasing a single electrode, i.e. single mode. This amplification factor is an indication the system's ability to enable the interdigitated sensors operation and thus improve its sensitivity through employing the generator collector technique. This data acquisition system was able to achieve an amplification factor of approximately 4 when detecting the FcCOOH, as seen from Figure 4.4. This verified that the system's ability to perform such measurements and thus augment the sensors sensitivity.

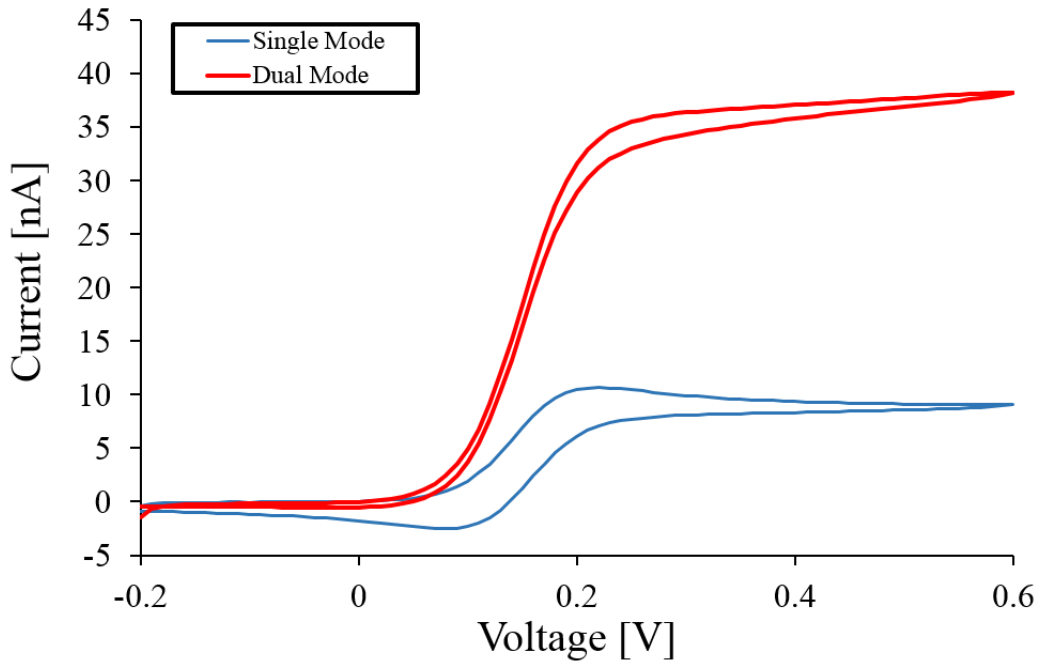


Figure 4.4: Cyclic Voltammogram fusing dual electrode proof of concept system at 100mV/s of interdigitated ultramicro band electrochemical sensor for single and dual electrode configurations (WE 2 maintained at -0.2 V for dual mode).

The system can also control two electrodes of an electrochemical sensor with similar accuracy to a benchtop potentiostat, as outlined in Figure 4.5. Here, the same test was performed on both the proposed system and a laboratory benchtop potentiostat. When comparing the two current outputs the variance between the proposed system and expected result from the benchtop potentiostat was minimal. The reduction potential varied by 10 mV and the peak current amplitude varied by 221 pA. Factors that may have caused a discrepancy between results include an electrochemical change on the sensor surface from run 1 to run 2 or polarisation of the reference electrode.

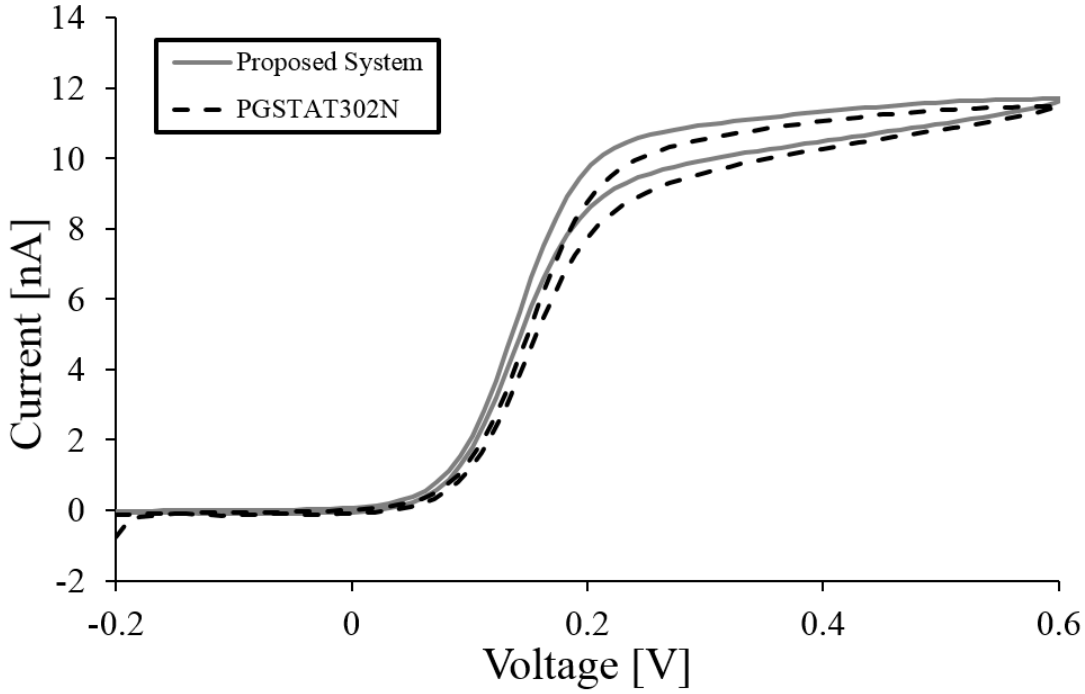


Figure 4.5 Generator Collector Cyclic Voltammogram of 1mM FcCOOH using an interdigitated ultramicro band sensor, swept at 100mV/s using the proposed system and a laboratory benchtop potentiostat.(WE2 maintained at -0.2).

4.3.1.4*Wireless Communication*

To allow for ease of use at the point of sample the system has to be wireless. A Bluetooth module called the HC-05 [16] is used for this purpose. As well as being low cost, it is an easy to use, ubiquitous Bluetooth module, which is compatible with mobile devices.

4.3.1.5*Smartphone Application*

An android application (app) has been developed using the MIT app inventor [17], which is a scratch based language for rapid prototyping of apps. The app allows the user to select and configure the necessary electrochemical test and read out the results on a graph in real-time. To ensure the adoption of the system by electrochemists, the app's user interface has been designed such that it is consistent

with the interfaces of existing laboratory potentiostats. The device can be programmed to perform a range of electrochemical tests and the user has the option of initialising the voltammetric sweep from either the maximum or minimum voltage. A ‘cleaning scan’ option is also available to apply a negative potential to the working electrodes for 30 seconds prior to the test. These are essential capabilities especially when developing new electrochemical sensors. There is also a user option to save the voltammetric results to a file storage service such as google drive. The scratch code developed for the application can be accessed in Appendix, section A.4.

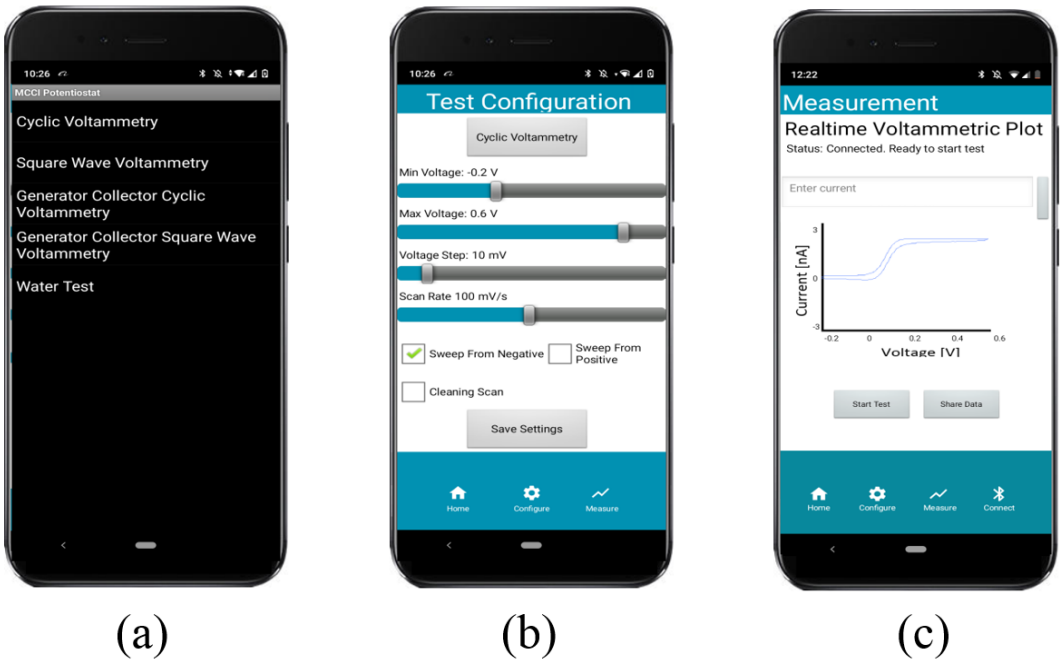


Figure 4.6: Proposed easy to use smartphone application with (a) Voltammetric test dropdown menu, (b) Voltammetric test configuration screen and (c) Real-time electrochemical test plot with wireless export option.

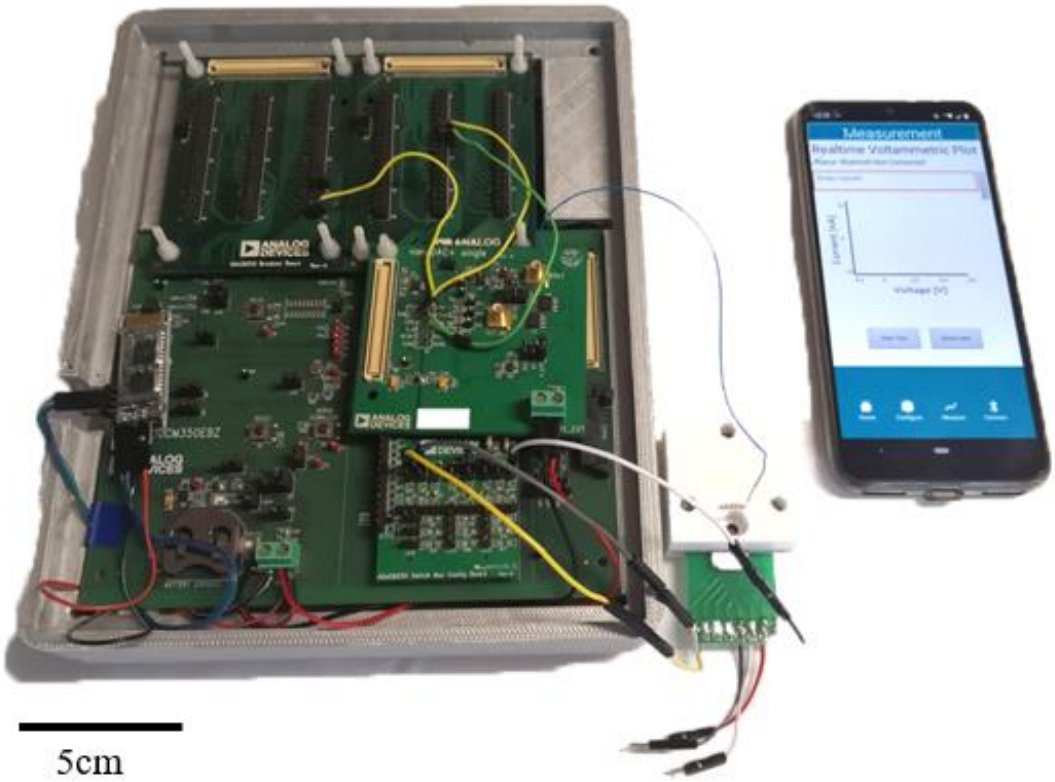


Figure 4.7: Proof of concept portable dual electrode system inside a 3d-printed enclosure, interfacing to an ultramicro electrochemical sensor with smartphone interface.

4.3.2 Custom Printed Circuit Board Realisation

Although the proof of concept is able to perform the necessary electrochemical tests, it is too large and is not sufficiently robust to be a viable solution for point of test measurements, as seen in Figure 4.7. Therefore, it was necessary to create a custom Printed Circuit Board (PCB) to reduce the cost and form factor of the system. This PCB also has to be battery operable to allow for field use. Another advantage of creating a PCB for the system is that the length of the AFE signal paths are reduced resulting in better noise performance. For the schematic capture and PCB design of the device, Easy PC is used [18]. The schematic and PCB layout of the design can be seen in the Appendix, section A.5.

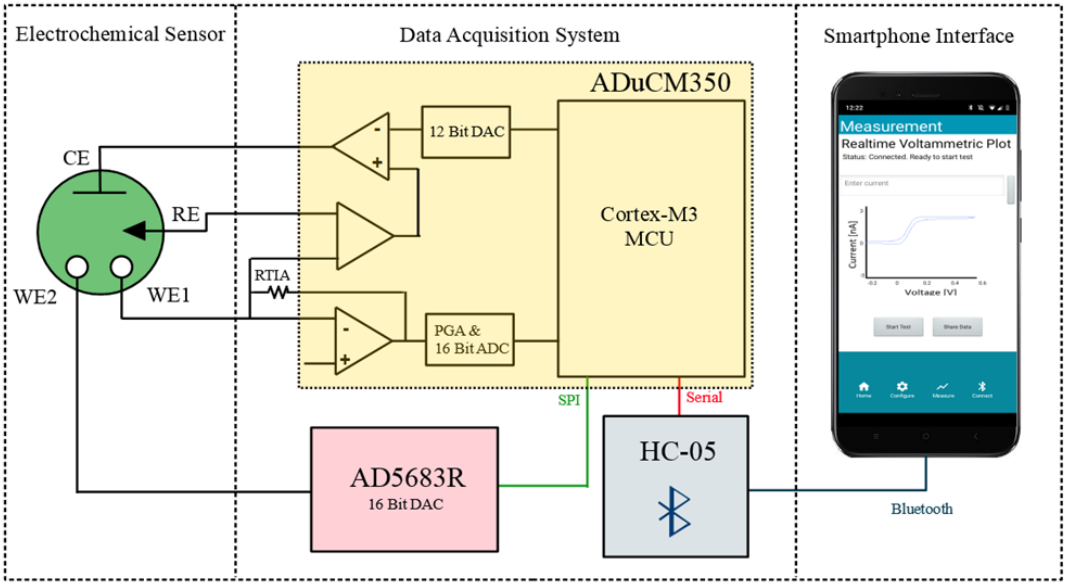


Figure 4.8: Block diagram of potable point of sample system, with separate electrochemical sensor. Data acquisition system consisting of the ADUCM350, the AD5683R connecting to the WE2, all controlled by the micro Controller in the ADUCM350. The HC-05 provides the necessary Bluetooth connection for the smartphone interface.

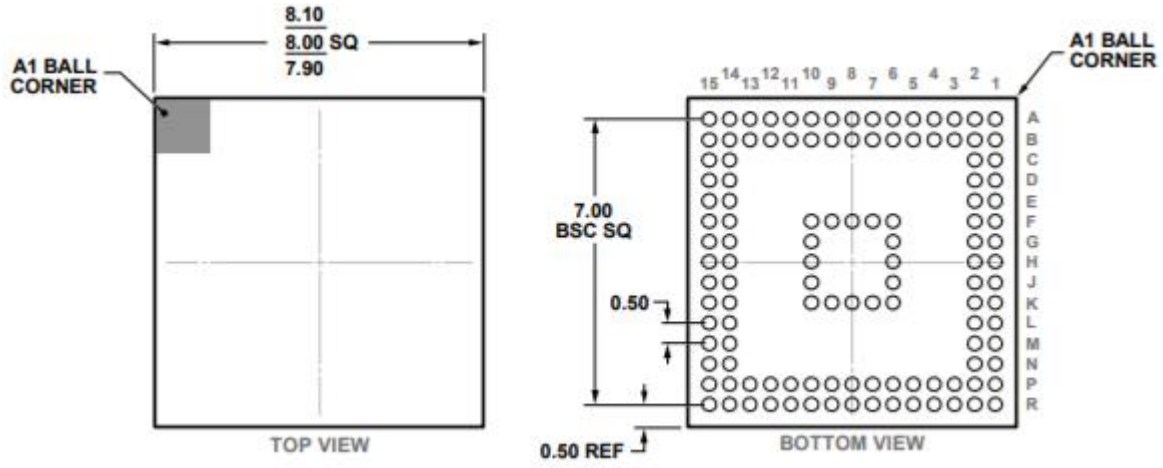


Figure 4.9: Top and bottom view of ADuCM350 IC package.This BC-120-3 package requires a multilayer board to route all required signals to and from the chip.

The ADuCM350 chip is contained in a BC-120-3 package. It has a relatively fine pitch of 0.5 mm between each of the contact pads. As a result of the fine pitch and the fact that the majority of the AFE contacts in the chip have to be interfaced to, a 6 layer PCB is used. This allows for a contact to be made with all the required pads

for the PCB design. An increased number of layers also allows for a smaller PCB footprint as components can be placed closer together. Through using both sides of the PCB and 6 copper layers, the final dimensions of the design is 57 mm x 30 mm.

4.3.2.1 *AFE Implementation*

Individual discrete analog components are placed as close as possible together on the PCB to limit noise, which is seen in the proximity of components on the top of each side of the PCB illustrated in Figure 4.10. Decoupling capacitors, RTIA and RCAL were prioritised when placing components in proximity to the ADuCM350. Similarly to the proof of concept, the RTIA and RCAL that are used are 10 MΩ but headers are also implemented to allow for different external resistor values to be used if required. A dedicated ground plane is used to provide low impedance signal paths and reduce electrical noise. A phoenix connector [19] enables user flexibility to interface their sensor with the system in whichever way is suitable for their sensing technology. This is also placed so that the potentiostatic signal path is made as short as possible.

4.3.2.2 *Portability Implementation*

To power the device a 18650, 1200mAh rechargeable lithium ion battery was used. A step up battery protection module is used to protect the battery from overcharging [20]. This module also has a buck boost converter to increase its output to 5 V. A buck-boost converter is a type of DC-DC converter that can produce an output voltage that is either higher or lower than the input voltage. It does this by controlling the duty cycle of a switching element e.g. a transistor. On the PCB, the 5 V from the module is used for the HC05 Bluetooth transceiver, which has a higher

voltage requirement. An Analog Devices, ADP3333 [21], linear regulator is used to provide a stable 3.3 V signal for the ADuCM350 and AD5683R.



Figure 4.10: Front and back of the 6 layer data acquisition PCB, dimensions; 57 mm by 36 mm. To minimise the footprint, the ADuCM350 was placed at the back of the PCB.

4.3.2.3*Device Cost*

The total cost of the system developed is €90.30 and a brief breakdown of costing is presented in Table. II. The cost is for a small run of 10 PCBs. If the components and PCB are purchased in bulk, the overall cost would be significantly cheaper. Nevertheless this is still is several orders of magnitude cheaper than laboratory grade equipment that have the capability of performing measurements in the nano amp range. Such a low cost should significantly lower the barrier of entry for future ultramicro scale electrochemical sensors being developed for use at the point of sample.

Table 4.2: System Cost Overview.

Item	Cost (€)
PCB	
Unit	8.02
Components	39.50
Assembly	37.00
	84.52
External Components	
HC-05	2.78
Li Battery & Charger	3.00
	5.78
Total Cost	**90.30**

4.3.3 Validation of the data acquisition PCB

4.3.3.1*Initial testing problems*

A design error in the initial PCB layout was that all vias were left exposed. This meant that a gold exposed pad was on each side of the surface of the PCB corresponding to most of the nets of the AFE as seen in Figure 4.10. A net is a connected group of nodes in a circuit. Although this is common practice in the majority of standard PCB designs, it was a significant design flaw here due to the sensitivity of the current measurements being taken. As a result, when the system was tested initially, there was an equivalent resistance in the region of 1 GΩ for open circuit voltammetric measurements, i.e. when the resistance was measured in the absence of a sensor. This resistance got smaller, the closer the corresponding WE vias were to the CE on the PCB surface. It was identified that the predominant reason for this short was residual solder flux from the nearby

CONN3 header. To rectify this, each PCB was cleaned with isopropyl alcohol. Once dried, three layers of PCB varnish was applied to the surface of the device. This PCB varnish would also protect the device from dirt and moisture when the system is utilised in the field.

4.3.3.2*Resistive Calibration*

To gauge the performance of the custom PCB, a CV sweep was performed across its voltage range using a 100MΩ resistor. It was benchmarked using the PGSTAT302N [22] and also compared to the ADuCM350 evaluation board. As seen in Figure 4.11 the custom PCB current output overlapped the benchtop potentiostat. The impedance measured through the line of best fit of the laboratory based potentiostat was 101.95 MΩ, while the line of best fit for the custom PCB was 101.85 MΩ. There was a gain error in for the evaluation board despite the fact that the same code was used for both devices. This reflects a significant improvement in accuracy of measurements through the development of a custom PCB for precision measurements.

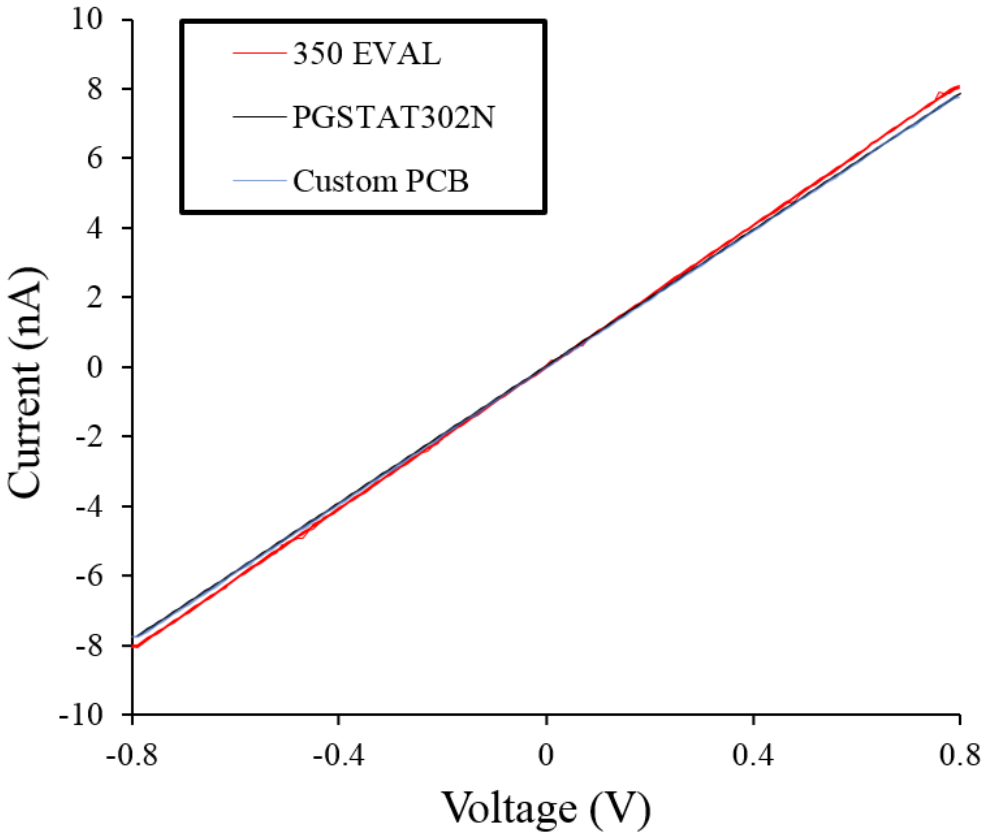


Figure 4.11: Cyclic Voltammetery scan across full range of ADuCM350 for the Custom PCB, ADuCM350 evaluation board and the Metrohm PGSTAT302N potentiostat.

A graph reflecting the deviation from the expected current value was taken across the ten cyclic voltammograms. This test was performed to illustrate that the use of a custom PCB improved noise performance of measurements. The expected current value was derived from the line of best fit of each of the voltammograms and subtracted away from the measured value. Any gain error was calibrated out to ensure only the variance of the current measured was taken into consideration. The evaluation board returned a standard deviation of 21.9 pA, while the custom PCB had a standard deviation of 16.4 pA. Signs of clipping can be seen at + 0.8V and -0.8V for both the custom PCB and EVAL board in Figure 4.12.

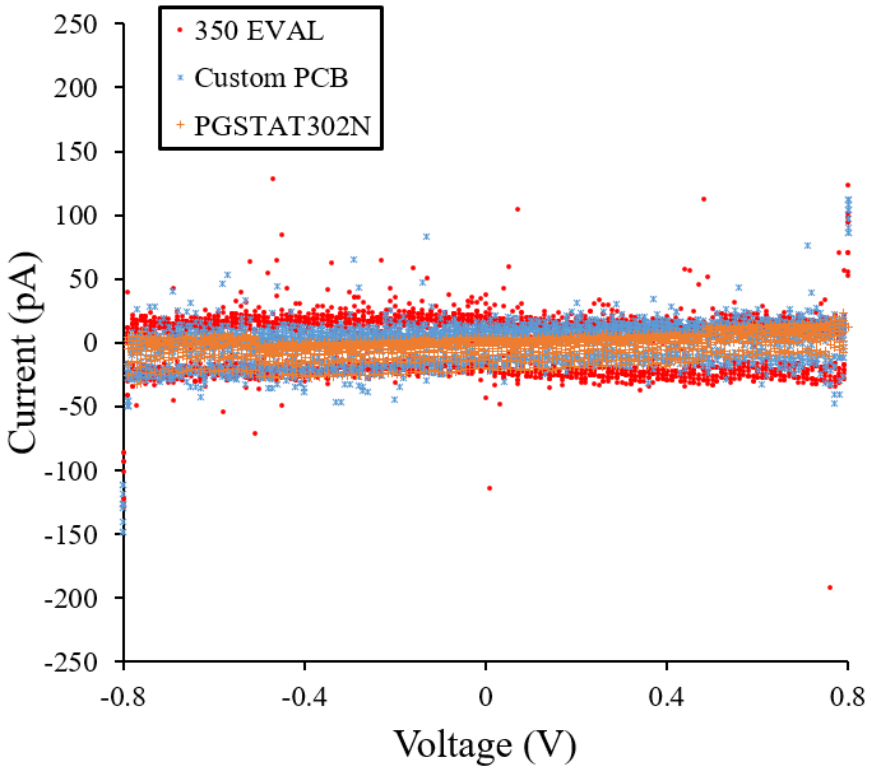


Figure 4.12: Current deviation from expected value for ten CVs swept at 200mV/s from - 0.8 V to 0.8 V using the ADuCM350 evaluation board, the custom PCB and the Metrohm PGSTAT302N.

Given that the same apparatus was used for each measurement, this figure reflects the improvement on noise performance through shortening the potentiostatic signal path. The standard deviation of the benchtop potentiostat was 7.8 pA. Measures that the PGSTAT302N takes for improved noise performance include, coaxial lines for each electrode, a faraday cage and superior precision current measurement circuitry.

4.4 Calibration of Sensor in River Lee Water

To present the full range of functionality of the system and verify its use as a portable potentiostat, a calibration curve was produced for the detection of dissolved oxygen in river water.

4.4.1 Dissolved Oxygen Sensor

This was performed using recently developed ultramicro band electrochemical sensors [23], [24]. As seen in Figure 4.13 (a), the sensor has the same topography as a Micro SD card, utilises six individual sensors, with a common integrated on chip platinum pseudo reference electrode and gold counter electrode of 50 nm thickness. The dissolved oxygen sensor consists of interdigitated platinum (WE Pt) and gold working electrodes (WE Au) microband array, shown in Figure 4.13 (b).

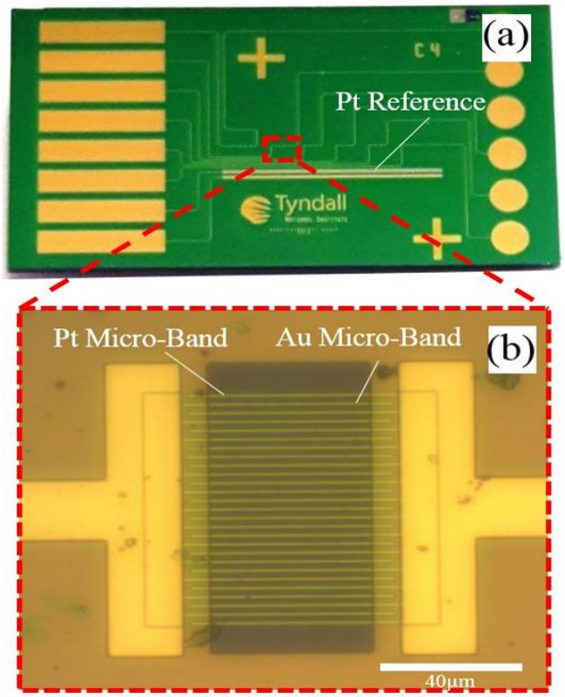


Figure 4.13: Tyndall National Institute electrochemical dissolved oxygen sensor, including, (a) Tyndall National Institute Electrochemical Sensor chip, (b) Microscopic view of gold and platinum deposited 1µm bands.

4.4.2 Electrochemical Reaction in Water for Dissolved Oxygen

The sensor generates peroxide (H_2O_2) at WE Au when a negative potential with respect to the Pt reference is applied. This is represented by the following two-electron oxidation-reduction reaction:

$$2\mathrm{H}^+ + \mathrm{O}_2 + 2e^- \rightarrow \mathrm{H}_2O_2. \quad (4.1)$$

Hydrogen peroxide produced is directly proportional to the concentration of oxygen present in the sample. The generated peroxide is subsequently oxidised at WE Pt array, which is represented as follows:

$$\mathrm{H}_2O_2 \rightarrow 2\mathrm{H}^+ + \mathrm{O}_2 + 2e^-. \quad (4.2)$$

The electrons gained by the WE Pt in this reaction are measured and used as an indication of the oxygen level present in the sample. Redox cycling can occur between the generator and collector as the reactions are reversible.

4.4.2.1*Dissolved Oxygen Voltammetric Test*

A CV scan was performed on a gold electrode, to produce the peroxide while a constant potential was maintained concurrently at a platinum electrode, to re-oxidise the peroxide back to oxygen. Due to the proximity of the gold and platinum electrodes the same chemical reaction could occur a multitude of times with an individual oxygen molecule. The redox cycling between WE Au and WE Pt electrodes increases sensitivity and selectivity of the oxygen measurement.

To execute the test using the proposed system, its 'extended voltage mode' was utilised. A CV was performed at WE Pt from 0.6 V to -0.9 V with a scan rate of 100mV/s, while the WE Au was maintained at 0.2 V potential throughout the test.

The voltage levels applied were with respect to the platinum on chip pseudo reference electrode. The current at -0.9 V potential of the resultant voltammogram at WE Pt corresponds to the oxygen concentration within the sample. Prior to the three tests at each concentration level, a cleaning scan was performed to remove any adsorbed residual species or platinum oxides, particularly from the platinum measurement electrode. As seen in Figure 4.14 (a), to perform the cleaning scan, a CV was performed on WE Au from 0.2 V to -0.8 V and WE Pt was maintained at -0.8 V. A scan rate of 100mV/s was used during this test.

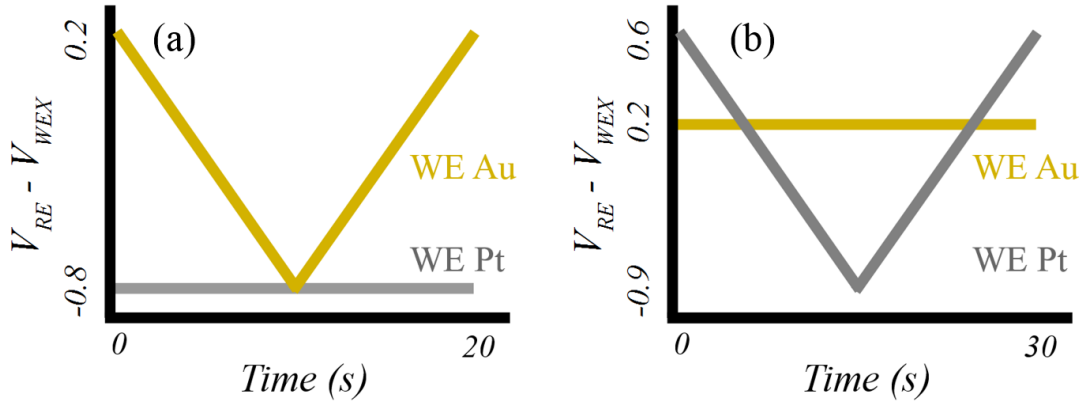


Figure 4.14: Voltages applied by system for dissolved oxygen measurement and electrode clean for, (a) Cleaning scan performed on micro-bands between dissolved oxygen measurements, (b) Voltammetric test required for dissolved oxygen.

4.4.3 Dissolved oxygen detection and calibration plot

Water samples were taken from the river Lee estuary, Cork, Ireland. These samples were deoxygenated using nitrogen gas to eight different oxygen levels and a commercial dissolved oxygen probe *[25]* was used to confirm their concentrations. The electrochemical sensor used consisted of two interdigitated arrays of 1µm bands, each band having 45 µm2 active surface area. There was an array of thirteen platinum bands and a gold band on each side of the platinum, amounting to fourteen fingers, which is depicted after use in river water under microscope in Figure 4.13

(b). Measurements were taken using the proposed system three times at each concentration level in order to discern a margin of error at each point in the dissolved oxygen calibration. Due to the re-oxygenation of the sample in the sensor holder, a new water sample was used for each measurement at every concentration level.



Figure 4.15: Water retrieval apparatus at site of water sample at River Lee Maltings, Cork.

As seen in Figure 4.17, there was a clear peak for the three scans corresponding to oxygen levels in the sample. Due to the nature of the sensor and holder used in Figure 4.16, long wires had to be used in the apparatus which may have led to the increased noise seen in Scan 1 of Figure 4.17. Despite the imperfect apparatus setup from a noise perspective, the results show that the proposed system is capable of performing repeatable electrochemical tests below the nano-amp current range. Jumps could be seen in the plots in Figure 4.17, particularly scan 1 due to the long wires used.

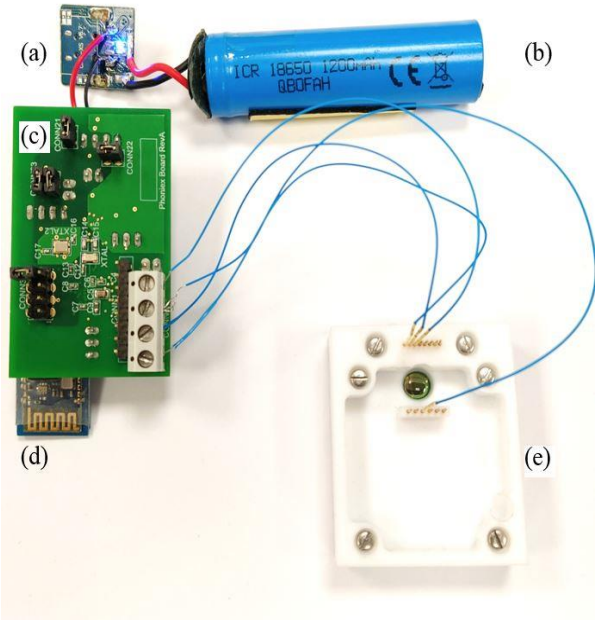


Figure 4.16: Dissolved oxygen measurement apparatus including, (a) Charger and Protection PCB, (b) Battery, (c) Proposed System PCB, (d) HC-05 Bluetooth Module, (e) Electrochemical Sensor.

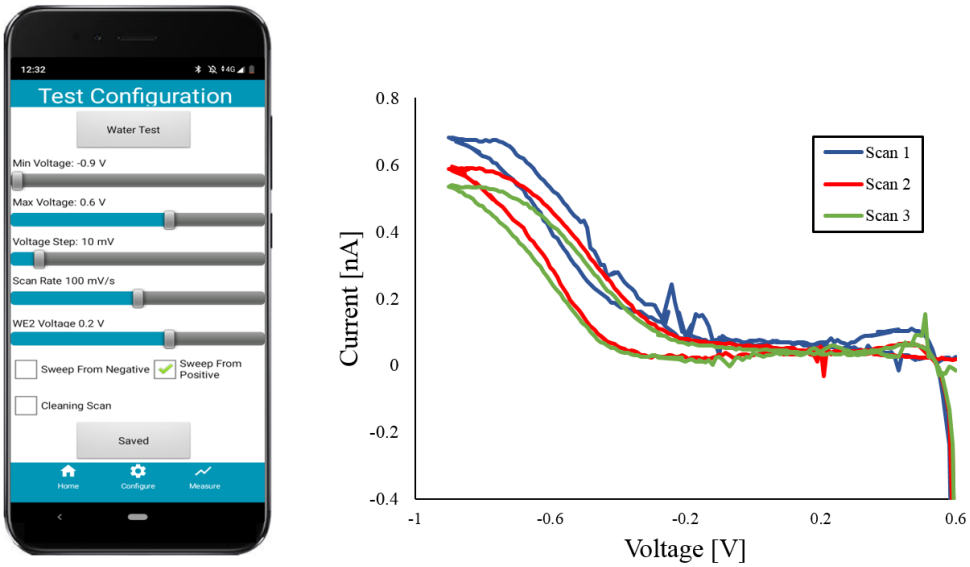


Figure 4.17: Screenshot of required dissolved oxygen measurement voltammogram configuration in Android smartphone application and three resultant current outputs recorded at a dissolved oxygen concentration of 3ppm, using the developed system. Note that the peak of these voltammograms represent the H202 bing oxidised back to H2 as outlined in equation 4.2.

Use of an anaerobic environment for the experiment was impractical due to the large number of calibration measurements required. As a result, one of the prominent sources of error in this experiment was as a consequence of the rapid re-oxygenation of the samples in the sensor sample well as a result of being exposed to the ambient environment. This error was more prolific the further oxygen concentration levels were from the 9 ppm saturated oxygen concentration of the sample. This was depicted by the larger error bars at concentrations between 0 ppm and 6 ppm in the calibration plot illustrated in Figure 4.18. Although the electrochemical test was initiated as soon as the sample was placed in the holder, oxygen would dissolve into the sample in transit to the sensor holder and throughout the duration of the test. The oxygen probe had an error associated with it of ± 0.2ppm for concentrations greater than 8ppm. Although river water was also a hostile matrix for detection of the dissolved oxygen species, Figure 4.18 shows that the proposed system is capable of inferring calibration curves from nano to ultramicro scale electrochemical sensors. The resultant R^2 value of 0.986 is in close alignment with results from similar sensors [23], using a laboratory grade potentiostat.

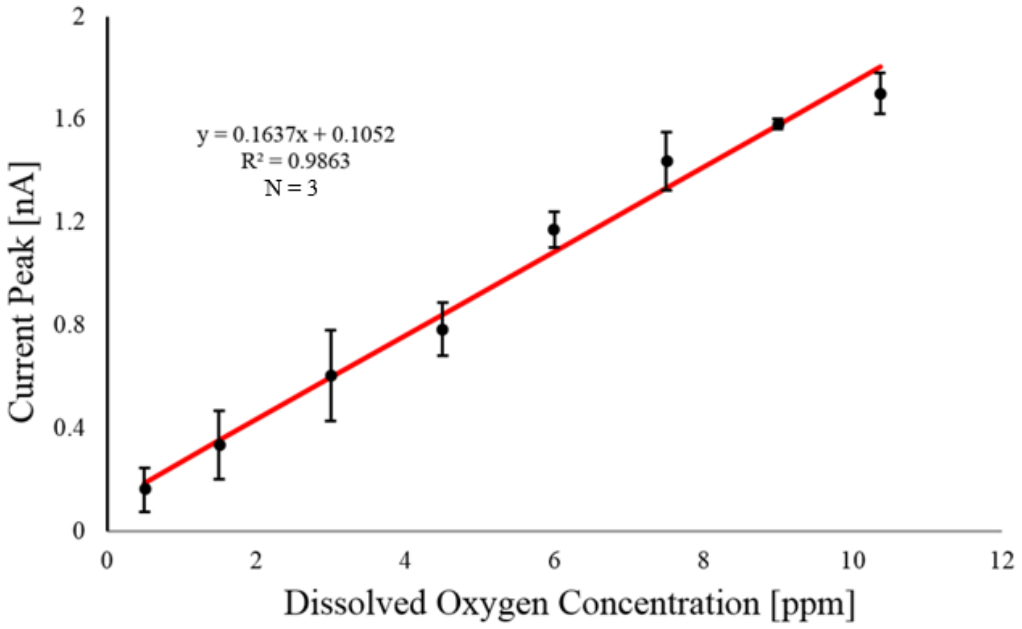


Figure 4.18: Dissolved oxygen calibration plot using river water.

4.4.4 Limitations of the System

In order to interface to some of the other Tyndall interdigitated sensors, particularly where the collector electrode is used for localised pH control [26], a wider applied potential range would be required from the system. In order to achieve this, a separate DAC would be required that could apply a wider voltage window and the common mode of the AFE would have to be increased from a value of 1.1V. This would involve creating a new system out of discrete components instead of the ADuCM350 and increase the overall cost of the device. This limitation is highlighted when comparing this work against other contemporary portable potentiostats as seen in Table 4.3. Another shortcoming of the device is that, unlike standard bipotentiostats, it cannot concurrently measure both working electrodes at the same time. Although it is not essential for getting a quantitate measurement of the concentration of an analyte in a solution for generator collector measurements, it can be used as an indicator of the health of the sensor and the efficiency of the generator

collector measurement. To achieve this, a separate TIA would have to be used at the WE2. Despite these limitations, this work offers a novel cost effective means of interfacing to dual electrode electrochemical sensors that return current values in the nano amp range.

Table 4.3: Comparison of portable voltammetric potentiostats.

System	CE Range (V)	Measurement Range	Bipotentiostat?	Size(mm)	User Interface	Development Stage	Cost	Year
Murphy et al.	±0.8	±100nA	Yes	57x36	App/Bluetooth	Research	$98	2020
MiniStat	±1.2	±100µA	No	27x20	App/Bluetooth	Open Source	$80	2020
Cheapstat	±0.99	100nA – 50µA	No	140x66	PC/USB	Open Source	<$80	2011
Dstat	±1.5	600fA (min limit)	No	92x84	PC/USB	Open Source	$120	2015
UWED	±1.5	±180 µA	No	51x34	App/Bluetooth	Open Source	$61.50*.	2018
Sensit Smart	-1.7 to 2	100nA – 5mA	No	43 x 25	App/Bluetooth	Commercial	$1250	2019
Interface 1010B	±12	10nA-1A	No	270x240	PC/USB	Commercial	$7600	-
Em Stat3	±5	1nA-10mA	No	67x50	PC/USB	Commercial	$1850	-
PalmSens 4	±10	100 pA to 10 mA	Yes	157x97	App/Bluetooth	Commercial	$4300	2019
1200C	±5	1nA-10mA	Yes	178x114	PC	Commercial	$3000	-

4.5 Conclusion

A low cost portable electrochemical data acquisition system is presented that can interface to nano and ultramicro scale electrochemical sensors. It is low cost due to the use of widely available commercial components. Portability is realised from the small form factor and battery operation, in addition to the wireless interface via Bluetooth to a standard smartphone. The custom smartphone app, ensures simple, consistent and robust interface. The complete system has the ability to perform voltammetric tests such as CV, SWV and generator collector voltammetry. Experimental data verifies that the potentiostatic system is fit for purpose and can be used to derive calibration curves from nano and ultramicro scale electrochemical sensors. As a result, the proposed device can be utilised as an integral tool for

developing proof of concepts for emerging nano scale sensors systems at the point of test.

References

[1] P. Ramnani et al., “Carbon nanomaterial-based electrochemical biosensors for label-free sensing of environmental pollutants,” *Chemosphere,* vol. 143, pp. 85-98, Jan. 2016.

[2] F. Van Rossem. et al., “Sensing oxygen at the millisecond time-scale using an ultra-microelectrode array (UMEA),” *Sensors and Actuators B: Chemical,* vol. 238, pp. 1008-1016, 2017.

[3] A.A. Arrocha-Arcos et al., “Electrochemical reduction of Bicarbonate to Formate with Silver Nanoparticles and Silver Nanoclusters supported on Multiwalled Carbon Nanotubes,” *Electrochimica Acta,* vol. 246, pp. 1082-1087, 2017.

[4] K. Dawson et al., “Fully integrated on-chip nano-electrochemical devices for electroanalytical applications,” *Electrochimica Acta,* vol. 115, pp. 239-246, Jan 2014.

[5] J.P.C. Da Costa et al., “Portable Laboratory Platform With Electrochemical Biosensors for Immunodiagnostic of Hepatitis C Virus,” *IEEE Sensors,* vol. 19, no. 22, pp. 10701-10709, 2019.

[6] G. Zhao and G. Liu, “A portable electrochemical system for the on-site detection of heavy metals in farmland soil based on electrochemical sensors,” *IEEE Sensors,* vol. 18, no. 14, pp. 5645 - 5655, 2018.

[7] A.U. Alam et al., “Fully Integrated, Simple and Low-cost Electrochemical Sensors Array for In Situ Water Quality Monitoring,” *ACS sensors,* vol. 5, no. 2, pp. 412-422, 2020.

[8] Palmsens, “Palmsens4-Potentiostat/Galvanostat/ImpedanceAnalyzer,” *[Online], Available:https://www.palmsens.com/shared/content/uploads/2017/03/PalmSens4-description-8.pdf.,* Accessed 07 03 2021.

[9] Metrohm, “Dropsens- μStat 400 Bipotentiostat/Galvanostat,” *[Online].Available:http://www.dropsens.com/en/pdfs_productos/new_brochures/stat400.pdf ,* Accessed 07 01 2020.

[10] S.D Adams et al., “MiniStat: Development and evaluation of a mini-potentiostat for electrochemical measurements,” *IEEE access,* vol. 7, pp. 31903-31912, 2019.

[11] C.Y. Huang et al., “Design of a portable mini potentiostat for electrochemical biosensors,” *2017 IEEE 2nd Advanced Information Technology, Electronic and Automation Control Conference,* pp. 200-203, March 2017.

[12] A. Ainla et al., “Open-source potentiostat for wireless electrochemical detection with smartphones,” *Analytical chemistry,* vol. 90, no. 10, pp. 6240-6246, 2018.

[13] A. Murphy et al., “Portable Data Acquisition System for Nano and Ultra-Micro Scale Electrochemical Sensors,” *IEEE Sensors,* vol. 21, no. 3, pp. 3210-3215, 2021.

[14] A. Murphy et al., “Generator Collector Voltammetry Data Acquisition for Nanowire Interdigitated Sensors,” *IEEE 18th International Conference on*

Nanotechnology (IEEE-NANO), 2018.

[15] Analog Devices, “Tiny 16-/14-/12-Bit SPI nanoDAC+, with ±2 (16-Bit) LSB INL and 2 ppm/°C Reference,” *Dec 2013 [Revised Dec 2016]*.

[16] I. Studio, “HC-05 - Bluetooth to Serial Port Module,” [Online]. Available: http://www.electronicaestudio.com/docs/istd016A.pdf. [Accessed 26 September 2018].

[17] MIT, “Mit App Inventor,” Available [https://appinventor.mit.edu/], (Assessed Jan 2021).

[18] Number One Systems, “Easy PC Schematic Capture and PCB Layout,” 2020.

[19] Camdenboss, “PCB TERMINAL BLOCKS,” Mildenhall, 2022.

[20] Bangood, “2Pcs 5V Lithium Battery Charger Step Up Protection Board Boost Power Module Micro USB Li-Po Li-ion 18650 Power Bank Charger Board DIY,” "https://www.banggood.com/2Pcs-5V-Lithium-Battery-Charger-Step-Up-Protection-Board-Boost-Power-Module-Micro-USB-Li-Po-Li-ion-1-p-1366320.html?cur_warehouse=CN&rmmds=search"[Assessed 2020].

[21] Analog Devices, “High Accuracy Ultralow IQ, 300 mA, anyCAP Low Dropout Regulator Rev B.,” Norwood, 2009.

[22] Metrohm, “PGSTAT302N, https://www.metrohm.com/en/products/electrochemistry/autolab-modular-line/PGSTAT302N (Assessed December 2021)”.

[23] I. Seymour et al., “Electrochemical detection of free-chlorine in Water samples facilitated by in-situ pH control using interdigitated microelectrodes,” *Sensors and Actuators B: Chemical*, vol. 325, p. 128774, 2020.

[24] A. Wahl et al., “Diffusion profile simulations and enhanced iron sensing in

generator-collector mode at interdigitated nanowire electrode arrays," *Electrchemica Acta,* vol. 277, pp. 235-243, 2018.

[25] Hach, "Intellical LDO101 Laboratory Luminescent/Optical Dissolved Oxygen (DO) Sensor, 3 m Cable," *[Online].Available: https://ie.hach.com/product.detail-print.version.jsa?id=24759305791,* [Accessed 10 03 2020].

[26] L.A. Wasiewska et al., "Reagent Free Electrochemical-Based Detection of Silver Ions at Interdigitated Micro Electrodes Using in Situ pH Control," *ChemRxiv,* 2020.

Chapter 5 EIS Disease Detection System

5.1 Introduction

Antimicrobial Resistance (AMR) is projected to cause ten million deaths a year by 2050 if no action is taken [1]. The main contributing factor to this is that antibiotics are being over administered to animals and it is making its way into the food chain. Some of the same antibiotic are used in both food animals and in human medicine. This will have the effect of rendering such medicines useless [2].

At present, the majority of disease diagnostics is both costly and time consuming for farmers. Most disease diagnostics are performed in a laboratory. Once a disease is suspected on a farm, a veterinarian must be hired to take blood samples. These samples are sent to the nearest diagnostics laboratory and results are sent back within 3-5 working days. The quality of the sample can deteriorate with time or get damaged in transit. While during this time period the suspected disease can spread throughout the herd. If the results return positive for a disease, the farmer must hire a veterinarian again to either administer or deliver the antibiotics. As a result of this time consuming, expensive process, blanket antibiotic doses are regularly pre-emptively administered across the entire herd instead.

An example where this disease diagnosis to treatment workflow occurs is in Bovine Respiratory Disease (BRD) in cattle [3], which can be seen in Figure 5.1. BRD inhibits the productivity of the animal and regularly causes death. It is the largest cause of mortality in feedlots, accounting for 45-55% of deaths and $54 million in treatment costs alone [4]. To address this problem we propose a system

that will detect the prevalence of BRD in blood samples on the farm. The final system will consist of a handheld reader and a disposable cartridge to hold the BRD sensor. Such a device will be distributed to vets which will enable them to diagnose cattle at the point of sample. If a test result returns positive using this device, the animal can be immediately quarantined and treated, ensuring the disease doesn't spread throughout the herd. As a result we project that there will be a significant reduction in over administration of antibiotics as only the animals that return positive test results will be treated.

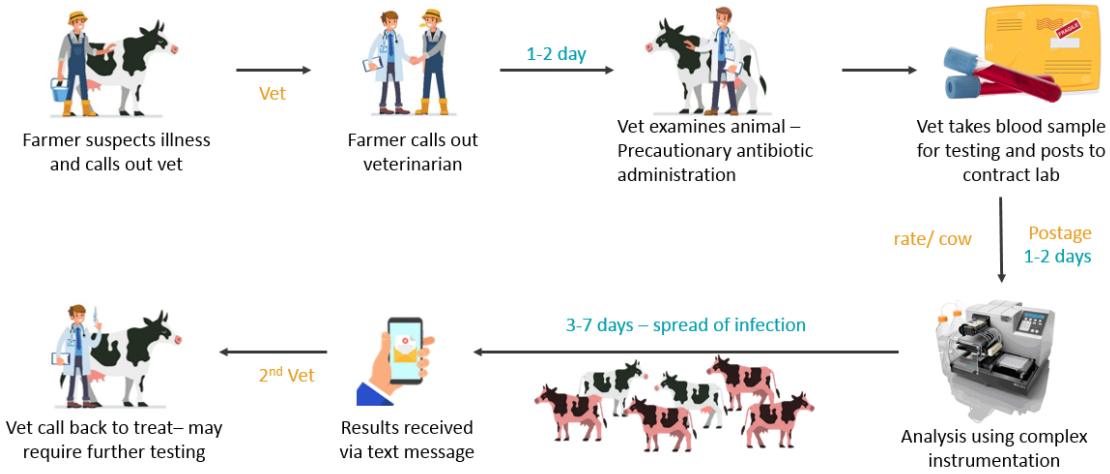


Figure 5.1: Current animal diagnostic method which can take 3 days or more due to the diagnosis being performed at a laboratory.

The effect that the proposed device will have on farm diagnosis workflow can be seen in Figure 5.2. The time taken to diagnose an animal should reduce from 3-10 days to 20 minutes. It should also offer a cost saving to the farmer as only one visit of the veterinarian is required. There is currently a trend for governing bodies, such as the European Union to enforce more legislation on the administration of drugs to food animals [5] hence, this testing will become a requirement in many countries. One of the challenges in realising such a system is creating an electronic interface for the

BRD sensors that have been developed. This chapter describes two iterations of an interface capable of being used to interrogate BRD electrochemical biosensors.

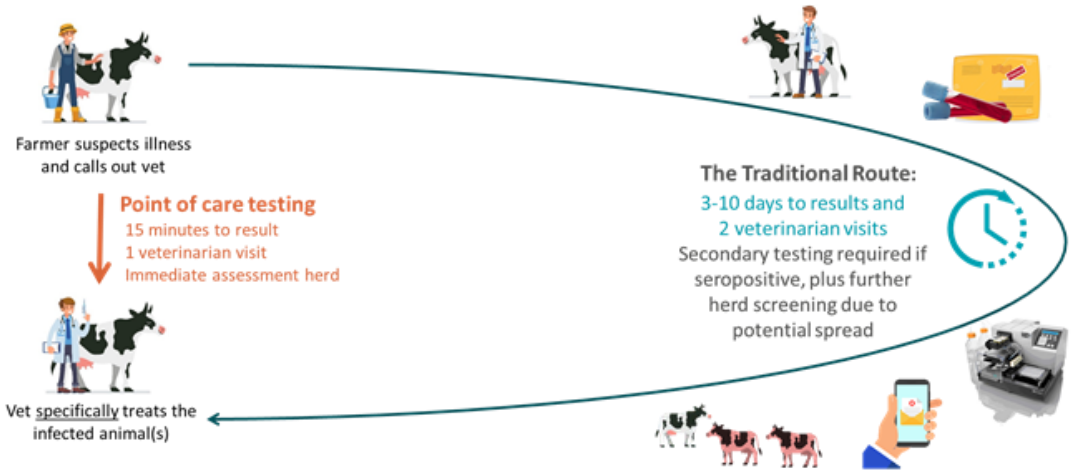


Figure 5.2: Proposed animal diagnostic methods, which will enable the veterinarian to take immediate action due to the 15 minute diagnosis.

5.2 Tyndall Immunosensors

Ultramicroband electrochemical immunosensors sensors are under development in the Tyndall National Institute that focus on the detection of the BRD respiratory pathogens [6]. Such pathogens include Bovine Viral Diarrhoea Virus (BVDV), Parainfluenza 3 (BPI3) and Infectious Bovine Rhinotracheitis (IBR) [7], [8], [9].

To selectively detect the individual pathogens, the UMEs must first be pre-modified with a capture biomolecule specific to the virus or antibody as shown in Figure 5.3. To attach the probe capture to the electrode surface, requires that the electrode surface is pre-treated. A polymer layer such as polyaniline is used to achieve this. To create a bond between the polymer and probe capture, a protein cross linker combination of EDC/NHS is used. The virus or antibody capture is subsequently deposited and a blocking agent called ethanolamine is used to inhibit non specific binding on the electrode surface.

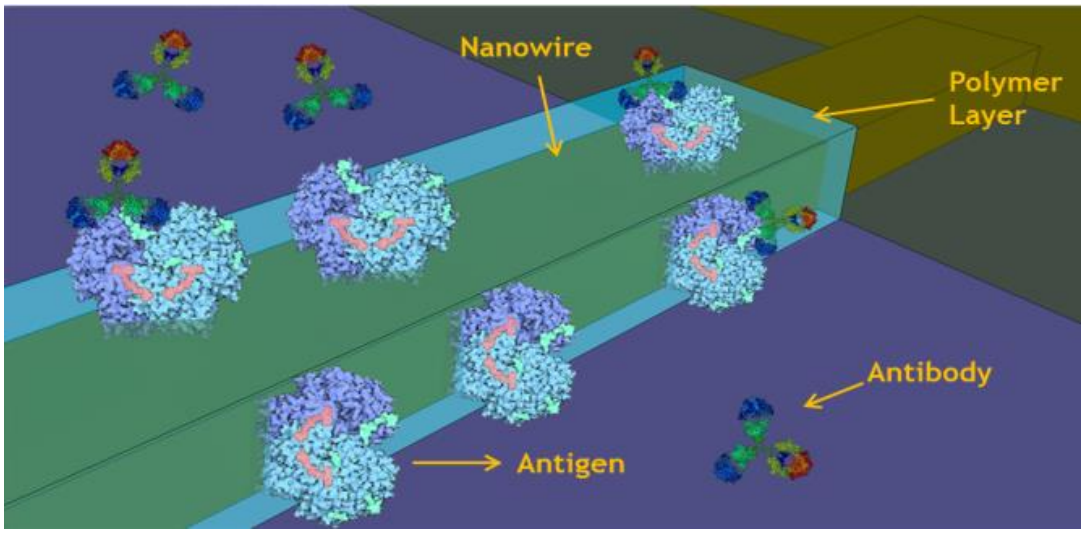


Figure 5.3: Animation of modified electrode surface where a polymer layer allows for the capture antigen to adhere to the nanowire surface.

A test is then performed on the electrode using buffer solution to attain a baseline measurement. The buffer solution is cleaned off the electrode and the serum sample is then deposited on the electrode surface. This is left to reside on the sensor for ten minutes to allow for the antibody or virus in question to bind to the surface of the electrode. The sample is then removed and a second measurement is taken using buffer solution once again. Due to the antibody or virus binding to the electrode, there will be an increase in impedance at its surface. This increase in impedance is due to the fact that the effective surface area of the UME should be reduced, thus reducing the probability of the redox probe reacting with the electrode. If there is a substantial or increase in impedance measured at the second test compared to the first, the sample is deemed to be infected.

5.3 CV Results

A diagnosis of serum samples for BVD through the use of a CV sweep was performed using the voltammetric portable potentiostat system described in Chapter 3. To determine the viability of the system for BRD diagnosis using the

ultramicroband sensors, the same test was performed on both the system and the Metrohm Autolab PGSTAT302N to detect BVD virus. To detect the virus, the BVD antibody was bound to the surface of an electrode through a series of chemical operations [6].

A baseline measurement was taken on the electrode using 1mM FcCOOH. As a control, serum without the BVD virus was deposited on the sensor for ten minutes as shown in Figure 5.4. A CV scan was subsequently performed using 1mM FcCOOH. The electrodes were then cleaned, using HB-SEP buffer and the BVD positive serum was left on the electrode for ten minutes. A final sweep was performed to diagnose the BVD positive serum.

As seen from Figure 5.5, there is a strong correlation between the commercial potentiostat and the ADuCM350 for each of the CV scans, despite differences that may have been caused by the evaluation board gain error or run to run electrochemical variation. This proves that the proposed system is fit for purpose for interrogation of BRD sensors using CV. As shown from the current magnitude comparison between the baseline and negative serum sample measurement there was a significant amount of nonspecific binding to the electrode surface. This shows that there was not sufficient blocking mechanisms active on this particular electrode surface to inhibit nonspecific molecules, such as bacteria, proteins, or other pathogens in the serum from binding. The current magnitude drop between the negative and positive CV scans indicates that the BVD virus has bonded to the antibody on the electrodes surface.

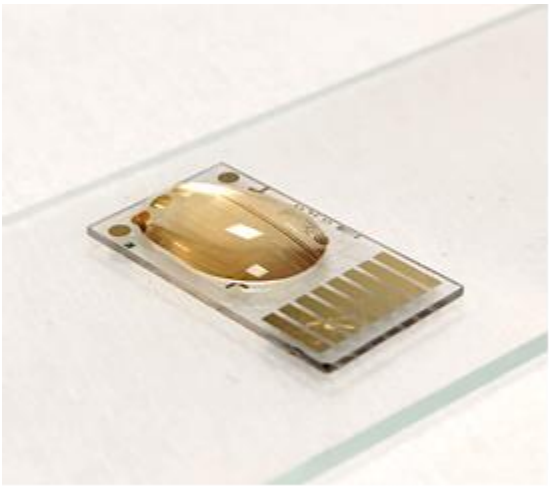


Figure 5.4: Serum sample residing on electrochemical sensor

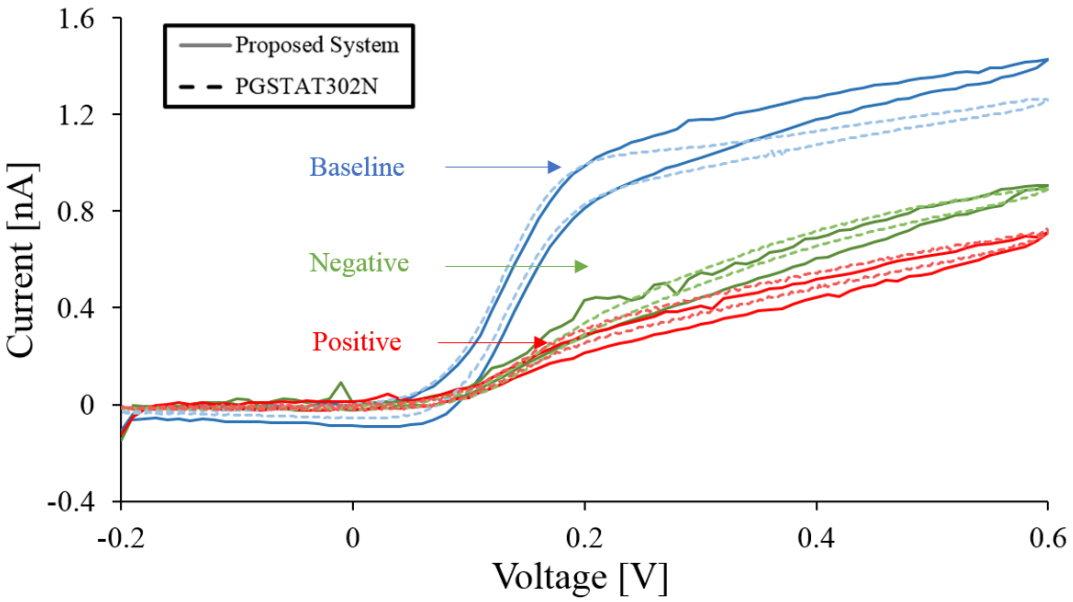


Figure 5.5: Cyclic Voltammogram of 1um microband electrochemical sensor using 1Mm FcCOOH for pre-test, negative BVD virus serum application and positive BVD serum application on Autolab PGSTAT302N and ADuCM350.

5.4 Portable Impedometric Potentiostat

EIS (Electrochemical Impedance Spectroscopy) is the test more commonly used to diagnose pathogens in the immunosensors as it provides a higher degree of sensitivity for interrogating the electronic characteristics of an electrode surface. The resultant Nyquist plot can be used to generate a Randles circuit, which, as described in Chapter 2, is an electrical model of the electrode surface**Invalid source specified.**.

5.4.1 Derivation of Specifications

The excitation signal used for the EIS test to diagnose serum samples is a 5 mV peak to peak amplitude AC signal, biased at 0.2 V. This signal is subsequently swept across a set range of frequencies. To diagnose the sample, the resultant diameter of the EIS Nyquist plot is used. As seen in Figure 5.6, the resultant plots are noisy as blood serum is a hostile matrix to use for analyte detection. This is because non specific molecules can bind to the electrode surface and inhibit readings. The diameter of the Nyquist plot, which corresponds to the charge transfer resistance of the reaction, increases for more concentrated BVD blood samples. Its diameter corresponds closely with the impedance value at 0.1 Hz.

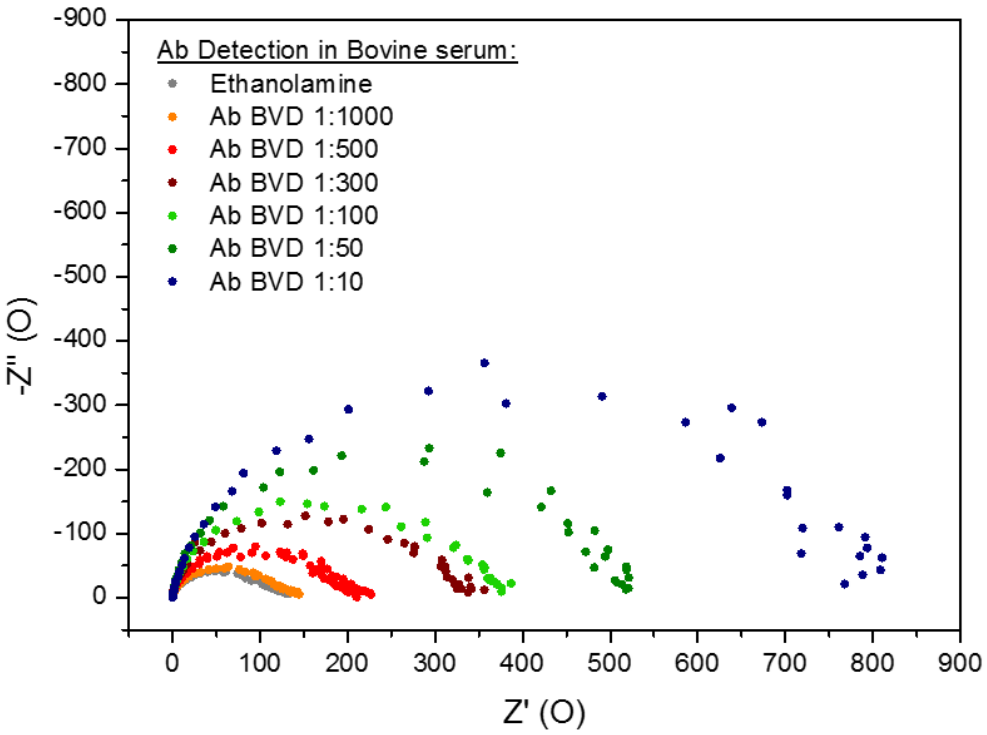


Figure 5.6: EIS plot for varying concentrations of BVD antibody for a nanowire electrochemical sensor using PGSTAT302N [13].

In order to make the proposed system as cost effective and efficient as possible, a narrower frequency range was identified in which a diagnosis would be possible. This meant that the complexity of the electronic interface, and it's measurement times are reduced. The frequency range of the system is 0.1 Hz to 10 Hz. This window was derived from Figure 5.7 as the greatest deviation between the impedance magnitude of positive and negative samples was in this frequency range. The frequency at which the highest impedance was observed corresponded to 0.1 Hz. As shown from Figure 5.8, the cut off between positive and negative serum samples is 700 MΩ so the required impedance that has to be measured is up to 1 GΩ. If the impedance result from the sensor is larger than 1 GΩ the sample is infected. From the graphs below, it could be seen that there was overlap region from 400 MΩ to 800 MΩ where there were both positive and negative samples. This means that the proposed system would struggle to make a definitive diagnosis for a proportion of samples that returned an impedance result in this region and thus the sample in question would require further investigation, which would most likely include forwarding the sample to a laboratory. This overlap window is currently limited by the variability of the sensor design and electrochemistry and it will reduce further with future improvements to the sensor design, therefore, a typical measurement value of 100 MΩ, seen in Table 5.1 was more appropriate, which is well within the capability of the proposed system.

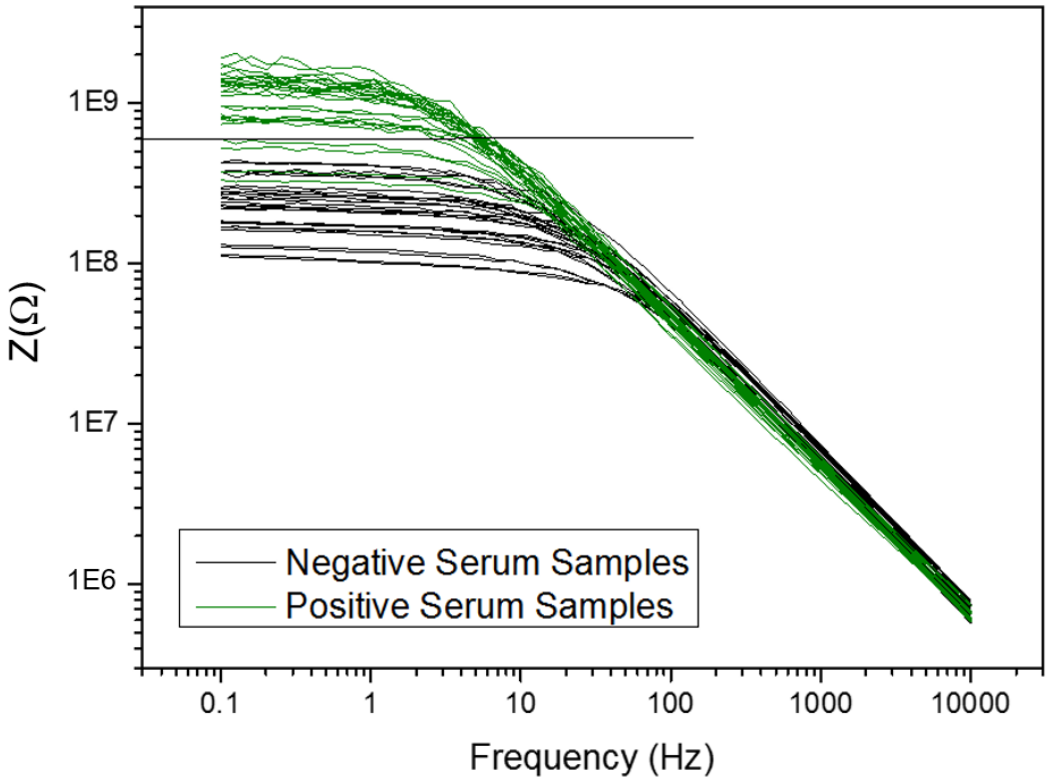


Figure 5.7: Bode plot of 100 different both positive and negative BVD samples using ultra microband electrochemical immunosensors.

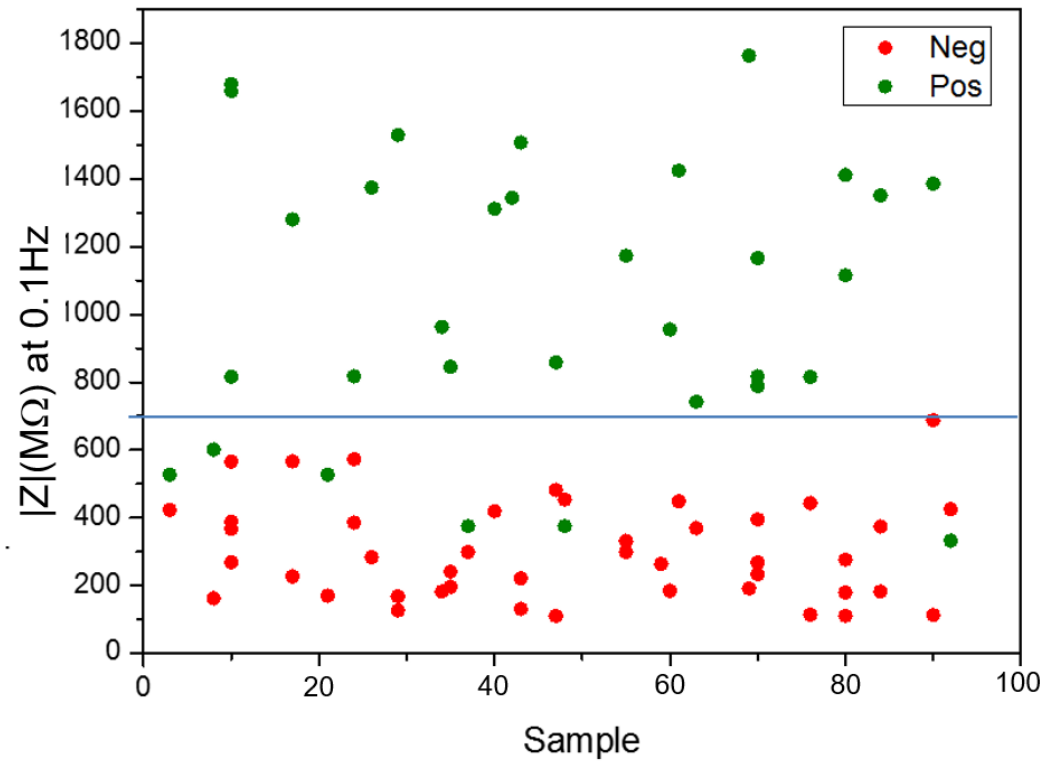


Figure 5.8: Scatter plot showing total impedance of various different BVD samples at 0.1 Hz using ultra microband electrochemical immunosensors.

Table 5.1: Impedance measurement system target specifications.

Parameter	Min	Typical	Max	Unit
Applied Signal Information				
Frequency Range	0.1	1	10	Hz
Amplitude		5		mV
DC Bias		0.2		V
Sensor Information				
Measured Impedance Range	10	100	1000	MΩ
Input Current from Sensor	5	50	5000	pA
Sensivity Aim (1% of Min.)		50		fA

5.4.2 ADuCM355 as a SoC for Impedance Measurements

Although the ADuCM350 is able to perform impedance measurements, the ADuCM355 [11] has a superior impedance measurement engine and also has additional switches that allow for external customisation of the AFE path. This was particularly useful for using an external low pass filter which will be discussed later in the chapter.

5.4.2.1 *DC Biased Excitation Signal Generation*

The ADuCM355 has an output DC range to the sensor of ± 1.2 V, therefore it is comfortably able to provide the required 200 mV DC bias. Two low power DACs are used to provide the DC bias. While, the potential at the WE is controlled by the Vzero 6 bit DAC output as shown in Figure 5.9, the 12 bit Vbias output determines

potential required at the RE. The excitation amplifier uses feedback from Vbias and Vzero to apply an appropriate voltage to the CE. A precision DAC is used to provide the AC excitation signal [12]. This signal can be programmed to be as low as 0.0016 Hz.

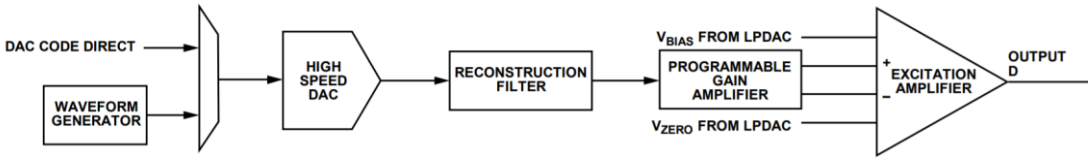


Figure 5.9: Overview of excitation signal generation path, used in the ADuCM355.

5.4.2.2*Signal Processing*

` Both the common mode node, TIA_N and the resultant TIA voltage node, TIA_P, as shown in Figure 5.11, are used for the differential ADC measurement. As seen from Figure 5.10, the signals are buffered and can be amplified by a factor of up to 9 through a programmable gain amplifier. An antialiasing filter is used to mitigate any out of band signals such as environmental electronic noise that would otherwise alias in-band when sampled degrading the signal of interest. The signal is once again buffered before it is digitised by the ADC.

Similarly to the ADuCM350, the ADuCM355 utilises a 16 bit ADC. The ADuCM355 also includes a dedicated digital DFT hardware acceleration block, which is used to process ADC output codes. The DFT block outputs a complex number which is representative of the overall DFT result. It uses a preselected number of ADC samples for the applied AC signal. The result from the DFT is sent to the Cortex M3 microcontroller via a die to die interface in the package. Programmable Sinc2 and Sinc3 filters are available for use on the signal path, these filters are useful for oversampling [13].

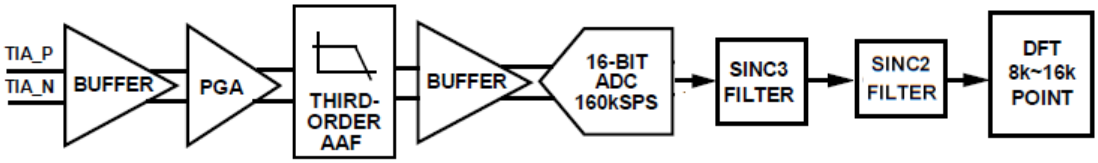


Figure 5.10: Block diagram of ADC, DFT and signal processing for EIS measurements using the ADuCM355.

5.4.2.3*Performing Impedance Measurements using the ADuCM355*

To perform an impedance measurement using the ADuCM355, the output current of a known calibration resistor is taken first and then compared against the unknown sensor impedance. This ratiometric measurement method compares the DFT outputs corresponding to the calibration resistor and sensor in question from the ADuCM355 as described below:

$$|Z_{sensor}| = \frac{I(s)_{Rcal}}{I(s)_{sensor}} \, x \, R_{cal.} \tag{5.1}$$

Where Z_{sensor} is the impedance of the electrochemical sensor, $I(s)_{Rcal}$ is the DFT calibration current and $I(s)_{sensor}$ is the DFT sensor current. An inbuilt function in the ADuCM355 calculates the relative phase of R_{cal} and the sensor, where the absolute phase is calculated using with the following equation:

$$Z_{sensor}(phase) = Ang(I(s)_{Rcal}) - Ang(I(s)_{sensor}). \tag{5.2}$$

Where *Ang()* is the function to calculate the phase angle.

5.4.3 Development of System

5.4.3.1*Trans-Impedance Amplifier*

As seen from table 5.1, the maximum input current to the TIA is 5 nA. The ADC input channel is optimised for a ± 0.75 V output range from the TIA.

Therefore, the sizing of the RTIA is based on that voltage range and is governed by the following equation:

$$RTIA = \frac{\mathrm{Vout}_{TIA}}{\mathrm{I}_{max}}, \tag{5.3}$$

and

$$RTIA = \frac{750\ \mathrm{mV}}{5\ \mathrm{nA}} = 150\ M\Omega. \tag{5.4}$$

Where, $Vout_{TIA}$ is the maximum input voltage swing into the TIA and I_{max} is the maximum current that must be measured by the system. The high speed TIA that is used for impedance measurements in the ADuCM355 has a programmable resistor matrix of values up to 160 kΩ. Unfortunately, this isn't large enough to measure the impedances associated with the Tyndall immunosensors, so an external resistor of 100 MΩ had to be used.

5.4.3.2*Calibration Resistor*

Due to the fact that the calibration resistor was used to perform a ratiometric measurement, a value was chosen that reflected a typical impedance measurement using the system. Therefore the calibration resistor chosen was 100 MΩ based on Table 5.1.

5.4.3.1*Low Pass Filter*

In order to improve the noise response the bandwidth of the proposed system is limited only to the necessary measurement window. Narrowing the measurement window from 0.1 Hz to 10 Hz meant that a low pass filter (LPF) stage could be used after the TIA stage to improve noise performance. A passive LPF is used with a cut

off frequency of 15 Hz, as is shown in Figure 5.11. The resistor used is 100 kΩ, while the capacitor is 100 nF. The cut off frequency of the RC filter is governed by following the equation:

$$f_c = \frac{1}{2\pi RC}, \tag{5.5}$$

and

$$f_c = \frac{1}{2\pi(100x10^3)(100x10^{-9})} = 15.92\ Hz. \tag{5.6}$$

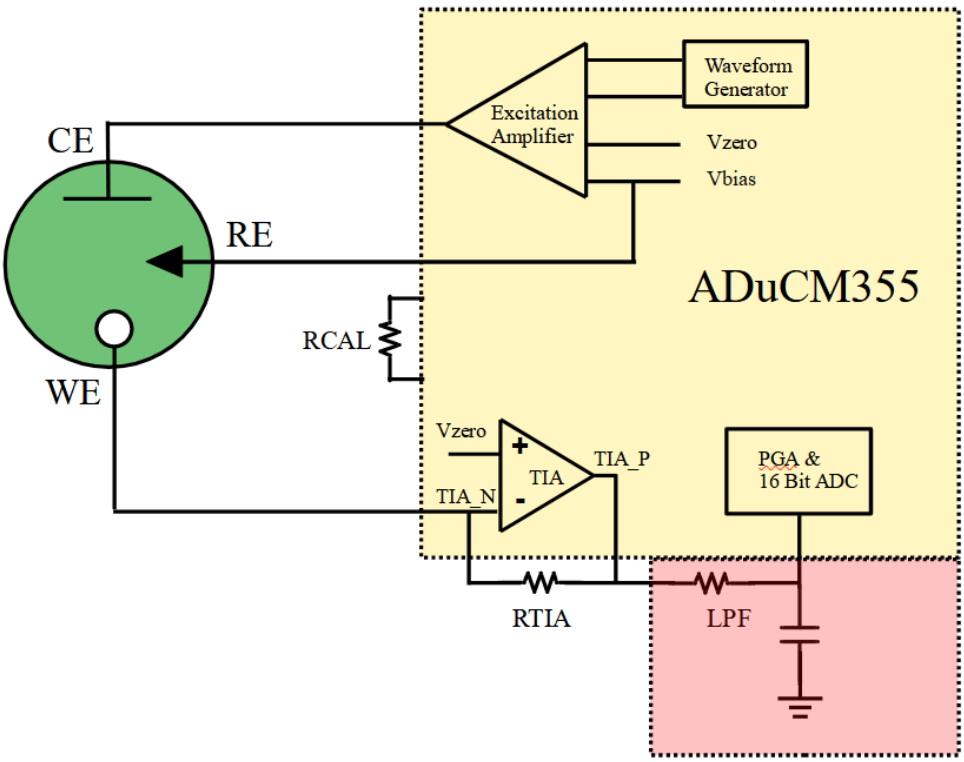


Figure 5.11: Simplified circuit diagram of EIS capture circuit, including the excitation amplifier, trans-impedance amplifier and low pass filter.

5.4.3.1*DFT Impedance Measurement*

The ADuCM355 DFT engine takes raw ADC output data from the AFE and transpose the current response into separate respective frequency bins. This is performed for both the RCAL and sensor measurements as seen in Figure 5.12. To attain an impedance magnitude result, the area underneath the spectral response of the sensor is compared to the known RCAL results. In the example in Figure 5.12, the RCAL is 100 MΩ and the dummy cell used is 200 MΩ. As seen in Table 5.2, different sampling frequencies were used that reflected the measurement frequency to fill the DFT bins. It was important to limit the measurement time as much as possible while maintaining accuracy to make the device a viable tool for use in the field.

Table 5.2: DFT parameters for different EIS excitation frequencies.

Frequency (Hz)	**DFT Number**	**Sampling Frequency (Hz)**	**Measurement Time (s)**
0.1 - 0.5	16384	250	32.7
0.51 - 5	16384	375	21.83
5 - 10	16384	1123	7.28

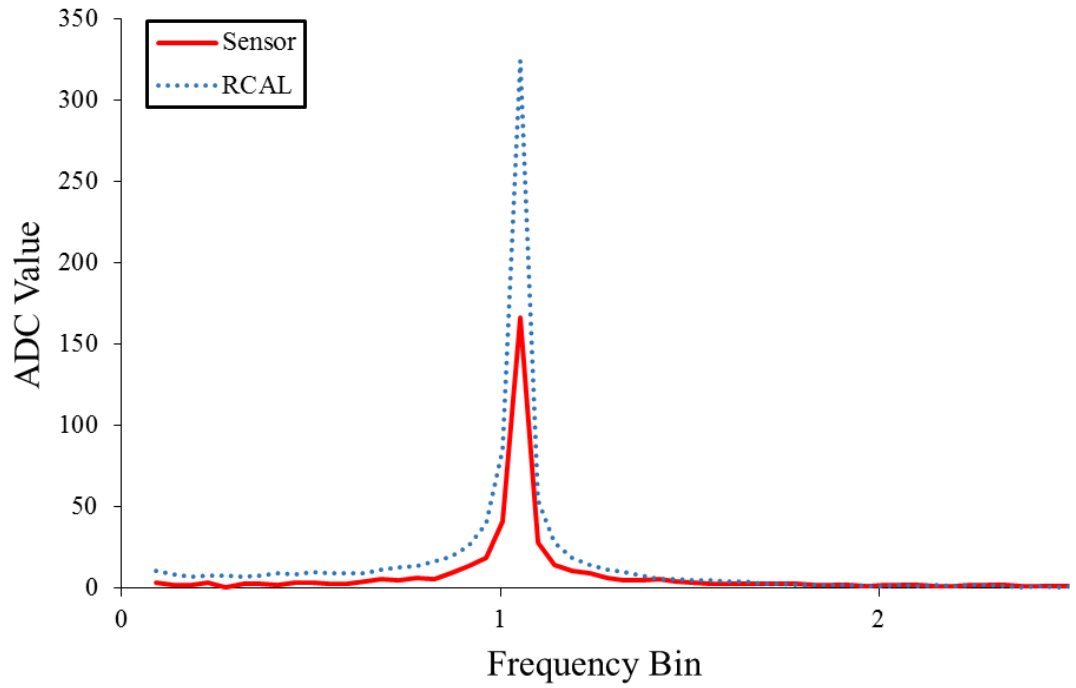


Figure 5.12: Spectral response for EIS measurement at 1Hz on 200MΩ resistor using ADuCM355, compared against the know external100 MΩ RCAL resistor.

5.4.3.1*Noise Improvements*

To portray the measures taken to improve noise performance of the device, the spectral response of the device was shown for measurements on a 200 MΩ dummy cell. The first iteration of the system used the ADuCM355 evaluation board. The predominant noise source was the 50 Hz mains hum from electrical equipment used in the test and nearby equipment. The current magnitude of the 50Hz DFT bin was 9 times larger than the current response at the 1Hz EIS measurement frequency. This out of band noise has to be nullified to achieve more accurate impedance measurements.

The most significant measure taken to improve the devices susceptibility to noise was to shorten the length of the signal path. This was achieved by optimising the length of the AFE signal tracks in the custom PCB as previously discussed. Figure 5.13 and Figure 5.14 shows that by reducing the length current measurement

signal path, the effects of ambient noise sources such as 50 Hz noise is minimised. The calibration resistor has a much shorter signal path as it is totally encompassed on the PCB, this resulted in the ambient 50Hz noise having a negligible effect on the measurement. Each of the sensors that the proposed system will interface to will have an associated extra length of signal path. In this instance, as a spark fun SD sniffer [14] is used to interface to the 200MΩ dummy cell.

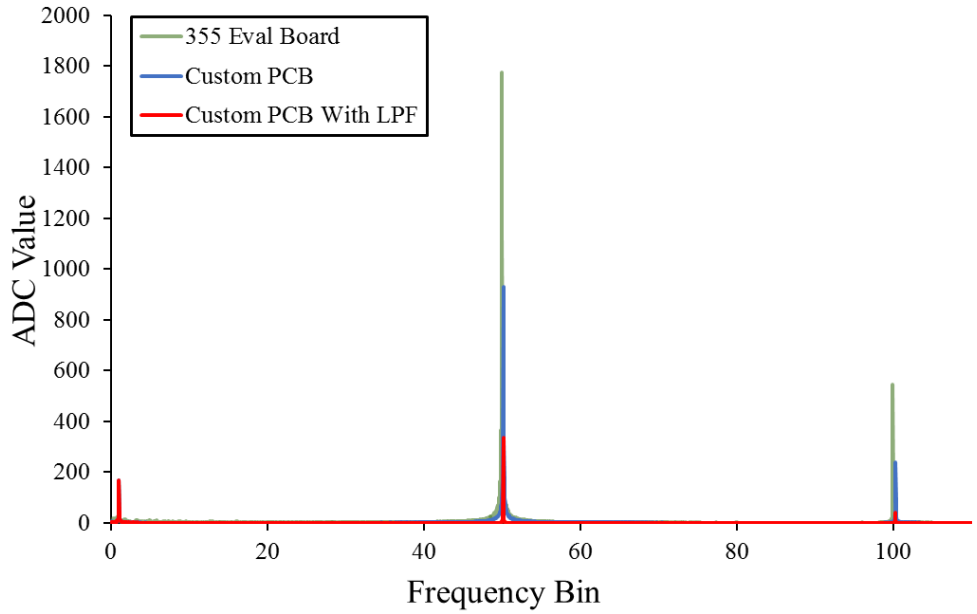


Figure 5.13: Spectral response of dummy cell signal path using different board configurations which shows that a shorter signal path and a LPF reduces the effect of ambient noise .

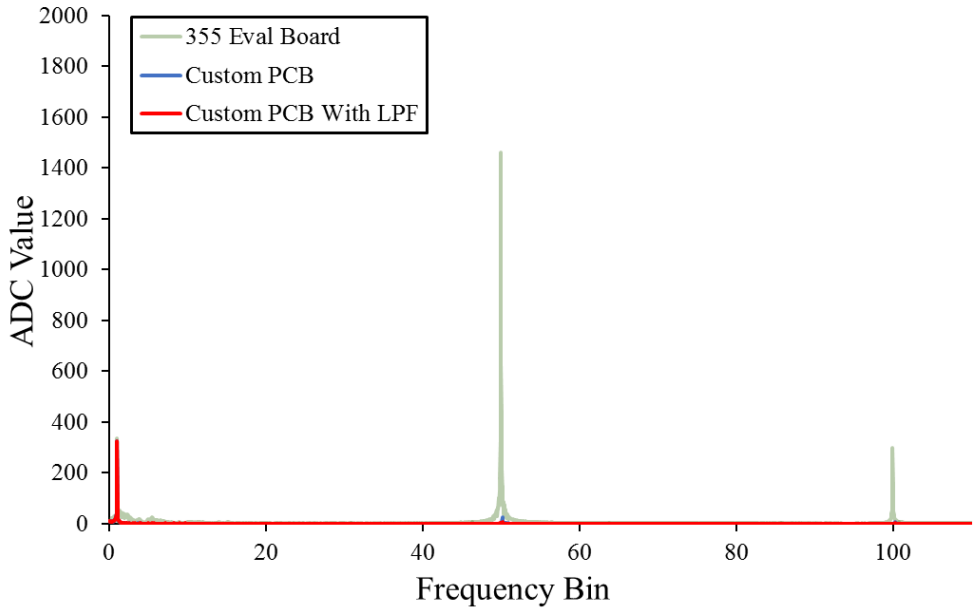


Figure 5.14: Spectral response of RCAL signal path using different board configurations which shows that a shorter signal path significantly reduces the effect of 50 Hz noise.

The 10 Hz passive low pass filter supressed out of band noise further. Figure 5.13 reflects this with significantly smaller current responses at 50Hz frequency and its 100 Hz harmonic.

5.4.4 PCB Implementation

The ADuCM355 utilised a CC-72-2 package, the dimensions of which can be seen in Figure 5.15. This package has less space underneath the chip compared to the ADuCM350. This meant that standard through hole vias weren't suitable to attain a signal path from the inside pads. Blind vias connect an outer layer to one or more inner layer but do not go through the PCB [15]. These had to be used to access some of the pins on the ADuCM355 chip. This contributed to a slightly more expensive PCB manufacturing cost.

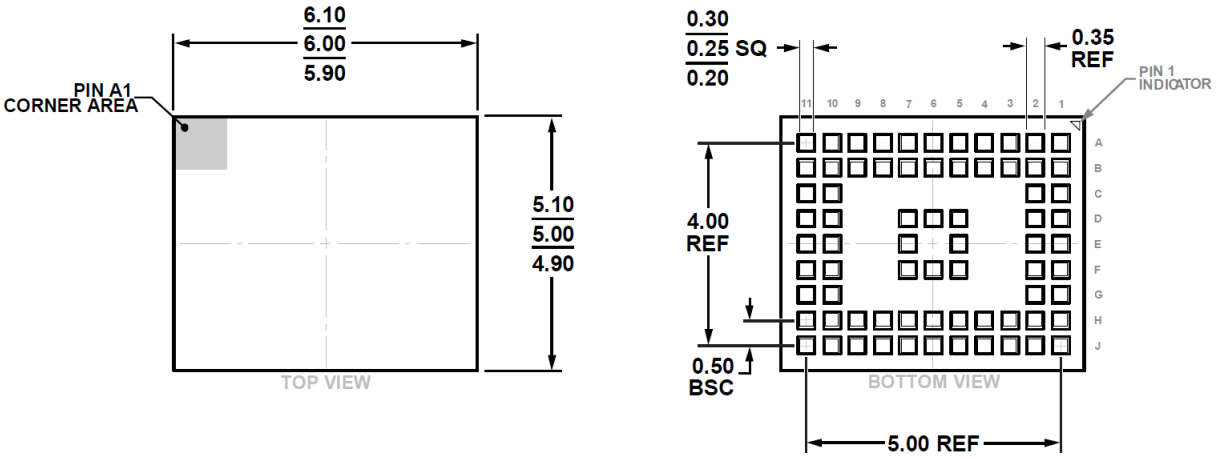


Figure 5.15: Top and bottom view of ADuCM355 chip.

5.4.4.1*AFE Implementation*

The system interfaces to the sensor via a female micro SD port. The signal paths of the ADuCM355 were made as short as possible to the SD port to mitigate parasitic noise. This is reflected in the proximity RTIA and RCAL, R1 and R2 to the ADuCM355 in Figure 5.16. Precision, low drift 100 MΩ resistors are used for RTIA and RCAL [16].

Although not part of the AFE, decoupling capacitors that are used for the ADuCM355 are placed as close as possible to their corresponding pin in the package for maximum performance.

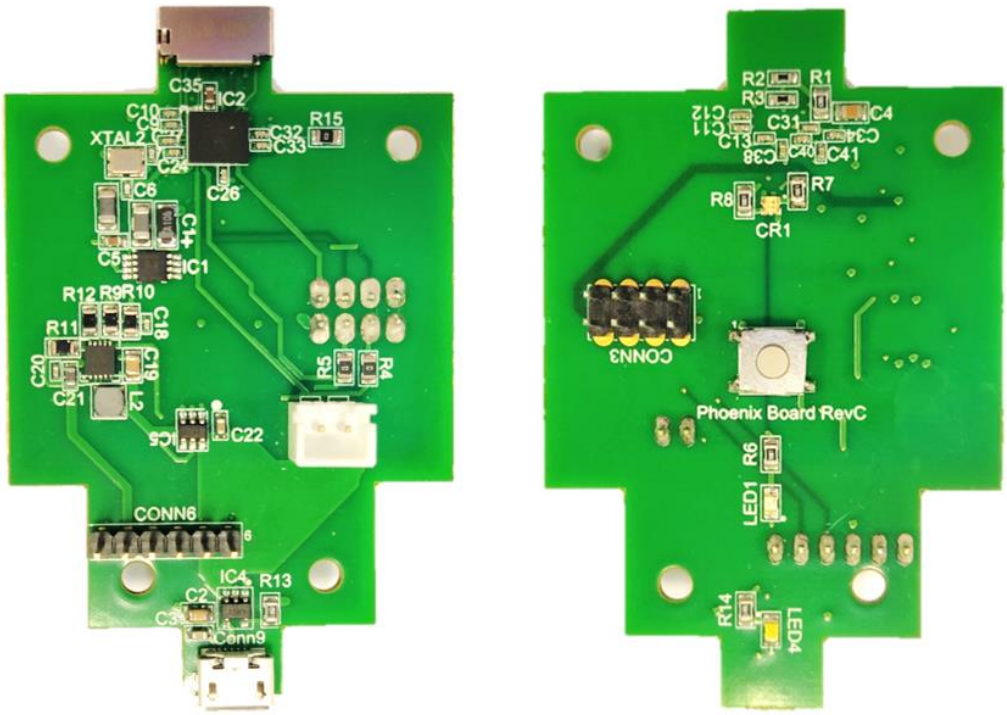


Figure 5.16: Front and back of portable EIS data acquisition PCB.

5.4.4.2*Industrial Design*

To improve the proof of concept, a commercial prototype of the system was made in conjunction with Dolmen Design and Innovation Consultants [17]. The device is designed to be an easy to use diagnosis tool for veterinarians on a farm. As well as the EIS PCB described in this chapter, the prototype also integrated the microfluidics system which is in development for use with electrochemical immunosensors. The sample can be delivered to the sensor through the sample inlet as seen in Figure 5.17. A first wash blister is broken to clean the sensor surface while the second wash blister delivers FcCOOH for a measurement to be performed.

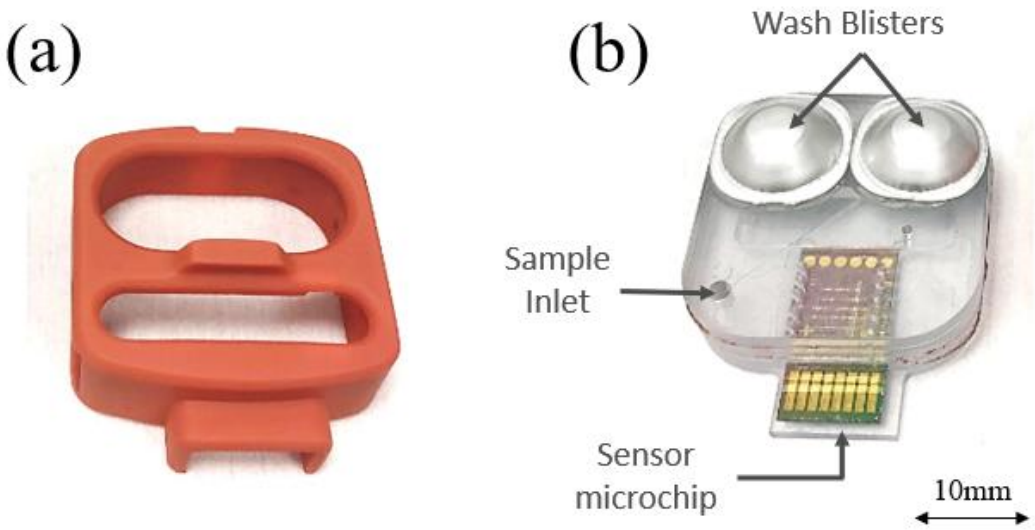


Figure 5.17: (a) Proposed Sensor Microfluidic Cartridge, (b) Proposed Sensor Microfluidic Platform which includes the electrochemical sensor under test, wash blisters and a sample inlet.

To create a device that would closely resemble the end product used by veterinarians, extra features were added to the EIS diagnosis PCB. The system was made battery rechargeable through the use of a charge protection IC on the PCB and an 1800 mAh LiPo battery [18]. Similarly to the previous PCB, the HC-05 was used to enable a Bluetooth connection via a smartphone application, which will be discussed later in this section. A boost converter is used to step up the battery voltage to 5V [19] and a linear regulator [20] is used to provide a stable 3.3V for the ADuCM355. To toggle the power of the device, an on off controller is used [21]. Indicator lights are utilised for to give feedback to the user based on the test result. Lights are also used to indicate whether a Bluetooth connection is made and to indicate the charging status of the device. These features were integrated into the system prototype which is shown in Figure 5.18. The schematic design and PCB layout was performed using Easy PC. The layout and schematic of the device can be seen in the Appendix, section A.5.

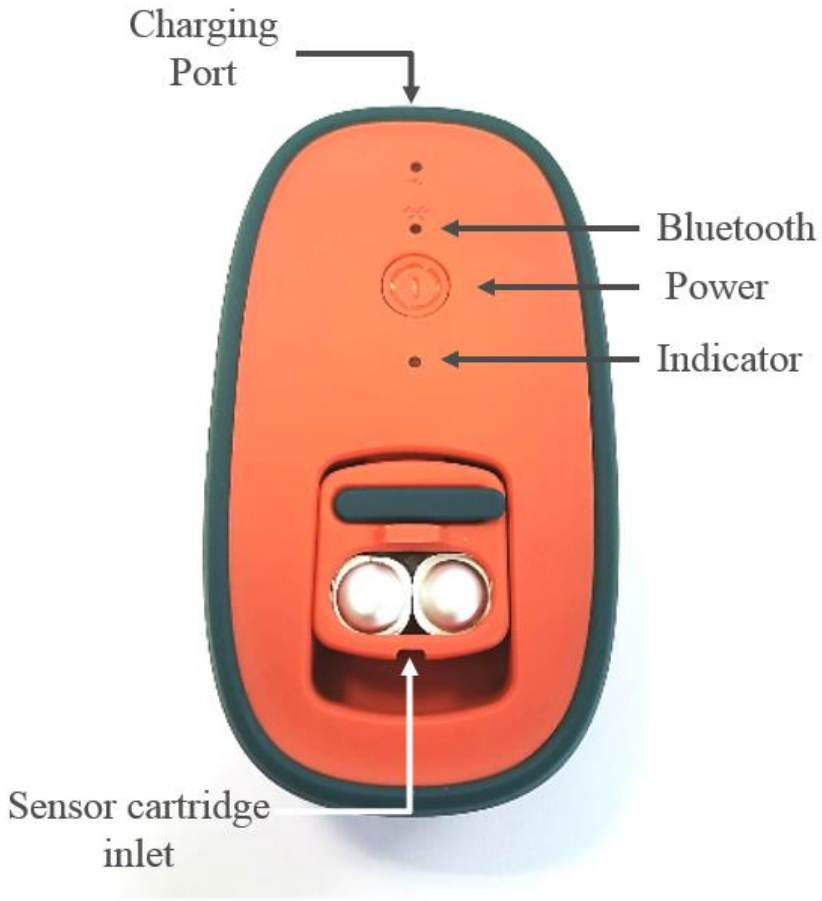


Figure 5.18: On farm diagnosis prototype device which includes the sensor cartridge and an inlet, indicator lights, a power button and charging port.

5.4.4.3*Device Cost*

The cost of the electronic components of the system is €186.01 as seen in Table 5.3. Similarly to the PCB in the last chapter, the prices are inflated as the PCB and components were purchased for a small run of 10 PCBs. Despite this, the electronics are still an order of magnitude less expensive compared to other portable devices that can perform impedance measurements in a similar range such as the Palm Sens 4 [22] and the Interface 1010B [23]. Such a comparison can be seen in Table 2.2.

Table 5.3: Cost of electronics in the proposed system.

Item	Cost (€)
PCB	
Unit	28.00
Components	43.57
Assembly	96.00
	167.57
External Components	
HC-05	2.78
LiPo Battery	15.66
	18.44
Total	**186.01**

5.4.4.4*User Interface*

A Bluetooth serial connection smartphone application is used [24] to interface to the portable EIS system. By entering a number from one to six, the user can initialise a test, selecting one of the six electrodes. The system subsequently prints the resultant phase and impedance data points to the screen. Once the test is completed, the user has the option of saving the dataset to a cloud service such as Google Drive.

5.5 Results

5.5.1 Device Calibration

5.5.1.1*Dummy Cell Calibration*

To characterise the system, while removing electrochemical noise, an EIS scan was performed using a range of dummy cells. These cells were used to represent the range of different impedances that the proposed system is required to

measure from an ultramicro scale electrochemical immunosensor. Each measurement was repeated using the PGSTAT302N, as shown in Figure 5.19 and Figure 5.21. A scan from 0.1 Hz to 10 Hz was performed using a 5 mV amplitude sine wave. The dummy cells were placed in a Faraday cage for the PGSTAT302N but were not for measurements using the custom PCB. The average error of the magnitude measurement was 1.29 %, while the phase error was 0.64º. The most important frequency measurement point for the system is at 0.1 Hz as it represents the charge transfer resistance of the system. This value is an important parameter used to diagnose samples later in the chapter. For 0.1 Hz, the average magnitude error was 1.80% while the phase error was 1.53º.

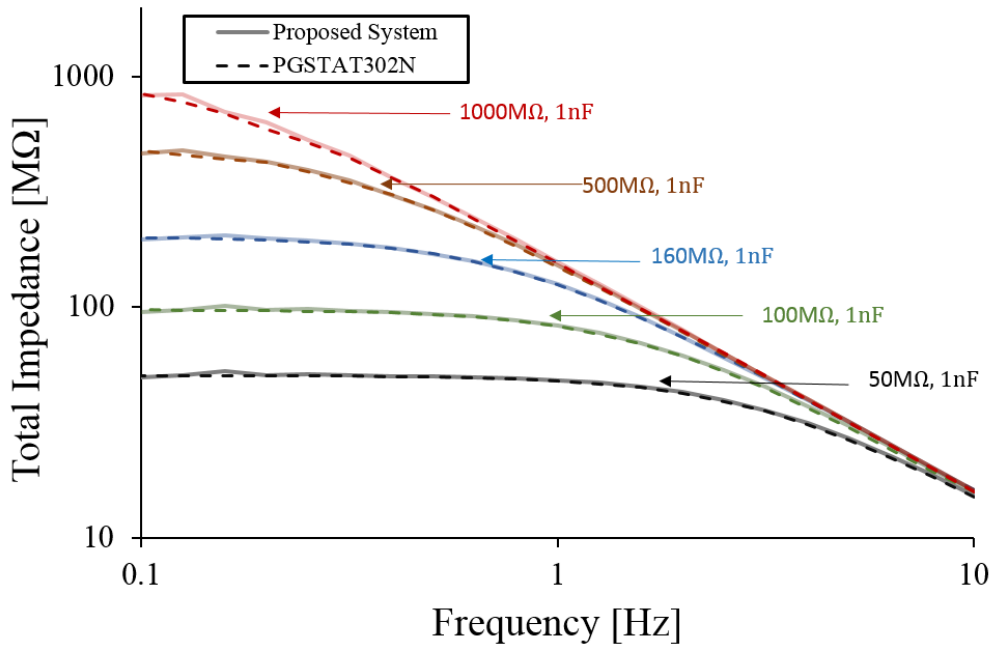


Figure 5.19: Magnitude response of system and Autolab PGSTAT302N, for EIS test using various dummy cells of similar impedance values expected from electrochemical ultramicro immunosensors.

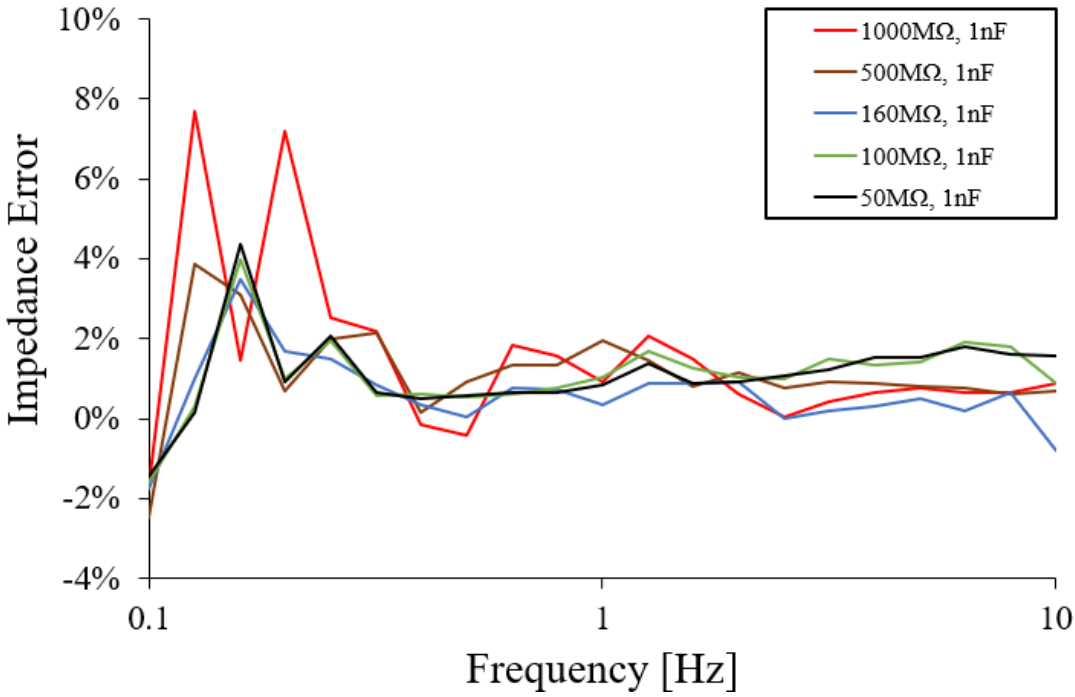


Figure 5.20: Error between of system and Autolab PGSTAT302N, for EIS test using various dummy cells of similar impedance values expected from electrochemical ultramicro immunosensors.

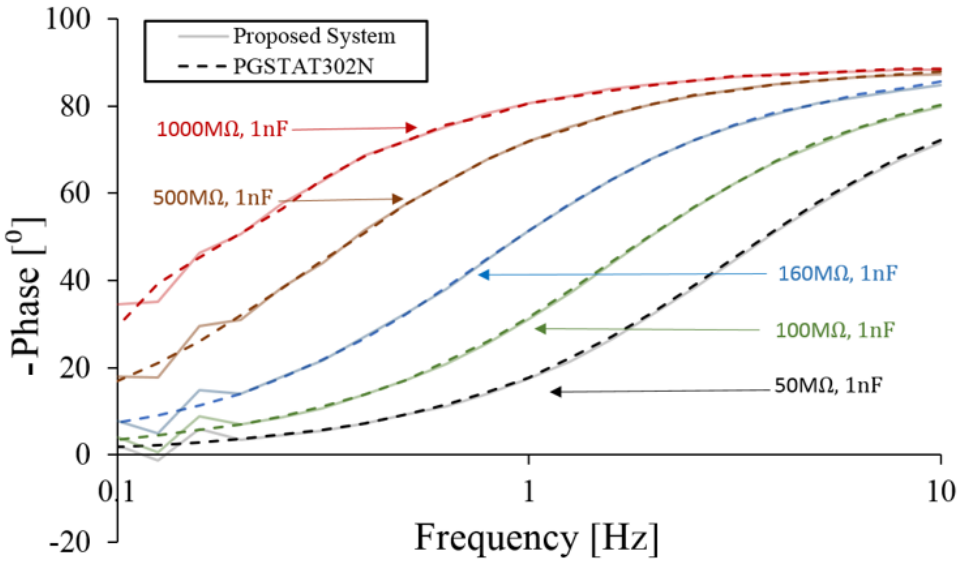


Figure 5.201: Phase response of system and Autolab PGSTAT302N, for EIS test various dummy cells of similar impedance values expected from electrochemical ultramicro immunosensors.

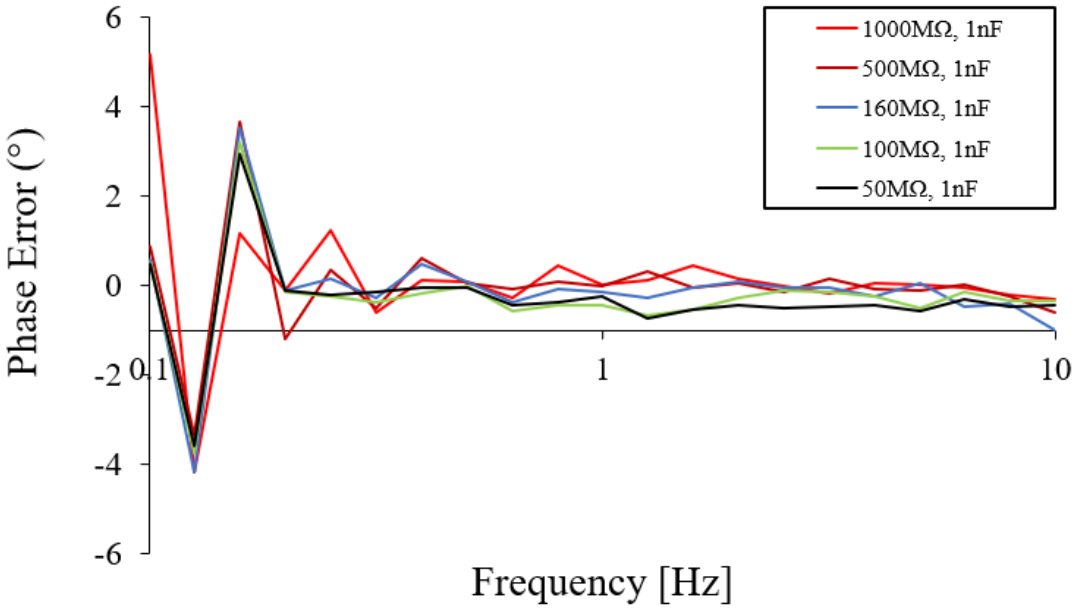


Figure 5.212: Phase response of system and Autolab PGSTAT302N, for EIS test various dummy cells of similar impedance values expected from electrochemical ultramicro immunosensors.

5.5.1.2*Electrochemical Cell Calibration*

To verify that the system could interface to electrochemical sensors with similar accuracy to benchtop equipment, EIS results were compared across a range of concentrations of FcCOOH. The tests were performed across a range of concentrations that would require the custom PCB to perform measurements across its full range of 10 MΩ to 1 GΩ. For voltammetric tests, such as CV, the relationship between the peak current and concentration is linear. For EIS, a more logarithmic relationship is seen.

Through performing measurements using electrochemical sensors in a laboratory environment, a number of issues were found. Firstly, the counter and reference pins on the custom PCB were incorrectly orientated in the custom PCB, meaning that the Sparkfun SD sniffer was required to interface to the correct pins, as

shown in Figure 5.23. Through interrogating the system during the test, it was found that there was DAC offset error, meaning that the bias voltage between the RE and WE wasn't correct. The DC bias being maintained between the RE and WE was incorrect by up to 12 mV, depending on the ADuCM355 chip used. This error was calibrated out of the each device by adding the offset voltage to the CE bias potential.

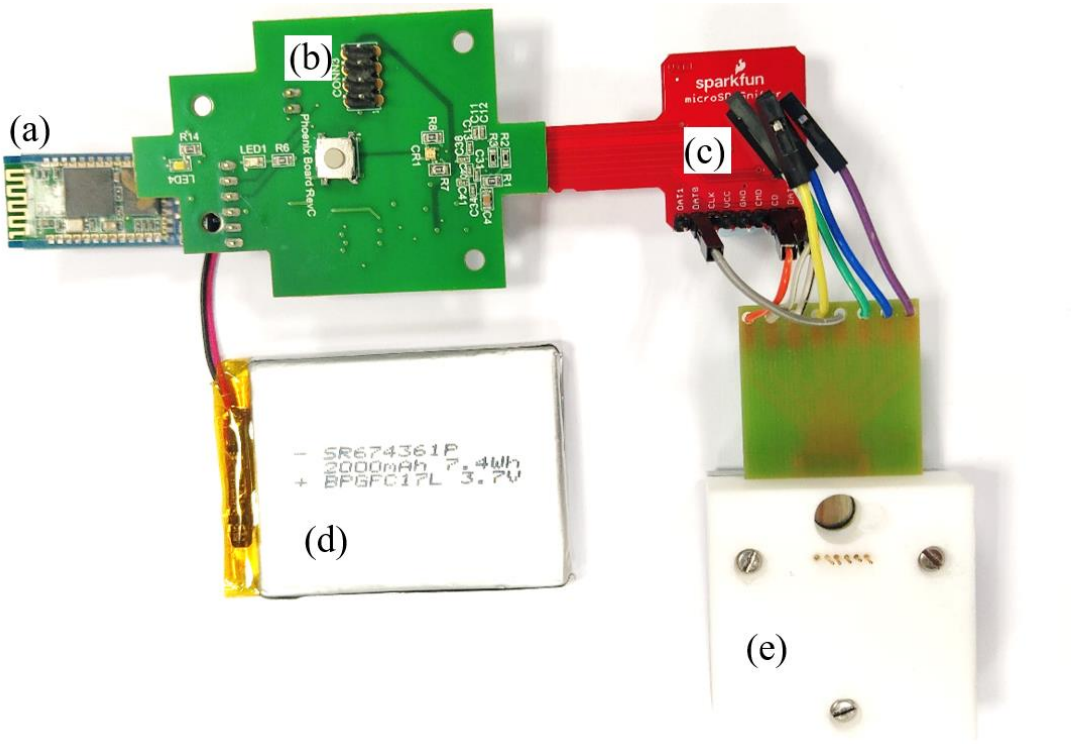


Figure 5.223: Measurement apparatus for EIS test; (a) HC-05 Bluetooth Module, (b) Proposed System PCB, (c) Sparkfun SD Edge connector,(d) Battery, (e) Electrochemical Sensor.

It was also found that through performing measurements in environments with a high degree of electromagnetic noise, such as a laboratory, the measurements were significantly distorted. Therefore, test results were obtained through the use of laboratory faraday cage. Test results were taken using a homemade Faraday cage, consisting of a box layered with tinfoil, to verify that the measurements could still be performed at a low cost in the field.

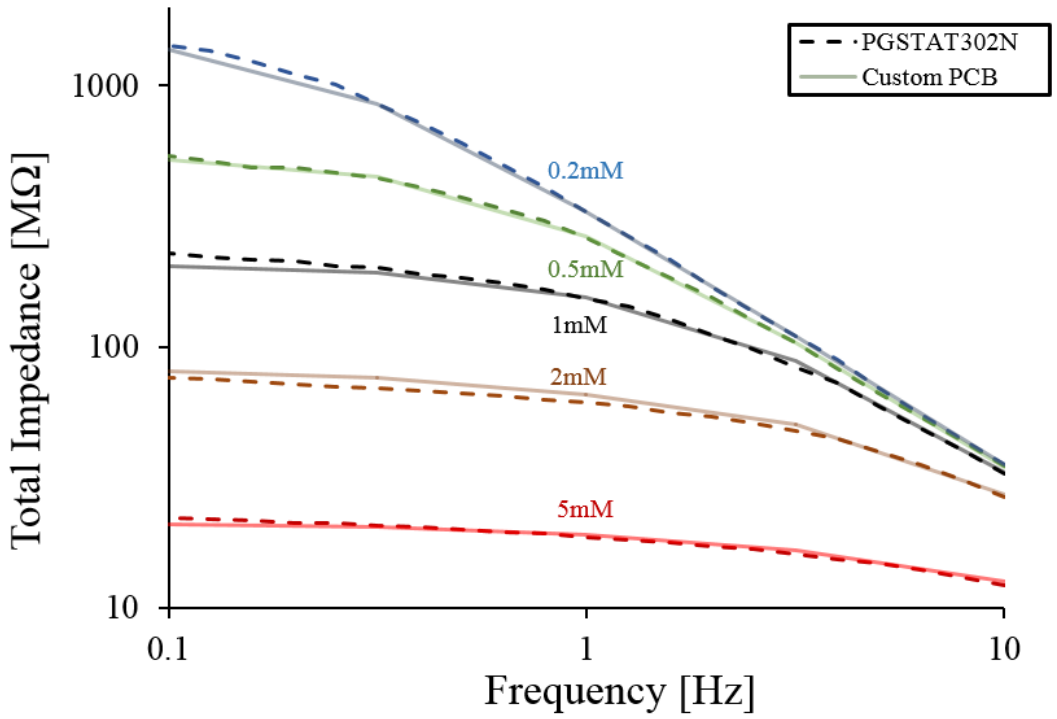


Figure 5.234: Magnitude response of EIS scan from 0.1 Hz to 10 Hz, AC amplitude 5 mV, 0.2 V DC bias for various concentrations of FcCOOH using both the custom PCB inside a low cost faraday cage and the PGSTAT302N for an ultra microband electrode.

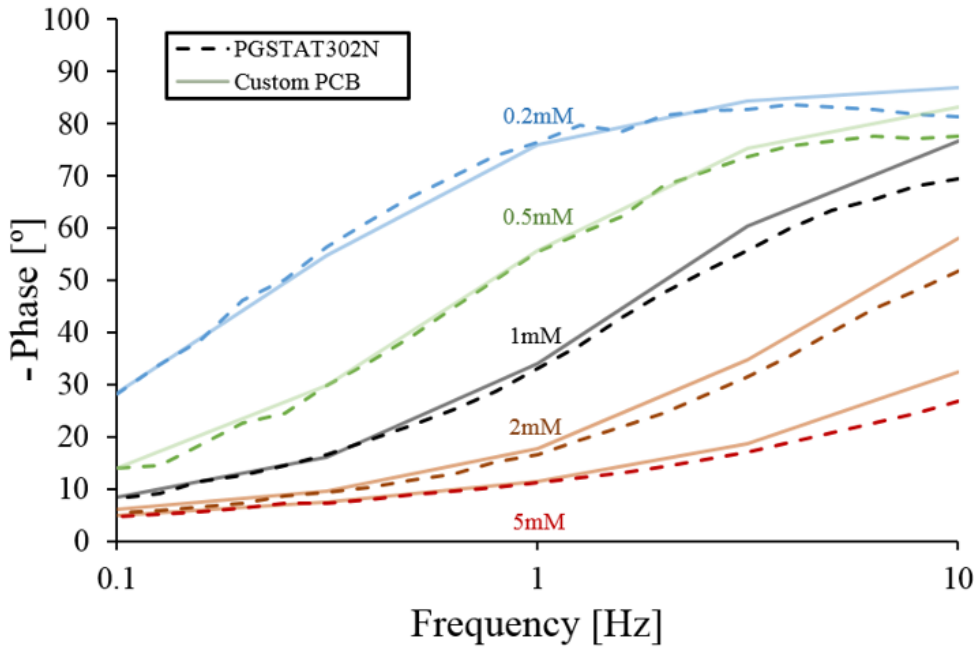


Figure 5.245: Phase response of EIS scan from 0.1 Hz to 10 Hz, AC amplitude 5 mV, 0.2 V DC bias for various concentrations of FcCOOH using both the custom PCB inside a low cost faraday cage and the PGSTAT302N for an ultra microband electrode.

Due to the fact that a single impedance measurement using the proposed system took up to two minutes at 0.1 Hz, two frequency data points were taken per decade as opposed to the ten points per decade of the PGSTAT302N. This amounted to five data points per scan resulting in a 12 minute test time. The likelihood of the sensor being damaged or its properties changing is increased through exposing the electrode to the electrochemical test over a long period of time. Ten separate EIS tests had to be performed on a single electrode in order to complete the experiment.

Tests were performed using a single electrode, measuring from the highest concentration to the lowest as shown in Figure 5.24 and Figure 5.25. Each test was performed on the custom PCB first and subsequently on the PGSTAT302N. The average magnitude error was 3.16 % while the phase error was 2.01 ^{0}. There is a clear correlation of all results between the custom PCB and PGSTAT302N which verifies that the system is fit for purpose. Furthermore, there is an R^2 value of 0.994

when the total impedance of ferrocene at 0.1Hz is plotted against ferrocene concentration, as shown in Figure 26.

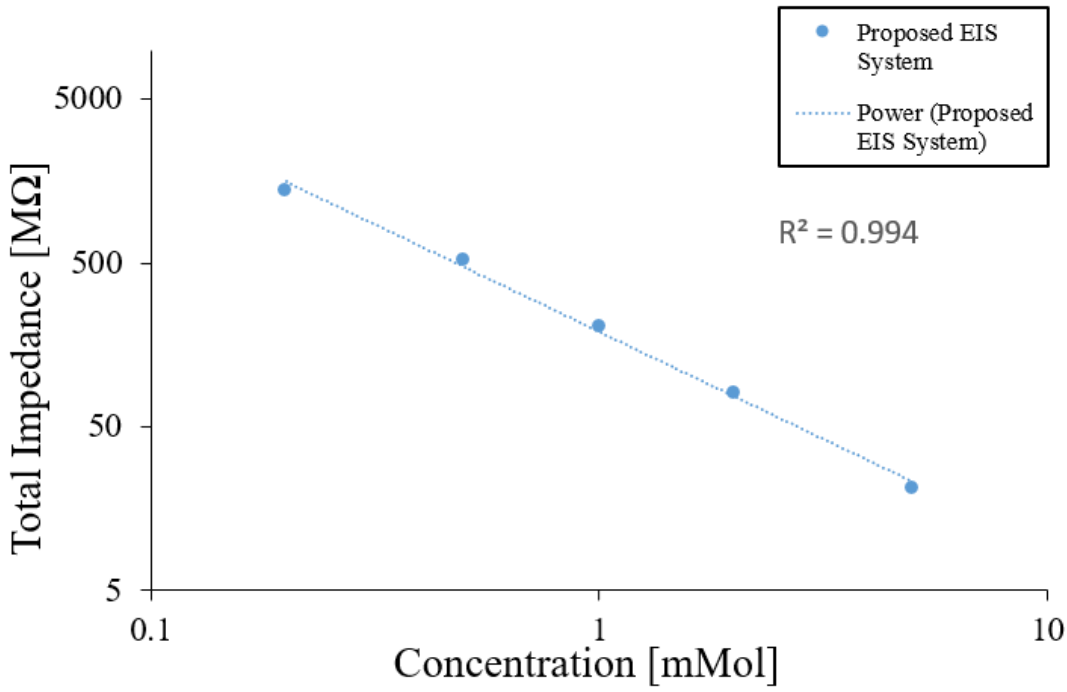


Figure 5.256: Calibration plot for EIS measurements using the proposed system at 0.1Hz in varying concentrations of Ferri-Ferrocyanide, n=1.

5.6 Limitations of System

One limitation of this system is that it is not suitable for use near noise sources, particularly large, high voltage equipment. This was evident when characterising the proposed system near an AIX200 atomic vapour deposition machine [25]. Despite using a faraday cage, the output was distorted and the resultant impedance measurement was incorrect by a factor of 15%, the effects of which are shown in Figure 5.25. A time domain representation of the sensor and RCAL signal can be seen in Figure 5.27, where the AIX200 was switched off. In order to accommodate for measurements to be taken near noise sources, guard traces

may need to be employed for AFE signal lines or a superior faraday cage, this is discussed in more detail in the future work section of this thesis.

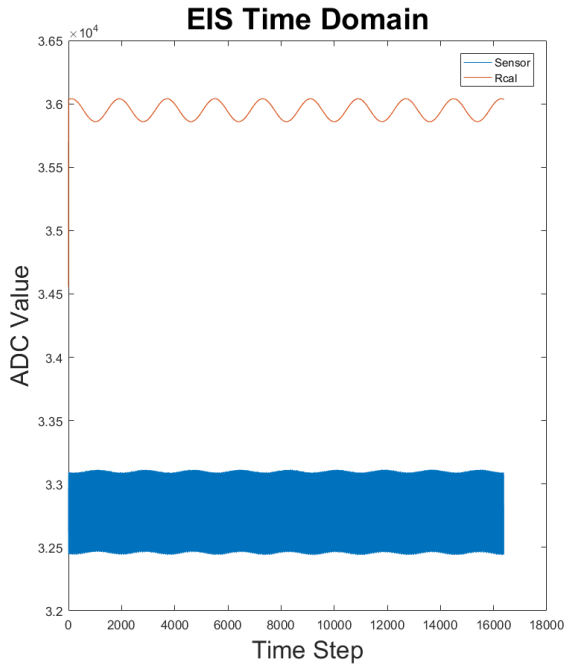


Figure 5.27: Raw ADC values of EIS measurement on 1 GΩ, 1 nF dummy cell using the proposed system in an environment without high volumes of ambient electromagnetic noise.

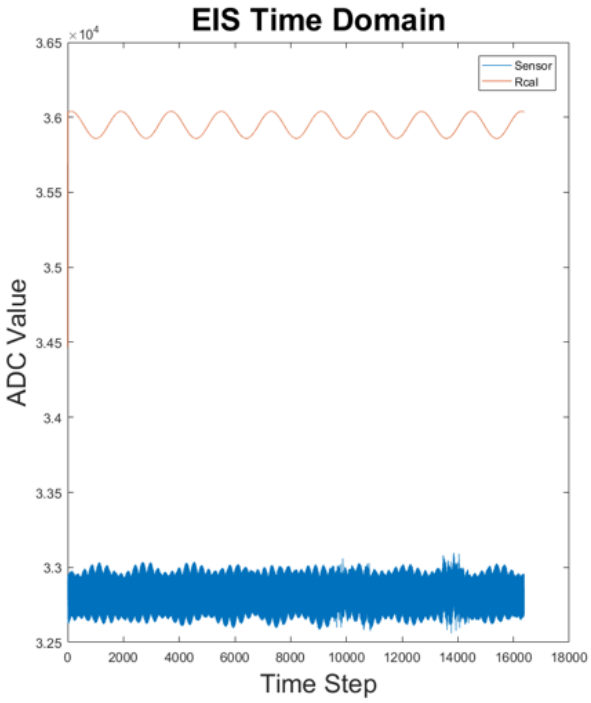


Figure 5.268: Raw ADC values of EIS measurement on 1 GΩ, 1 nF dummy cell, with measurements taken in proximity to the AIX200 atomic vapour deposition machine.

5.7 Field Results

` When the EIS data acquisition system was realised there were no BRD immunosensors readily available as the NTG group were redeveloping their fundamentals. Immunosensors that were used for the detection of Potato Virus Y (PVY) [26], in plants were at the field test development stage. Therefore the EIS data acquisition system was used on these sensors to prove that it is fit for purpose as a portable disease diagnostics reader.



Figure 5.29: Two potato plants in Teagsc, Carlow, unhealthy on the left, healthy on the right.

Samples were taken from potato plant leaves from both a plant that was visibly infected by PVY and one that was not, as seen in Figure 5.29. Plant extract was removed from the leaf and mixed with HEPES buffer. The solution was left to reside on the electrochemical sensor surface for fifteen minutes. The sensor surface was then cleaned and ferriferrocyanide was deposited on the sensor surface. An EIS scan was subsequently performed over five data points from 0.1 Hz to 10 Hz. As seen in both the phase and magnitude plots in Figure 5.30 and Figure 5.31, there is a clear differentiation between the positive and negative PVY samples for each of the five electrodes.

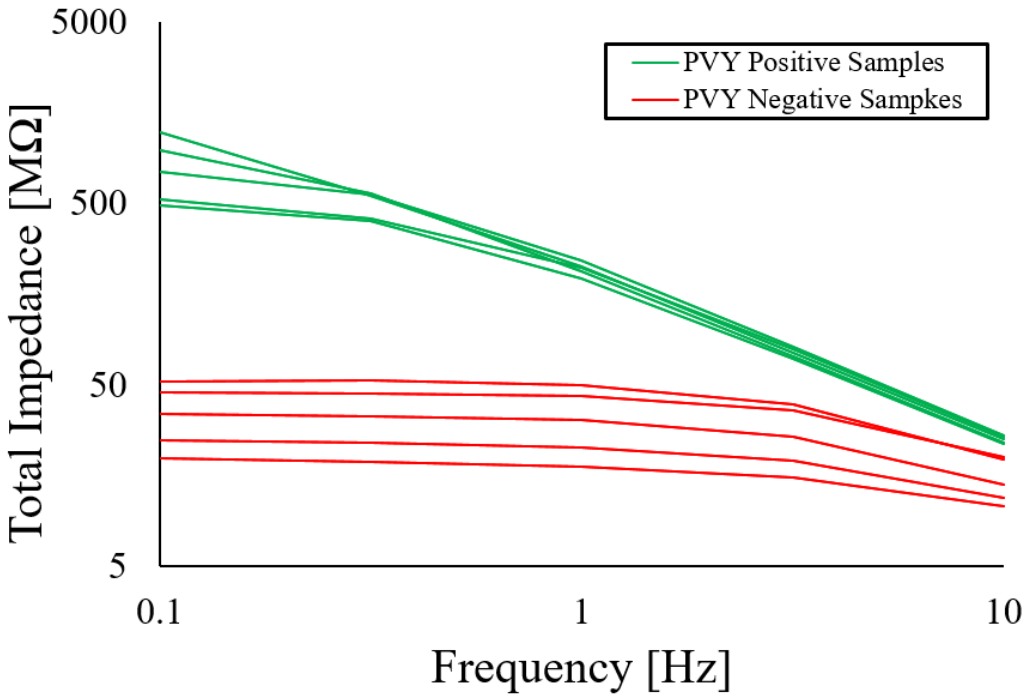


Figure 5.30: Bode plot of impedance magnitude of a positive and negative PVY sample on 0.1Mm Ferryferrocyanide using ultramicroband immunosensors, performed by the developed data acquisition system in Teagasc Carlow.

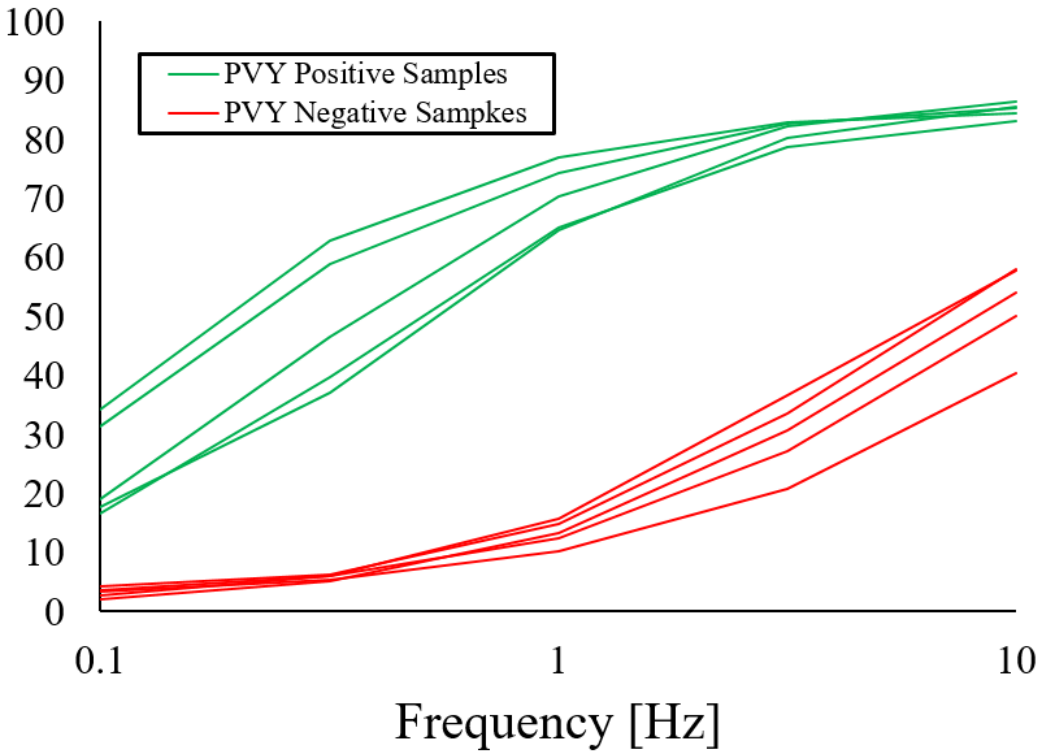


Figure 5.31: Bode plot of impedance magnitude of a positive and negative PVY sample on 0.1Mm Ferryferrocyanide using ultramicroband immunosensors, performed by the developed data acquisition system in Teagasc Carlow.

The diagnosis reference point of each measurement was defined as the total impedance at 0.1 Hz. The positive PVY samples exhibited a mean of 790 MΩ, and the standard deviation of the positive PVY sample population was estimated to be 277 MΩ using the formula:

$$\sigma = \frac{\sum(x-\mu)^2}{N} = 277M\Omega \tag{5.7}$$

Where x is a sample in the population, μ is the mean of the population and N is the population size. By taking the null hypothesis as the PVY negative samples mean, 35MΩ, the z value with respect to the positive PVY population can be described as:

$$Z = \frac{x-\mu}{\sigma} \tag{5.8}$$

Where x is the observed value of the null hypothesis, the mean of the negative PVY samples, μ is the mean of the PVY positive samples and σ is the standard deviation of the positive PVY samples.

$$Z = \frac{35\text{M}\Omega - 790\text{M}\Omega}{277M\Omega} = -2.72 \tag{5.9}$$

This Z value lies 99.35 percentile, thus it is reasonable to reject the null hypothesis. This indicates that the proposed diagnosis system is fit for the detection of PVY in potato crop.

5.8 Conclusion

A portable EIS data acquisition system is presented, that is suitable to interface to ultramicro electrochemical sensors. The system was verified by comparing experimental data from both dummy cells and electrochemical sensors against laboratory equipment. The experimental results verified that the system is capable of interfacing to the electrochemical immunosensors used for BRD, which were outlined earlier in this chapter and for PVY. This work will help enable the cost effective development of proof of concepts for emerging ultramicro electrochemical biosensors. Table 5.4 shows that this work is comparable to the state of the art despite using a 5mV AC input signal.

Table 5.4: Comparison vs State of the Art

System	Frequency Range	Measurement Range	Phase Error	Magnitude Error	User Interface	Cost	Year
This Work	**0.1Hz-10Hz**	**1MΩ-1GΩ**	**0.64º**	**1.29%**	**App/Bluetooth**	**230$**	**2021**
Grassini et al. [27]	0.01Hz-100kHz	100Ω-10GΩ	3º	5%	PC/USB	160$	2018
Lentka [28]	0.1Hz-100kHz	1Ω -10MΩ	1º	1.5%	PC/USB	-	2017
Sensit Smart [29]	0.016Hz-200kHz	10Ω-100MΩ,	-	-	App/Bluetooth	1250$	2019
Interface 1010B [23]	10uHz - 20kHz	<1mΩ >1GΩ	1º	1%	PC	7600$	2017
PalmSens 4 [22]	10uHz - 1MHz	<1Ω >1GΩ	1º	1%	App/Bluetooth	4300$	2019

5.9 References

[1] World Health Orginisation, “No Time to Wait: Securing the future from drug-resistant infections,” WHO, April 2019.

[2] World Health Organisation, “Global action plan on antimicrobial resistance,” WHO, 2015.

[3] R. W. Fulton, “Bovine respiratory disease research (1983–2009),” *Animal health research reviews,* vol. 10, no. 2, pp. 131-139, 2009.

[4] K. K. Johnson, “Market impacts of reducing the prevalence of bovine respiratory disease in United States beef cattle feedlots,” *Frontiers in veterinary science,* vol. 4, p. 189, 2017.

[5] European Parliment, “Regulation (EU) 2019/4 of the European Parliment and of the Council of 11 December 2018on the manufacture, placing on the market and use of medicated feed, amending Regulation (EC) No 183/2005 of the European Parliament and of the Council and repealing Co,” Brussels, 2019.

[6] N. Creedonet al., “Label-free impedimetric nanoband sensor for detection of both Bovine Viral Diarrhoea virus (BVDV) and antibody (BVDAb) in serum,” *ChemRxiv,* 2018.

[7] C. Schelp et al., “BVD diagnosis: an overview,” *Berliner und Munchener tierarztliche Wochenschrift,* vol. 116, no. 5-6, pp. 227-233, 2003.

[8] M.E. Theurer et al., “Systematic review and meta-analysis of the effectiveness of commercially available vaccines against bovine herpesvirus, bovine viral diarrhea virus, bovine respiratory syncytial virus, and parainfluenza type 3 virus for mitigation of bovine respiratory di,” *Journal of the American Veterinary*

Medical Association, vol. 246, no. 1, pp. 126-142, 2015.

[9] W. Yates, “A review of infectious bovine rhinotracheitis, shipping fever pneumonia and viral-bacterial synergism in respiratory disease of cattle,” *Canadian Journal of Comparative Medicine,* vol. 46, no. 3, p. 225, 1982.

[10] Z. Wang et al., “Equivalent Impedance Models for Electrochemical Nanosensor-Based Integrated System Design,” *Sensors,* vol. 21, no. 9, p. 3259, 2021.

[11] Analog Devices, “Precision Analog Microcontroller with Chemical Sensor Interface,” Analog Devices, Norwood, MA, 2020.

[12] Analog Devices, “ADuCM355 Hardware Reference Manual,” Analog Devices, Norwood, MA, 2020.

[13] N. Creedon, "Sensing at nanostructures for agri-food and enviromental applications ", Doctoral dissertation, University College Cork, 2018.

[13] S.R. Norsworthy. et al., "Delta-Sigma Data Converters: Theory, Design, and Simulation", New York: Wiley, 1997.

[14] Sparkfun, TOL-09419, Sparkfun micro SD Sniffer, Boulder, Colorado, 2021.

[15] C. Coombs. Jr., Coombs' Printed Circuits Handbook, Sixth Edition, McGraw-Hill: New York, 2007.

[16] Ohmite Mfg. Co., “Precision High-Value High-voltage Wraparound Chip,” Ohmite Mfg. Co., Chicago, 2021.

[17] Dolmen Design and Innovation Consultants, “https://www.dolmen.ie/about,” Dublin, 2021.

[18] RS Pro, “Lithium Polymer Rechargable Battery Pacl Tested and approved to

UN38.3," Dublin, (Assessed 2021).

[19] Texas Instruments, "TPS6120x Low Input Voltage Synchronous Boost Converter With 1.3-A Switches," Dallas, 2014.

[20] Analog Devices, "High Accuracy Ultralow IQ, 300 mA, anyCAP Low Dropout Regulator," Norwood, 2009.

[21] Maxim Intigrated, "On/Off Controller with Debounce and ±15kV ESD Protection," San Jose, 2008.

[22] PalmSens, PalmSens4 Potentiostat/Galvanostat/Impedance Analyzer Rev 1, Accessible (https://www.palmsens.com/wp-content/uploads/2020/07/PalmSens4-description.pdf), Houten, 2021.

[23] Garmy Instruments, Interface 1010 Potentiostat/Galvanostat/Zero Resistance Ammeter, Accessible (https://www.gamry.com/assets/Uploads/Interface-1010-Brochure-2020.pdf), Philadelphia, 2019.

[24] K. Morich, Serial Bluetooth Terminal (https://play.google.com/store/apps/details?id=de.kai_morich.serial_bluetooth_terminal&hl=en_IE&gl=US), (Assessed Jan 2022), Google Play Store, 2016.

[25] Aixtron, "Aix200 (aix200), (https://snfexfab.stanford.edu/guide/equipment/aix200-aix200), (Assessed Dec2021)," Stanford University, 2021.

[26] A.V Karasev and S.M. Gray, "Continuous and emerging challenges of potato virus Y in potato," *Annual Review of Phytopathology*, vol. 51, no. 1, pp. 571-586, 2013.

Chapter 6 Conclusions and Future Work

6.1 Conclusions and Summary

The purpose of this thesis was to develop low cost portable systems that could interface to nano-scale electrochemical sensors. To achieve this, commercial potentiostatic SoC's developed by Analog Devices were used. This dramatically reduced costs as an array of discrete components weren't required to interface to the sensors. Such devices should lower the barrier of entry of portable, in field measurements for the next generation of electrochemical sensors.

In Chapter 3, a proof of concept system was developed to interface to ultra microband electrochemical sensors using the ADuCM350. The system, which comprised of an evaluation board for the ADuCM350 was programmed to perform CV and SWV, which were the most commonly used voltammetric tests in the NTG group. Calibrations were performed using both a dummy cell and an electrochemical cell over a range of concentrations to verify that the ADuCM350 SoC was capable of performing measurements at a similar degree of accuracy to benchtop equipment.

In Chapter 4, the systems capability was extended to enable it to interface to dual WE electrochemical sensors. Through the addition of a DAC, Generator Collector voltammetric tests could be performed, augmenting the sensitivity of measurements that could be taken in the field. A PCB was developed to improve noise performance and reduce the form factor to a size suitable for field measurements. The PCB was made battery rechargeable and could be configured with a smartphone application through Bluetooth. The system was validated through

the generation of a calibration curve of dissolved oxygen in river water using an ultramicroband interdigitated sensor and the developed system.

In Chapter 5, a new portable system was developed to perform EIS. This was to enable the detection of biological agents using the ultramicroband sensors in the NTG group. Through the use of the ADuCM355, a portable device was developed that could perform impedance measurements from 10 Hz to 0.1 Hz, measuring magnitudes of up to 1 GΩ. The system was validated by comparing the phase and magnitude response from various dummy cells using the device developed and a laboratory potentiostat. Measurements were also compared from electrochemical sensors, using varying concentrations of FcCOOH, to ensure the device was fit for purpose. The portable system was used to diagnose potato plants for potato virus Y in Teagsc Carlow.

6.2 Future Work

For future iterations of the voltammetric measurement device described in Chapter 3 and 4, the main improvement that can be iterated is increasing the applied voltage range of the device. If the voltage range was increased from the current ± 0.8 V to ±2V, it would enable measurements to be taken in the field for a wider range of nano-scale electrochemical sensors. This can be achieved through the use of the ADuCM355. Intelligence could also be integrated into the system, allowing for instantaneous concentration readings to be made.

For the EIS data acquisition system, work should be done to allow for measurements to be taken more quickly. Through the use of the DFT engine of the ADuCM355 in this work, impedance measurements can be taken at a low cost but are time intensive. To make the system more feasible for field measurements by a veterinarian, a new system may have to be built using the lock in amplifier technique, as described in Chapter 2. This can be done using either discrete components or preferably on a custom IC so the electronics can be integrated as much as possible with the sensor to improve noise performance.

Appendices

A.1 Acronyms

AC	Alternating Current
ADC	Analog to Digital Converter
AFE	Analog Front End
Ag/AgCl	Silver / Silver Chloride
AMR	Antimicrobial Resistance
ARM	Advanced RISC Machines
BPI3	Parainfluenza 3
BRD	Bovine Respiratory Disease
BVDV	Bovine Viral Diarrhoea Virus
CE	Counter Electrode
CV	Cyclic Voltammetry
DAC	Digital to Analog Converter
DC	Direct Current
DFT	Discrete Fourier Transform
EDC	Ethylene Dichloride
EIS	Electrochemical Impedance Spectroscopy
FRA	Frequency Response Analyser
HDMI	High Definition Multimedia Interface
IBR	Infectious Bovine Rhinotracheitis
IR	Current/Resistance
LCD	Liquid Crystal Display
LPF	Low Pass Filter
NHS	N-Hydroxysuccinimide
RE	Reference Electrode

RISC	Reduced Instrumentation Set Computer
PC	Personal Computer
PCB	Printed Circuit Board
Ph	Power of Hydrogen
Pt	Platinum
PuTTY	Popular SSH and Telnet Client
SARS-CoV-2	Severe Acute Respiratory Syndrome Coronavirus-2
SD	Secure Digital
SWV	Square Wave Voltammetry
TIA	Trans-Impedance Amplifier
UART	Universal Asynchronous Receiver-Transmitter
UME	Ultra-Micro Electrode
USB	Universal Serial Bus
WE	Working Electrode
WE1	Working Electrode 1
WE2	Working Electrode 2

A.2 Peer Reviewed Publications

1. **A. Murphy**, I. Seymour, A. O'Riordan, I. O'Connell, " Portable Data Acquisition System for Nano and Ultra-Micro Scale Electrochemical Sensors", IEEE Sensors Journal, 21, 3, 3210-3215, 2021.
2. Z. Wang, **A. Murphy**, A. O'Riordan, I. O'Connell, " Equivalent Impedance Models for Electrochemical Nanosensor-based Integrated System Design", MDPI Sensors Journal, 2021.
3. I.Seymour, T. Narayan, N. Creedon, K. Kennedy, **A. Murphy**, R. Sayers, E. Kennedy, I. O'Connell, J. Rohan, A. O'Riordan, " Advanced Solid State Nano-electrochemical Sensors and System for Agri 4.0 Applications", MDPI Sensors Journal, 2021.
4. **A. Murphy**, N. Creedon, A. O'Riordan, I. O'Connell, " Data Acquisition for Ultramicroband Bovine Respitory Disease Electrochemical Immunosensors" in IEEE International Symposium on Circuits and Systems (ISCAS), Seville, 2020.
5. **A. Murphy**, K. Hanley, N. Creedon, A. O'Riordan, I. O'Connell, "Advanced data acquisition for emerging nano-electrochemical sensors" in IEEE International Instrumentation and Measurement Technology Conference (I2MTC), Houston, 2018.
6. **A. Murphy**, I. Seymour, A. O'Riordan, I. O'Connell, " Generator Collector Voltammetry Data Acquisition for Nanowire Interdigitated Sensors" in IEEE International Conference on Nanotechnology (IEEE-Nano), Cork, 2018.
7. K. Hanley, **A. Murphy**, N. Creedon, A. O'Riordan, D. O'Hare, I. O'Connell, " Current Readout Circuit for Point-of-Care Infectious Disease Diagnostics in Animal Health" in IEEE Nordic Circuits and Systems Conference (NORCAS), Tallinn, 2018.

A.3 Publications Submitted

1. **A. Murphy**, F. Diaz, A. O'Riordan, I. O'Connell, "Portable Electrochemical Impedance Spectroscopy Data Acquisition System for

Ultra-Micro Scale Electrochemical Immunosensors", IEEE Sensors Journal, 2023.

A.4 Code Used

1. C. files for EIS and Amperometric measurements can be found in the following link: https://github.com/aidanmurfie/PhD_Thesis
2. Scratch code for the App described in Chapter 4 can be found in the following link: https://github.com/aidanmurfie/PhD_Thesis
3. Please contact ivan.oconnell@mcci.ie for queries regarding other files in this thesis.

A.5 PCB Schematics and Layouts

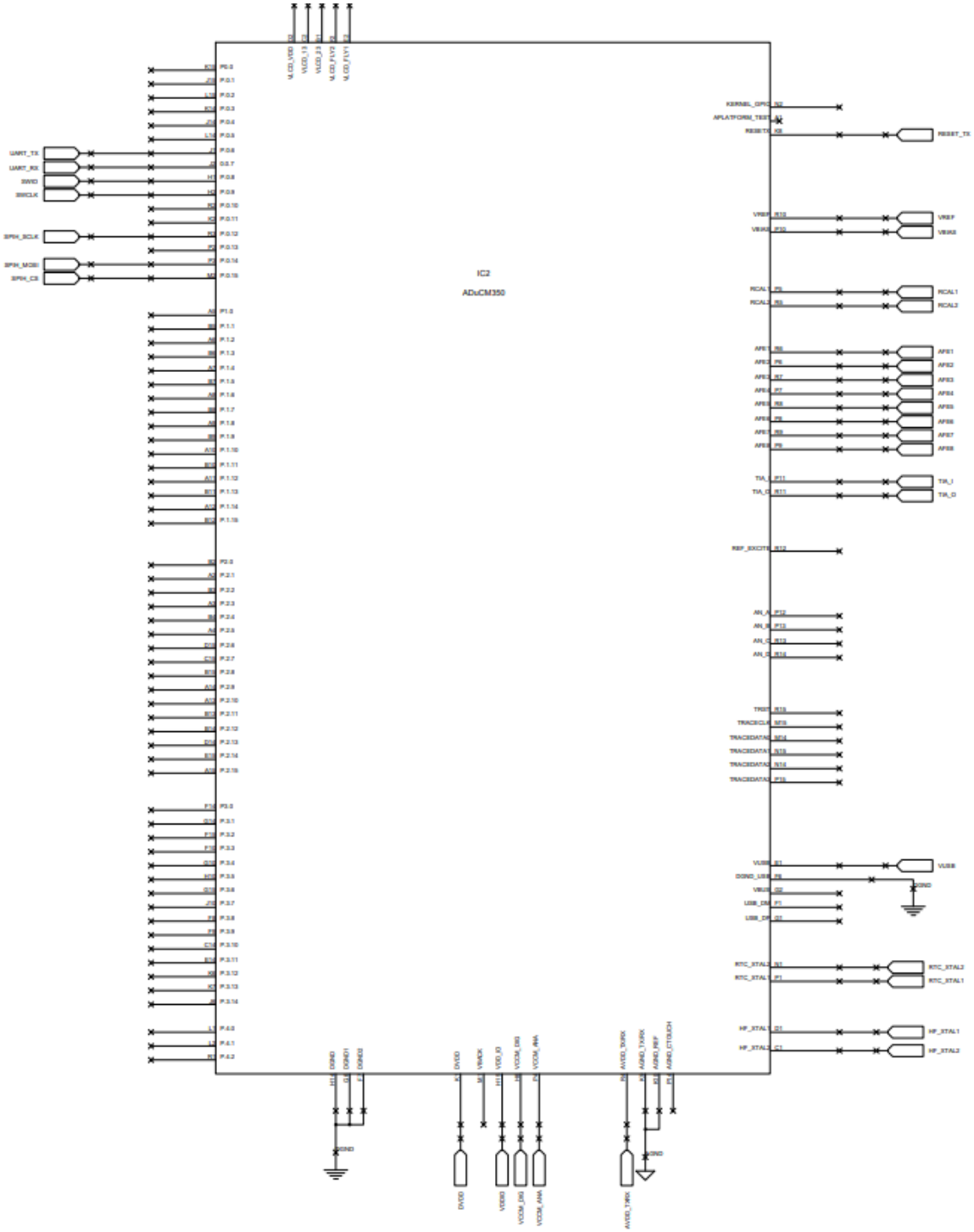


Figure A.1: ADuCM350 schematic for voltammetric potentiostat PCB.

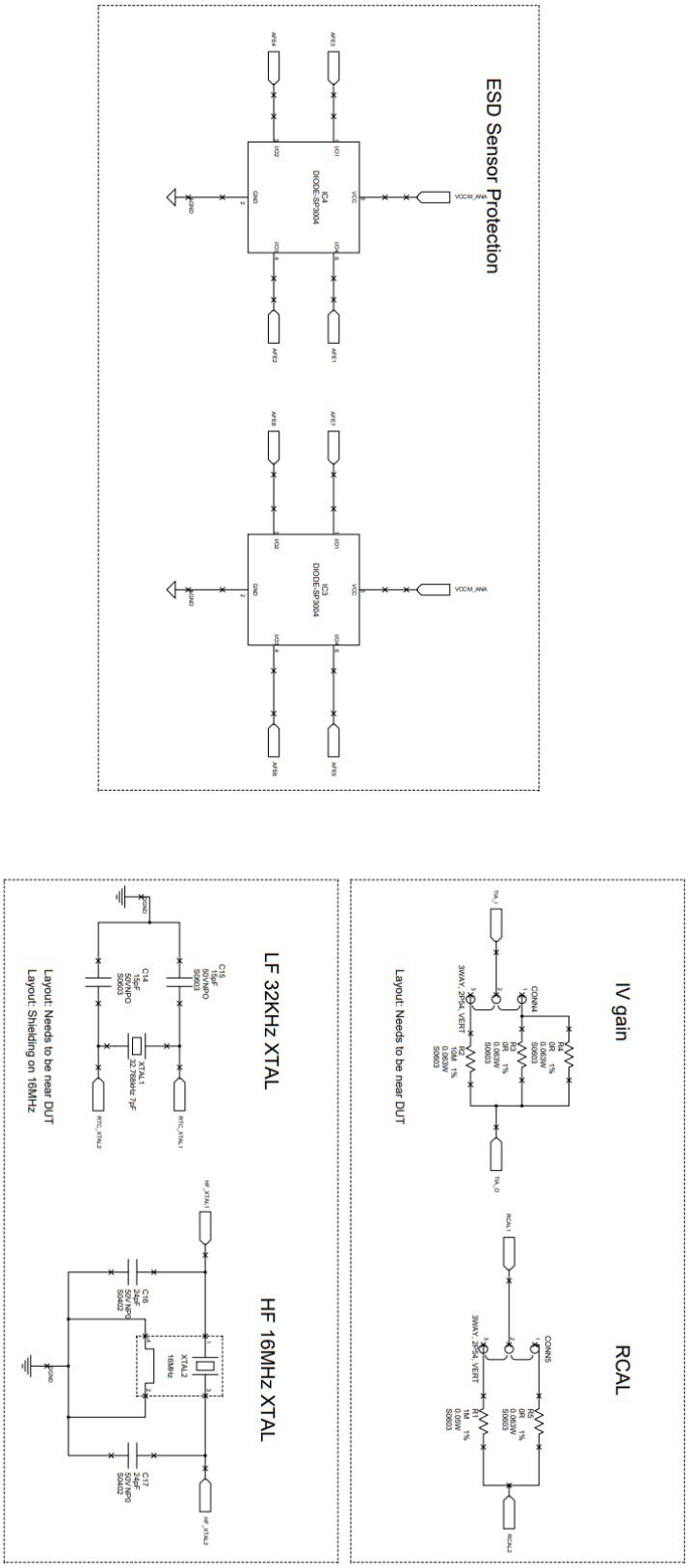


Figure A.2: Oscillators, AFE connections and sensor protection for voltammetric potentiostat PCB.

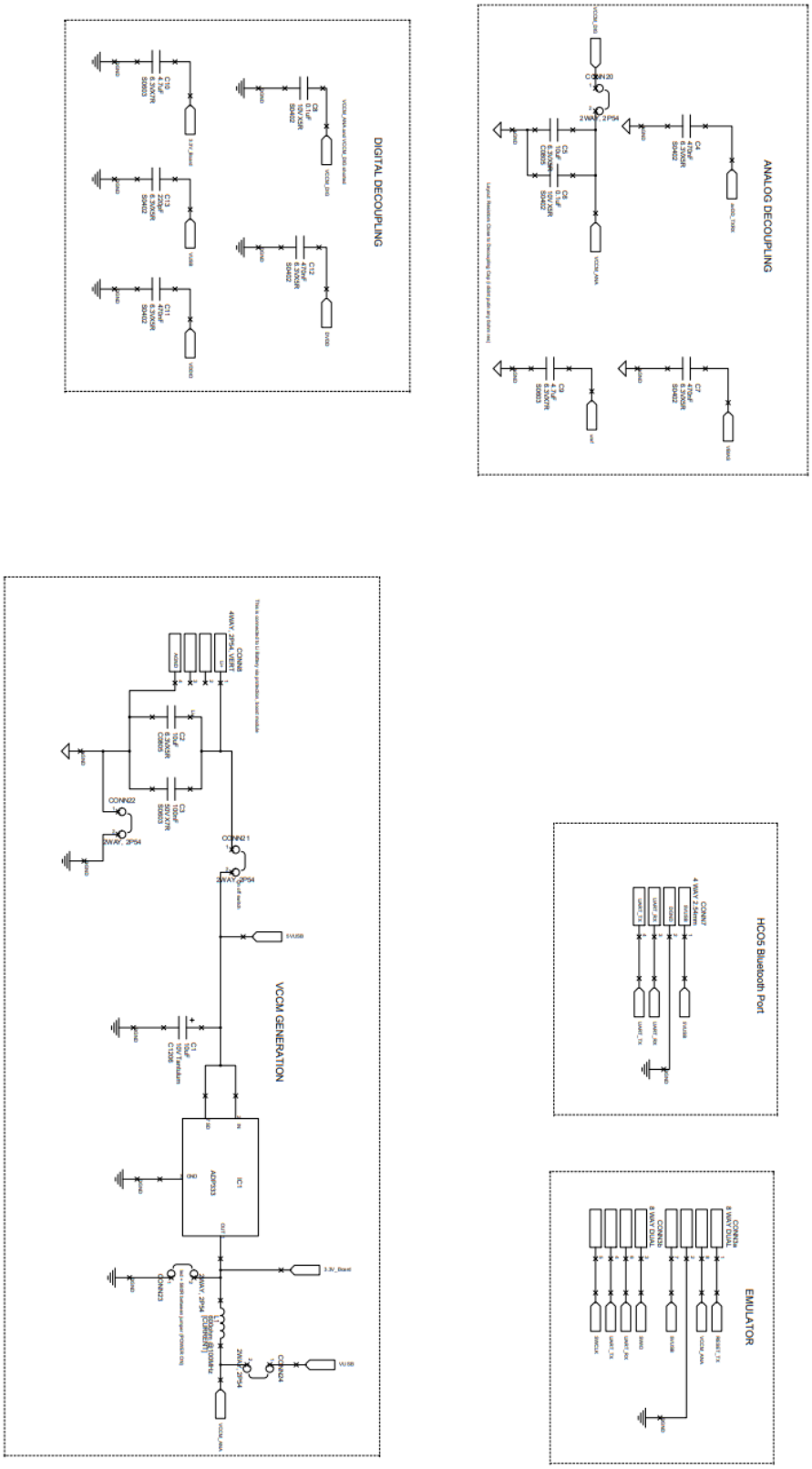


Figure A.3: Oscillators, AFE connections and sensor protection for voltammetric potentiostat PCB.

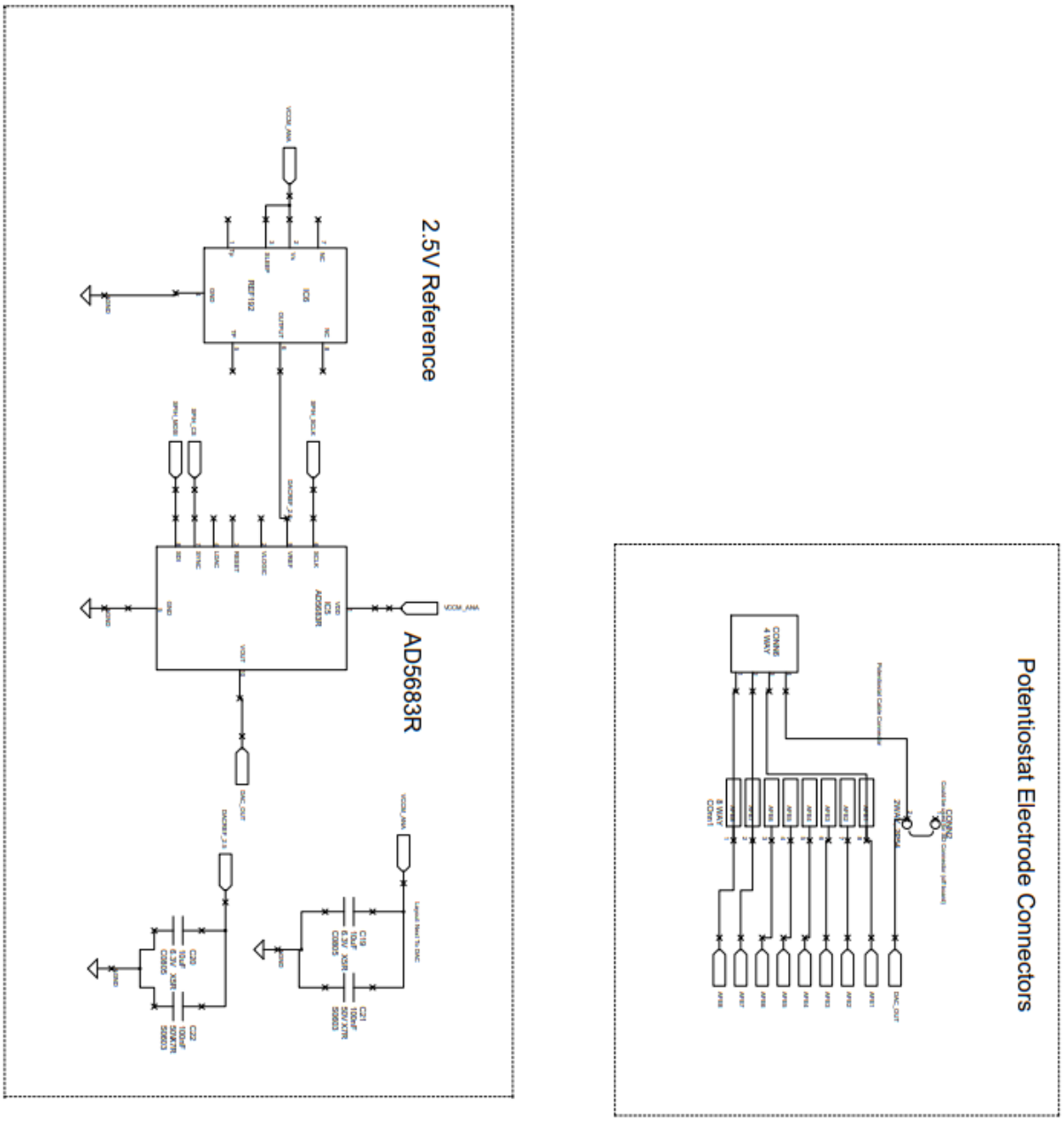


Figure A.4: AFE connections and external DAC for voltammetric potentiostat PCB.

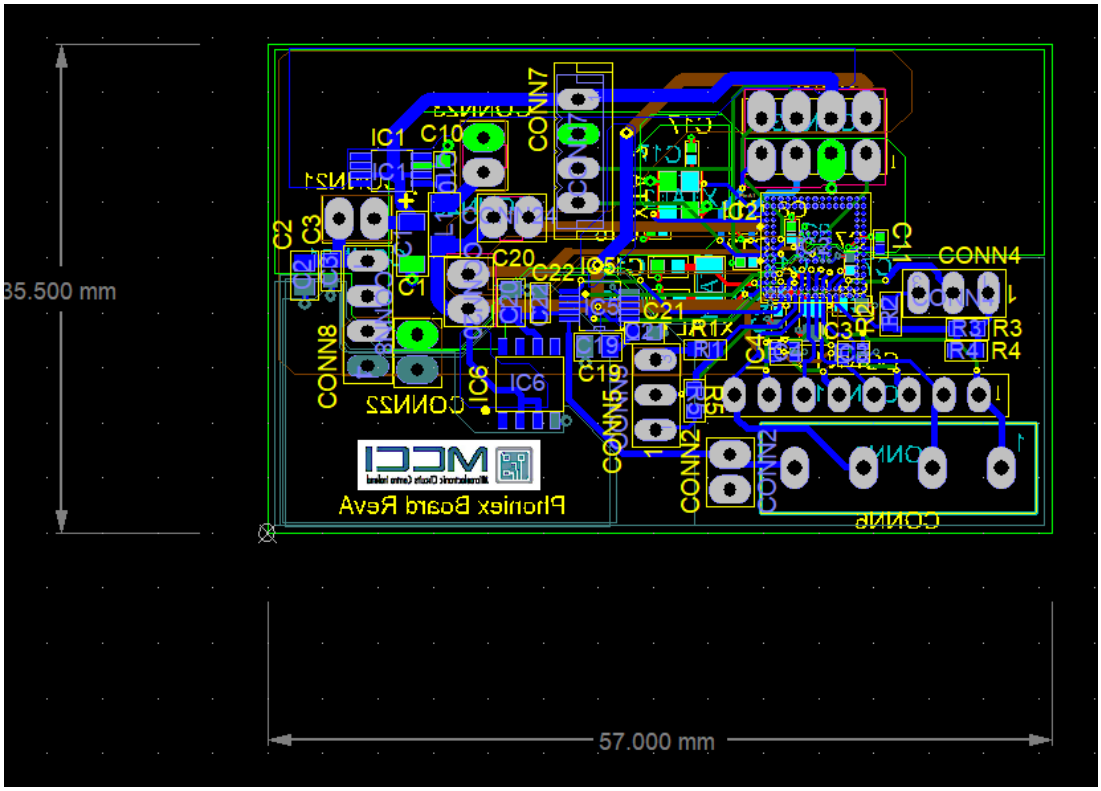


Figure A.5: All layers of voltammetric potentiostat PCB (poured shapes excluded).

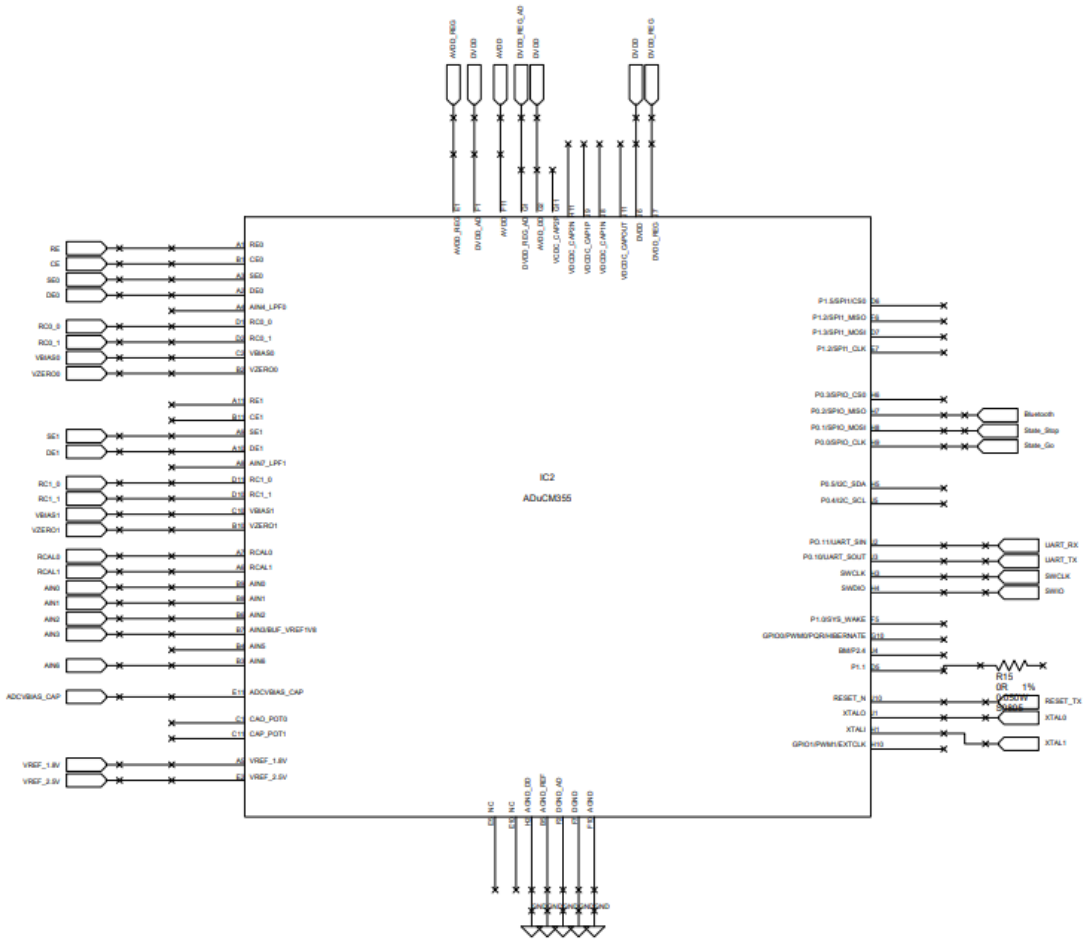


Figure A.27: ADuCM355 schematic for EIS PCB.

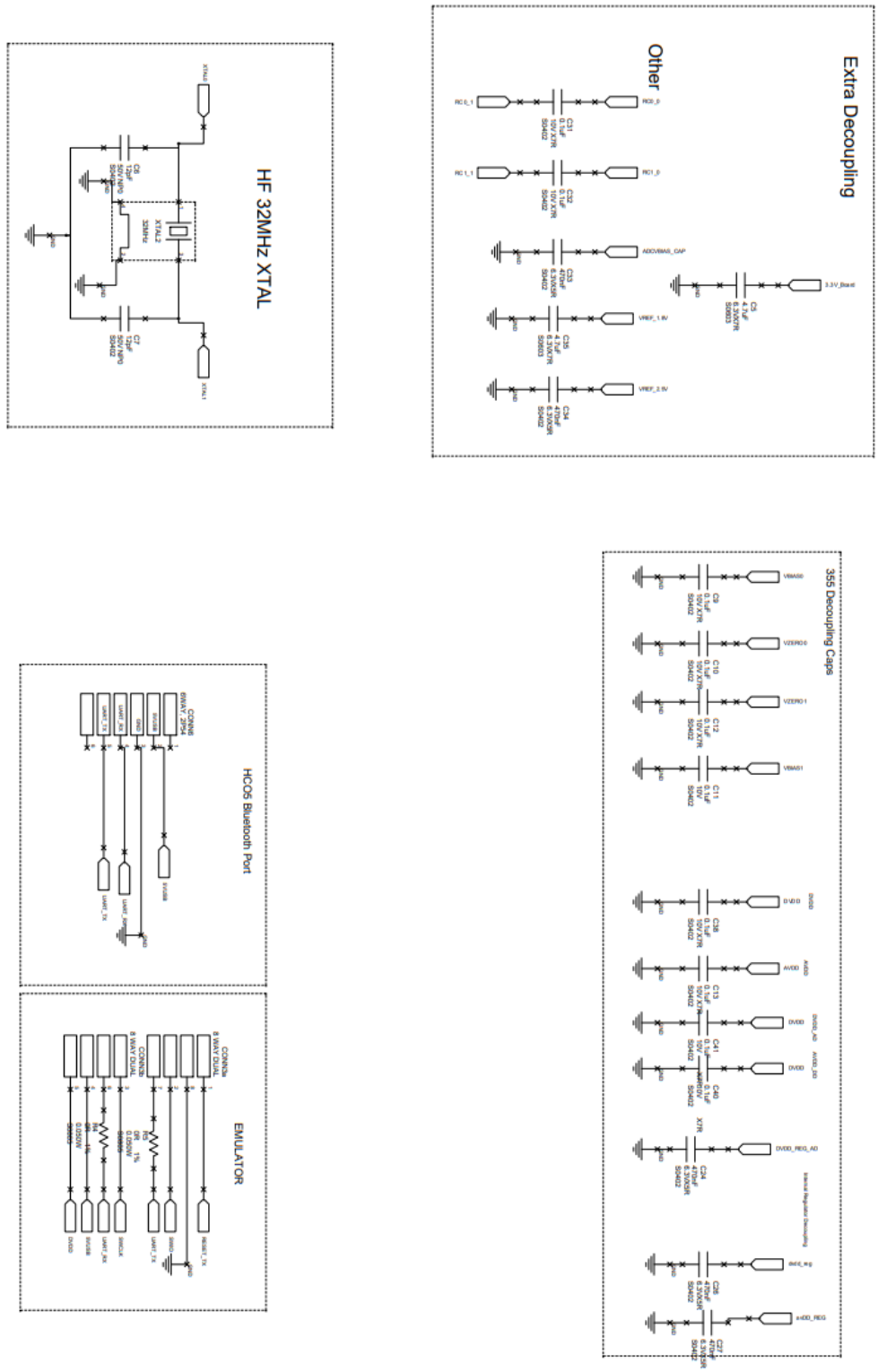


Figure A.7: Analog decoupling, resonator, programmer and Bluetooth schematic for EIS PCB.

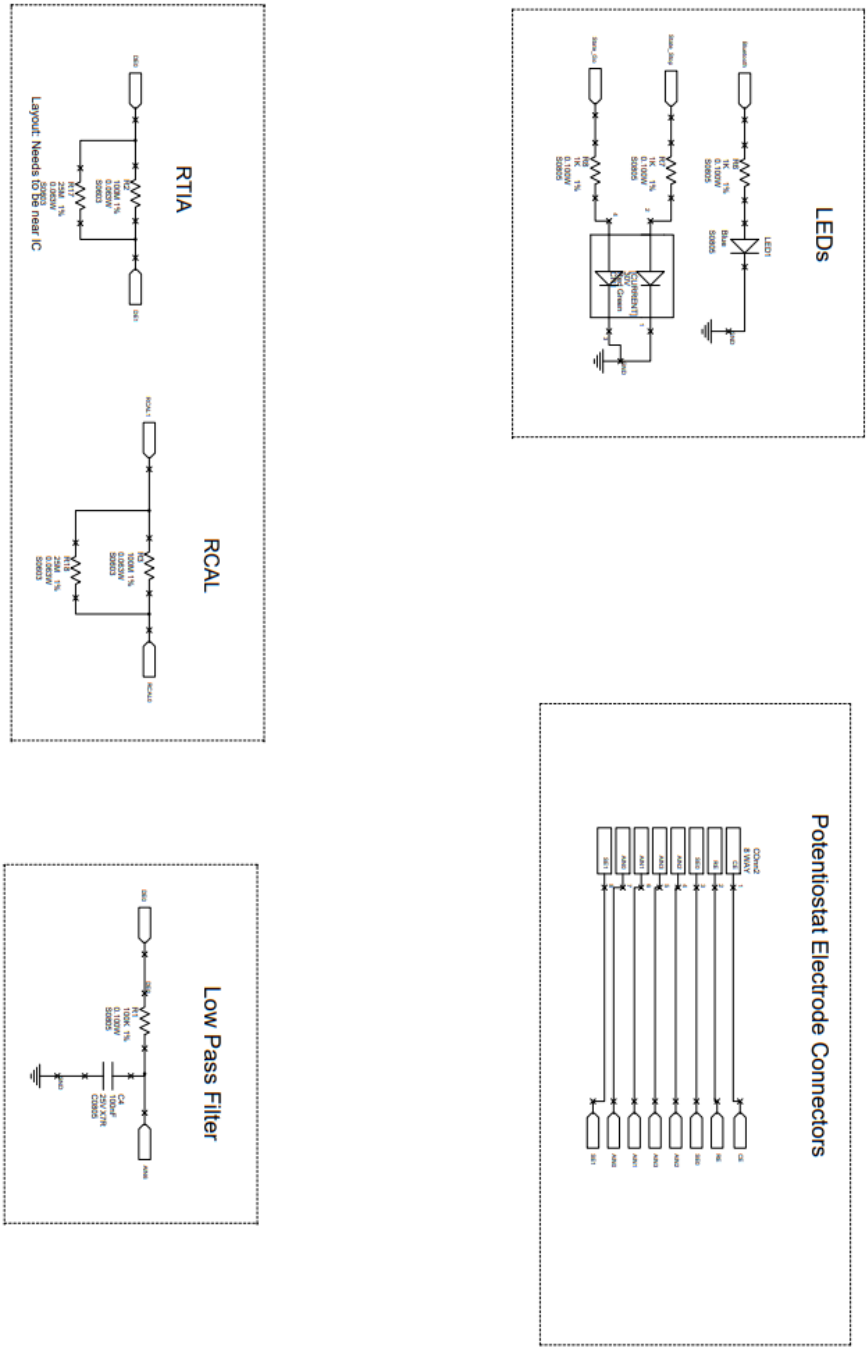


Figure A.8: AFE connections and indicator lights schematic for EIS PCB.

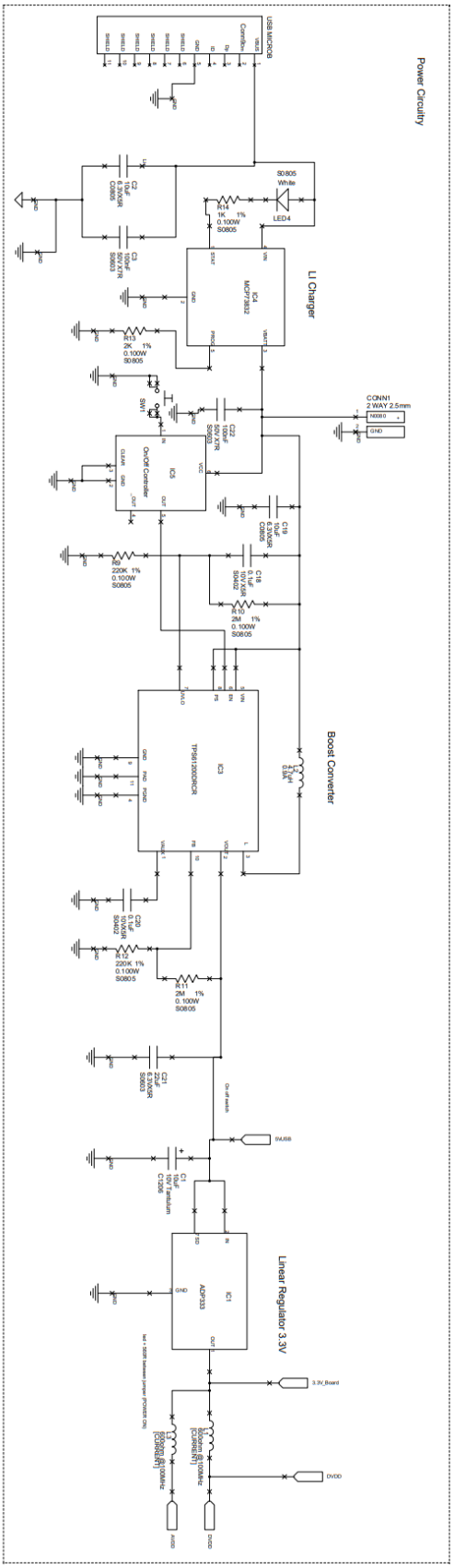


Figure A.9: Power Management schematic for EIS PCB.

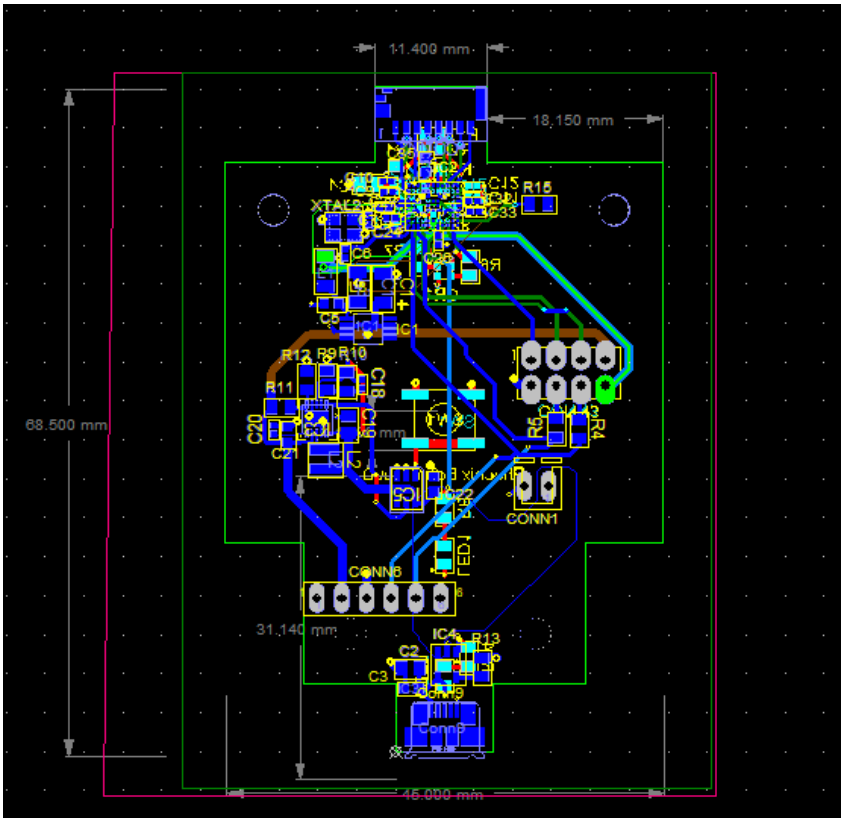


Figure A.10: All layers of EIS PCB Layout (poured shapes excluded).